Investigation of Functional Group Distributions on Modified Mesoporous Silica

---

Dissertation

zur

Erlangung der naturwissenschaftlichen Doktorwürde (Dr. sc. Nat.)

vorgelegt der

Mathematisch-naturwissenschaftlichen Fakultät

der

Universität Zürich

von

Nando Gartmann

von

Castrisch GR

Promotionskomitee

Prof. Dr. Roger Alberto (Vorsitz)

Prof. Dr. Heinz Berke

PD Dr. Dominik Brühwiler (Leitung der Dissertation)

Zürich, 2012

Acknowledgement

I am deeply grateful to PD Dr. Dominik Brühwiler for giving me the opportunity to carry out this thesis under his supervision. I am thankful for him always taking time when a new problem needed discussion. With his continuous support and excellent advice he gave very helpful contributions to my work.

Prof. Dr. Roger Alberto is acknowledged for the chairing of my defence and acting as the representative for my dissertation before the faculty.

Prof. Dr. Heinz Berke is thanked for being a member of my promotion committee.

For financial support I acknowledge the Swiss National Science Foundation (Project 200020-117591) and the European Commission (Marie-Curie RTN Nanomatch, Grant No. MRTN-CT-2006-035884).

I am much obliged to all former members of the Brühwiler group, especially to Christina, Christophe, Hanna, Igor, Jan, Le-Quyenh and Thomas (in alphabetical order) for helpful discussions, good advice and a really nice working atmosphere.

I also want to thank the whole ACI for providing a good working environment and most notably the friends I made in the institute during my time here, in particular Roman, Miri, Balz, Dani, Migi, Alois, Michi and Alex.

I want to thank Mine Ince from the Universidad Autonoma de Madrid for the fruitful collaboration and the very productive week she spent at the University of Zürich. Great thanks goes to Georg Meseck from the PCI for providing me with high quality SEM images without which my work would have been far more difficult.

I want to thank my parents for their continuous support and their encouragement during my whole studies, also to my parents-in-law for the support they give to my wife and me in many everyday life situations where somebody is needed.

Last but not least, the warmest thanks go to the two most important girls in my life Lisa and Lily, for being the center of my life.

Abstract

Based on its structural and chemical properties such as a large surface area, a large pore volume, a narrow pore size distribution, an easily modifiable surface and a high biocompatibility, mesoporous silica is the material of choice for many applications in catalysis, chromatography, sensing, adsorption, drug delivery and optical devices. All of these applications require functionalization of the surface, often with a certain degree of selectivity for external and internal surfaces. It is therefore essential to understand and control the placement of functional groups on the mesoporous silica surface. Trialkoxyaminosilanes are well established functionalization agents for mesoporous silica, because they offer a wide range of options for further derivatization.

This work tackles important problems to be faced in the functionalization of mesoporous silica surfaces, e.g. selectivity for the external surface, but it also contains studies on structural and morphological changes to mesoporous silica and the embedding of mesoporous silica and zeolites in thin polymer layers from wet films.

Two different types of mesoporous silica are functionalized with aminopropyltrialkoxysilanes and further labeled with fluorophores to visualize the functional group distribution. The influence of many factors, such as solvent polarity, reaction time, reaction temperature and trace water content on the distribution of different aminopropyltrialkoxysilanes is investigated, and a pathway for the selective functionalization of the external surface is shown. The analysis of the functionalized mesoporous silica is conducted with various methods: Scanning electron microscopy to visualize particle size and shape, UV/Vis absorption and luminescence spectroscopy to quantify the degree of functionalization and labeling, nitrogen sorption to determine the pore size and pore volume, and confocal laser scanning microscopy to image the distribution of the fluorescent labels throughout the porous particles. It is shown that the combination of nitrogen sorption analysis and confocal laser scanning microscopy is a versatile tool for the analysis of functional group distributions.

Structural and morphological modification of mesoporous silica is performed by layer-by-layer deposition of different small siloxanes to influence the pore size, and by synthesizing mesoporous silica in the presence of a cosurfactant to tailor the particle shape. These changes are monitored by scanning electron microscopy, nitrogen sorption, and pore size probing with a sterically demanding luminescent molecule.

In the second part of this work, the formation of patterns upon the embedment of porous silicate particles in a polymer matrix by wet film techniques is investigated. The patterns are visualized by fluorescence microscopy.

Kurzfassung

Die strukturellen und chemischen Eigenschaften von mesoporösem Silikat, wie z.B. die grosse Oberfläche, das grosse Porenvolumen, die enge Porengrössenverteilung, die einfach zu modifizierende Oberfläche und die hohe Umweltverträglichkeit, lassen es zum Material der Wahl für viele Anwendungen in Bereichen wie Katalyse, Chromatografie, Sensorik, Adsorption, Wirkstofftransport und optische Anwendungen werden. Für alle diese Anwendungen wird eine Modifizierung der Oberfläche, oft mit Selektivität für die innere oder äussere Oberfläche, benötigt. Das Verständnis und die Kontrolle der Platzierung solcher funktionellen Gruppen auf der Silikatoberfläche sind daher sehr wichtig. Trialkoxy-aminosilane sind weit verbreitete Funktionalisierungsstoffe für mesoporöse Silikate, da diese eine breite Palette weiterer Derivatisierungen ermöglichen.

Diese Arbeit beschäftigt sich mit wichtigen Fragestellungen, die bei der Funktionalisierung der Oberfläche mesoporöser Silikate auftreten, wie z.B. Selektivität für die äussere Oberfläche, und enthält Untersuchungen zu strukturellen und morphologischen Veränderungen an mesoporösem Silikat, sowie zur Einbettung von mesoporösem Silikat und Zeolithen in dünne Polymerschichten.

Zwei unterschiedliche mesoporöse Silikate werden mit Trialkoxyaminosilanen funktionalisiert und mit Fluoreszenzfarbstoffen modifiziert um deren Verteilung sichtbar zu machen. Der Einfluss vieler Faktoren wie z.B. die Polarität des Lösungsmittels, Reaktionszeit, Reaktionstemperatur und Gehalt an Spurenwasser auf die Verteilung der funktionellen Gruppen wird untersucht, und ein Weg zur selektiven Modifizierung der äusseren Oberfläche wird aufgezeigt. Zur Analyse von funktionalisiertem mesoporösem Silikat werden verschiedene Methoden verwendet: Rasterelektronenmikroskopie um Partikelform und -grösse zu untersuchen, UV/Vis und Lumineszenzspektroskopie um den Funktionalisierungs-grad zu quantifizieren, Stickstoffsorption um die Porengrösse und das Porenvolumen zu bestimmen, und konfokale Laserrastermikroskopie um die Verteilung der funktionellen Gruppen im porösen Partikel zu analysieren. Es wird gezeigt, dass die Kombination aus konfokaler Laserrastermikroskopie und Stickstoffsorption ein vielseitiges Werkzeug zur Analyse der Verteilung funktioneller Gruppen darstellt.

Strukturelle und morphologische Veränderungen an mesoporösen Silikaten werden auf zwei Arten vorgenommen, einerseits eine Schicht-für-Schicht Anlagerung von kleinen Siloxanen an die Oberfläche um die Porengrösse zu beeinflussen, andererseits die Zugabe eines Co-Tensids während der Silikatsynthese um die Form und Grösse der Partikel anzupassen. Die Veränderungen werden mittels Rasterelektronenmikroskopie, Stickstoffsorption und Porengrössensondierung mittels eines sterisch anspruchsvollen lumineszierenden Moleküls verfolgt.

Im zweiten Teil der Arbeit wird die Bildung von Mustern, welche bei der Einbettung von porösen Silikatpartikeln in dünne Polymerschichten entstehen, mittels Fluoreszenzmikrosko-pie untersucht.

List of Abbreviations

APDIPES	3-Aminopropyldiisopropylethoxysilane
APDMMS	3-Aminopropyldimethylmethoxysilane
APTES	3-Aminopropyltriethoxysilane
APTMEES	3-Aminopropyltrimethoxyethoxyethoxysilane
ASNCs	Arrays of silica nanochannels
BET	Brunauer-Emmett-Teller
BJH	Barrett-Joyner-Halenda
BTESPA	Bis(triethoxysilyl)propylamine
CLSM	Confocal laser scanning microscopy
CTAB	Hexadecyltrimethylammonium bromide
C_{12}TAC	Dodecyltrimethylammonium chloride
CTAC	Hexadecyltrimethylammonium chloride
DFT	Density functional theory
DMPS	Dodecamethylpentasiloxane
FITC	Fluorescein isothiocyanate
F127	Pluronic F127 (triblock copolymer: $HO(CH_2CH_2O)_{106}(CH_2CH(CH_3)O)_{60}(CH_2CH_2O)_{106}H$ / $EO_{106}PO_{60}EO_{106}$
MCM	Mobil Composition of Matter
MTMS	Methyltrimethoxysilane
PMMA	Polymethylmethacrylate
PSD	Pore size distribution
P123	Pluronic P123 (triblock copolymer: $HO(CH_2CH_2O)_{20}(CH_2CH(CH_3)O)_{70}(CH_2CH_2O)_{20}H$ / $EO_{20}PO_{70}EO_{20}$
SBA	Santa Barbara Amorphous
SBAs	Spherical SBA particles
SDA	Structure directing agent
SEM	Scanning electron microscopy

TEOS	Tetraethoxysilane
TBOS	Tetrabutoxysilane
TMB	1,3,5-Trimethylbenzene
THF	Tetrahydrofuran
TLC	Thin layer chromatography
TR	Texas Red
T8	Octakis-(dimethylsiloxy)-t8-silsesquioxane

Table of Contents

PART I: Mesoporous Silica

PART II Patterns of Porous Silicates in Polymer Thin Films

APPENDIX

PART I

Mesoporous Silica

1. Introduction

Since the discovery of the mesoporous silica of the M41S type in 1992 by the Mobil company[1, 2] these materials have aroused large interest in the scientific community. In the past twenty years, many mesoporous materials were developed, differing in size, shape, pore diameter and pore system symmetry.[3] Due to their large surface areas, their large pore volumes, their convenient functionalizability and their low toxicity, these materials are of particular interest in various fields, e.g. catalysis[4-6], chromatography[7], sensing[8], adsorption[9, 10] and drug delivery[11, 12].

For most of these applications a unique functionalization of the pore surface, the pore entrances and the external particle surface is needed, hence it is important to develop methods to control the distribution of functionalization agents on the surface. In the case of a drug delivery device, the functionalization of the internal pore surface would be adapted to provide ideal drug adsorption and the external surface functionalization would be responsible for blood stability, prevention of aggregation, and targeting,[13] whereas a gate mechanism could be installed at the pore entrances for zero-loss transport in the body. A similar system can also be used for cell labeling.[14] The pore surface is functionalized with the labeling agent (e.g. fluorescent or radio label), whereas the functionalization on the external surface is adapted for efficient cellular uptake.

A further example for the application of mesoporous silica featuring site specific functionalization is the research on heavy metal adsorbents for water purification conducted by the group of Fryxell[10]. The important steps in the purification of water are the capture of the heavy metals by the adsorbents and the recollection of the adsorbents from the water. Mesoporous silica with heavy metal binding groups (e.g. thiols for Hg, Pb and Cd) in the pore body and a slightly hydrophobic functionalization on the external surface are ideally suited for this application. The adsorbing phase takes up the heavy metals from the water and due to the slight hydrophobicity of the external surface, the adsorbent will slowly resurface. Such a system is not limited to water purification, thiol functionalized mesoporous silica can also be used for removing Hg from contaminated vacuum pump oil.[10]

The above mentioned applications of functionalized mesoporous materials require selective functionalization of internal and external surfaces as well as convenient analytical methods for the analysis of the functional group distribution. For this analysis, nitrogen sorption and fluorescent labeling combined with confocal laser scanning microscopy (CLSM) analysis is very effective[15] because general functionalization trends as well as subtle differences can be distinguished with the combination of optical data and the information about changes in pore size and pore volume upon surface functionalization. Large mesoporous particles with a well defined pore system such as SBAs[16-18] and most notably ASNCs[19] are suited best for these analytical methods.

2. Theory

2.1 Mesoporous Silica

Mesoporous silica consists of amorphous corner sharing SiO_4 tetrahedra featuring regular porous structures. According to IUPAC, a material is defined as mesoporous if its pore diameter lies between 2 nm and 50 nm (Fig. 1).[20] The surface of these materials is covered with hydroxy groups with a density of 3-4 groups per nm^2,[21] depending on the material and its treatment. Such mesoporous silica can be prepared with different pore geometries, e.g. hexagonal (MCM-41/SBA-15), laminar (MCM-50) or cubic (MCM-48) (Fig. 2). These materials feature high surface areas of approximately 700 to 1500 m^2 per gram of material.

Fig. 1 Nomenclature of porous materials according to IUPAC.[20]

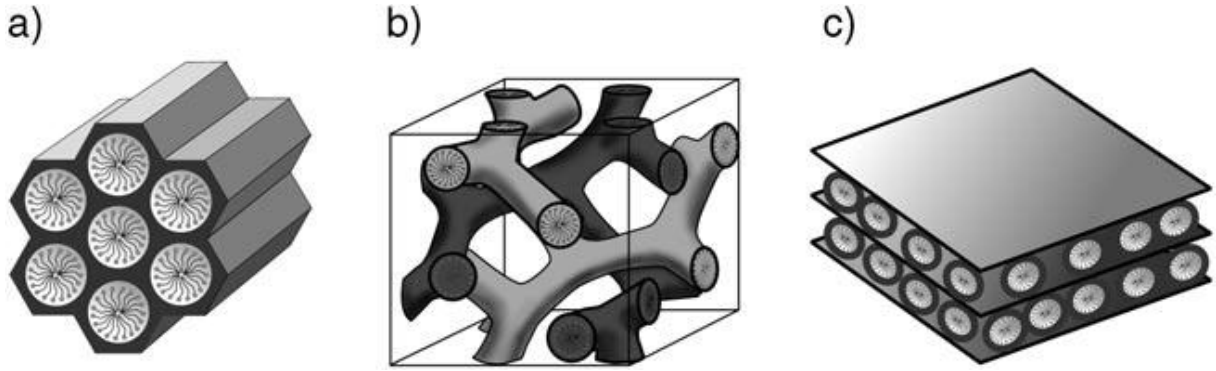

Fig. 2[22] Model of a hexagonal (a), cubic (b) and laminar (c) pore system.

In the so called liquid crystal templating (Fig. 3), the well ordered pore system develops due to the formation of supramolecular aggregates of surfactants in solution as structure directing agents (SDA).[22] These aggregates form a lyotropic liquid crystalline phase, which leads to the assembly of the amorphous mesoporous silica composites upon addition of a silica precursor such as a tetraalkoxysilane. To obtain the porous materials, the SDA is removed postsynthetically by calcination or extraction.

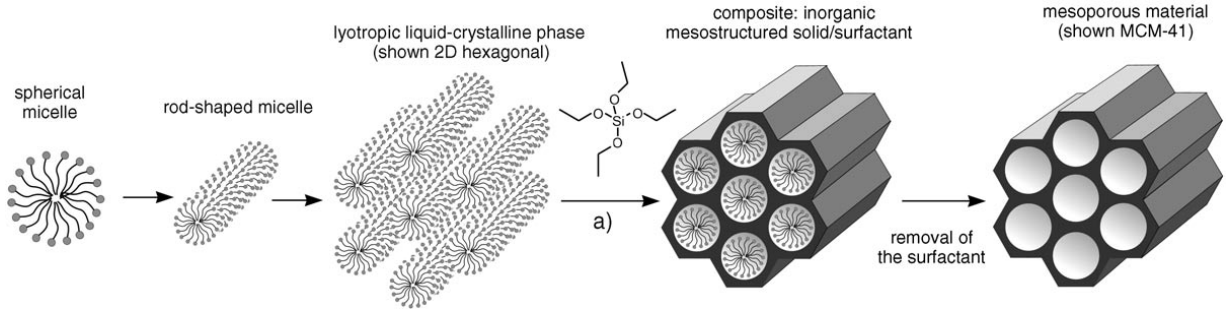

Fig. 3[22] Synthesis pathway of mesoporous silica with a hexagonal pore system.

An important requirement for the mesoporous silica to form is therefore the interaction between the SDA and the silica precursor. These interactions are categorized into different mechanisms[23, 24](Fig. 4). In the original approach,[1, 2] the M41S class, long-chain alkyltrimethylammonium halides are used as SDA. Under synthesis conditions in a basic aqueous solution, the -SiOH groups are deprotonated and interact directly with the positively charged ammonium groups. In case of SBA materials, which were developed at UC Santa Barbara in 1998,[25, 26] a non-ionic triblock copolymer consisting of polyethylene oxide and polypropylene oxide is employed as SDA and the synthesis is performed in a slightly acidic aqueous solution. Therefore, the interaction between the SDA and the silica is non-ionic and based on hydrogen bonding. If a highly acidic solution (pH < 2) is used together with a cationic SDA, as is the case in the synthesis of arrays of silica nanochannels (ASNCs[19]), both silica precursor and SDA are cationic and therefore the halide counter-anion acts as mediator.

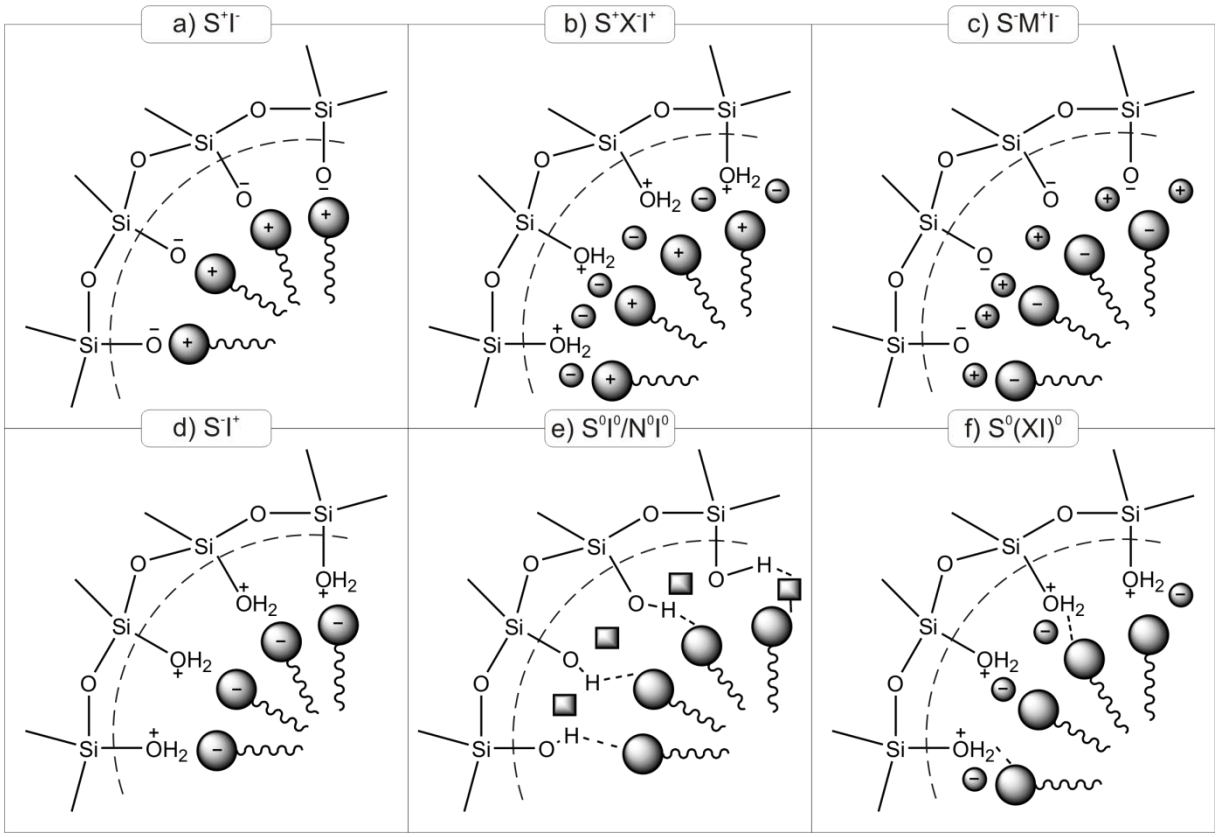

Fig. 4 Interactions between SDA and silica, cationic SDA in basic (e.g. MCM-41)(a) or acidic (e.g. ASNCs)(b) solution, anionic SDA in basic (c) or acidic (d) solution, neutral SDA in neutral (e) or acidic (e.g. SBA-15)(f) solution.

In our work, mesoporous silica materials featuring a hexagonal pore system are applied exclusively. The most prominent examples of these materials are MCM-41 and SBA-15. MCM-41 is usually synthesized hydrothermally, but can also be prepared in a room temperature procedure.[27] It features a narrow pore size distribution (PSD) around 4 nm (Fig. 5) and non-porous pore walls with a thickness of approximately 1 nm. In contrast to MCM-41, SBA-15 shows a larger pore size which is distributed around 7 - 8 nm (Fig. 5) and it also features thicker pore walls. SBA-15 exhibits intrawall porosity, this means that the

hexagonally arranged mesopores are interconnected by mostly microporous channels.[28, 29] The intrawall porosity can be up to 30 % of the total porosity[30] and depends to some extent on the synthesis temperature.[31]

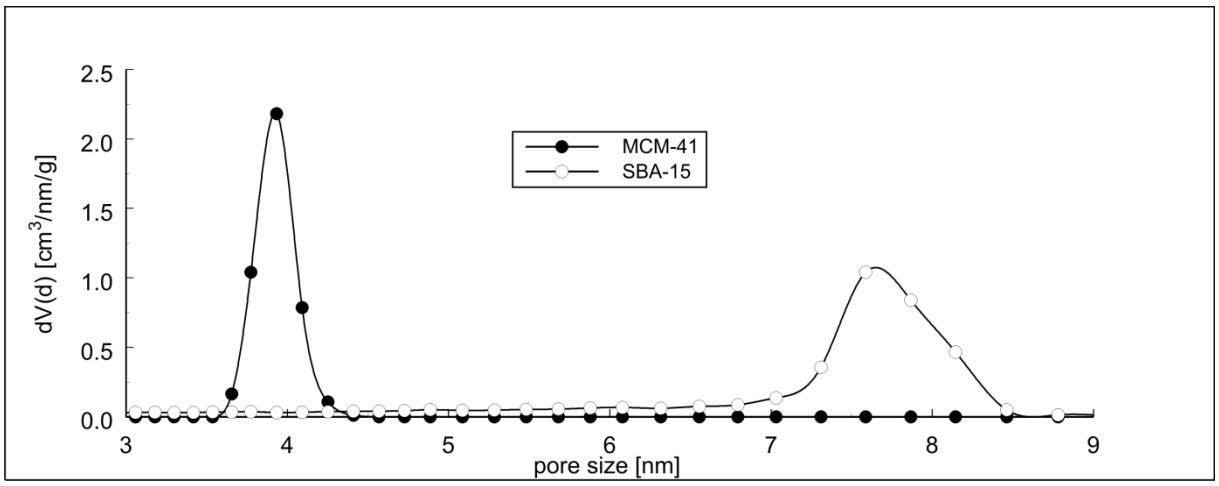

Fig. 5 PSD of MCM-41 and SBA-15, calculated with DFT from the N_2-adsorption isotherm.

Due to the fact that both MCM-41 and SBA-15 do not exhibit regular morphological properties such as size and shape, these materials are not well suited for analysis by optical methods like CLSM. Therefore, other materials have to be investigated. Our materials of choice were on the one hand large spherical particles of the SBA-15 type (SBAs) that were reported by Ma et al.[17] and later in a similar synthesis by Katiyar and Pinto[16, 18] , and on the other hand arrays of silica nanochannels (ASNCs) reported by Kievsky and Sokolov[19] (Fig. 6).

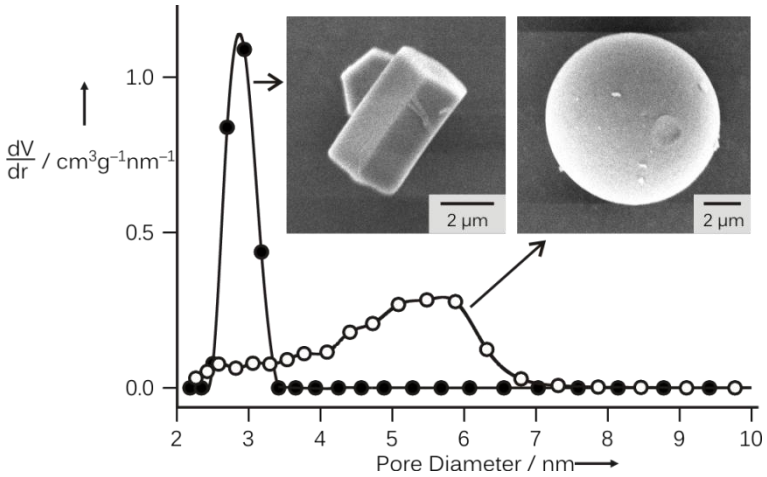

Fig. 6 PSD and SEM images of ASNCs (left, filled circles) and SBAs (right, empty circles).

SBAs has the drawback that the PSD is broad and ranges from 2.5 nm to 7 nm, and the nanochannels are not arranged in a parallel fashion throughout the particle. The ASNCs however feature a narrow PSD around 3 nm and contain unidirectional channels over the whole hexagonally shaped particles.

2.2 Functionalization & Labeling

Functionalization of mesoporous silica with organic moieties can easily be achieved by condensing alkoxysilanes or chlorosilanes with a functional organic residue to the surface hydroxy groups. There are two different pathways for functionalization (Fig. 7), namely postsynthetic functionalization, where the organosilane groups are grafted to the surface of the fully synthesized material and co-condensation, where the organosilane is introduced during the formation of the mesoporous framework.

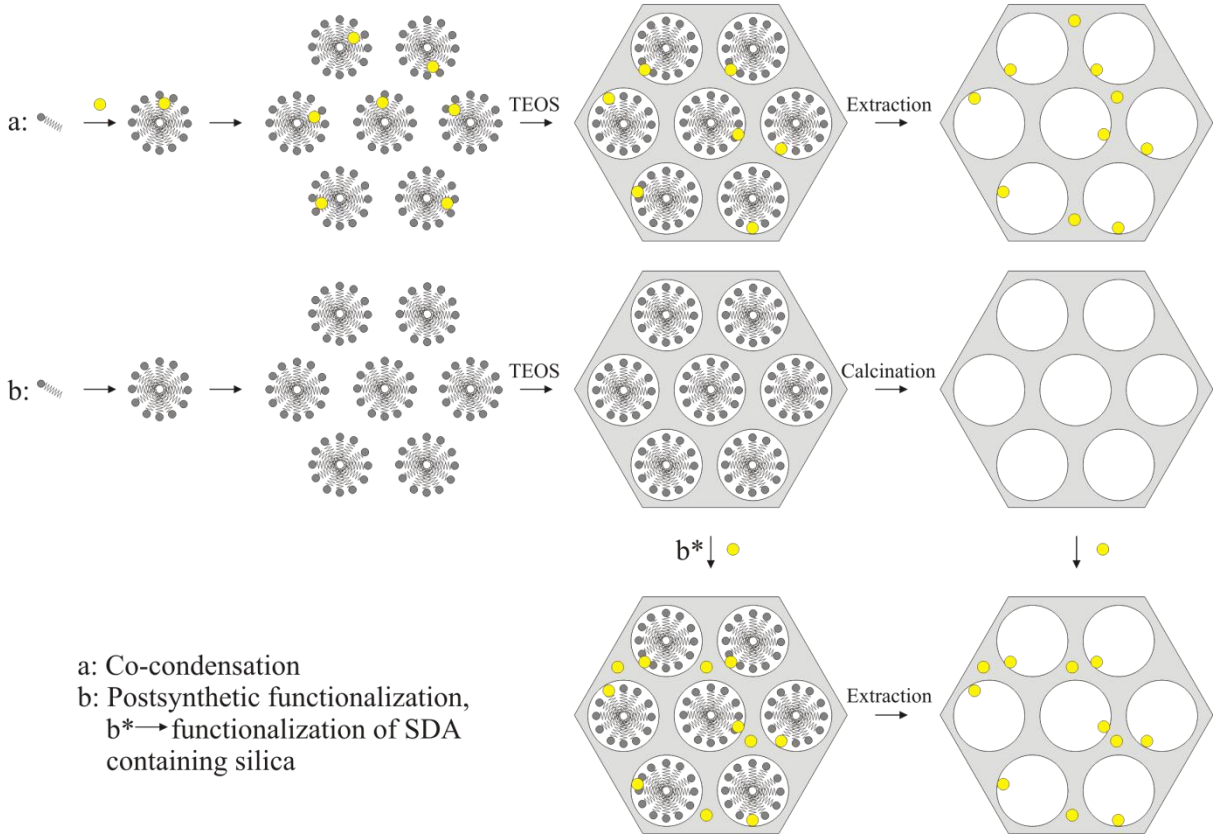

Fig. 7 Implementation of a functional group (yellow) in different reactions.

Although the co-condensation method is a convenient way to achieve a nearly uniform distribution, it is not suited for most applications because it affects pore size and particle morphology and it is almost impossible to control the functional group distribution. In postsynthetic functionalization, however, pore size, pore system geometry, particle size and particle morphology are given by the preformed mesoporous silica material. The distribution of functional groups can be controlled by different means, such as protection followed by selective deprotection of the mesoporous silica surface with fluorenylmethoxycarbonyl-(Fmoc)-modified silanes on certain parts of the surface.[32] The functionalization also depends strongly on the functionalizing agent. Highly reactive chlorosilanes react quickly with the silica surface and have the tendency do bind to the highly accessible silanol groups on the external surface.[33] Another influence on the functionalization occurs through the presence or absence of the SDA inside the pores. The SDA slows the migration of the functionalization agent in the pores and therefore directs the functionalization towards the external

surface.[34, 35] Other prominent influences on the distribution are polarity of the solvent,[36, 37] the functionalization agent,[38] and the trace water content of the functionalization reaction mixture.[39]

For the work in this thesis, mainly trialkoxyaminopropylsilanes were applied, as they are among the most widely used precursors for surface modification of silica. If the distribution of these precursors can be controlled, the distribution of further modifications can be controlled concomitantly.

In the grafting process (Fig. 8), the aminosilane first physisorbs to the silica surface via a hydrogen bond. Subsequently, the silane forms a covalent bond with the surface, liberating an alcohol (in the case of alkoxysilanes). The aminosilane is typically bound to the surface by one or two Si-O-Si bridges.

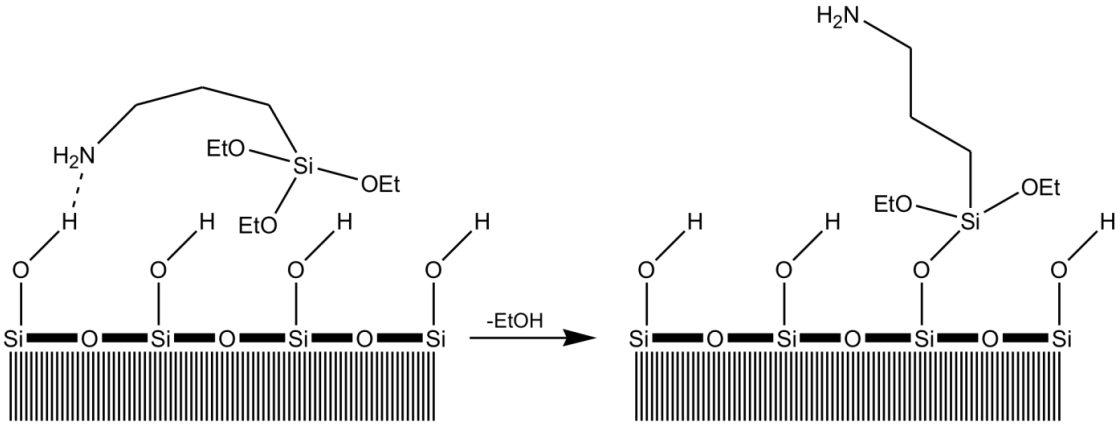

Fig. 8 Grafting of 3-aminopropyltriethoxysilane (APTES) to a silica surface.

To analyze the positioning of the amino groups on the surface, CLSM is applied. Therefore, a fluorescent label needs to be attached to the amino groups.

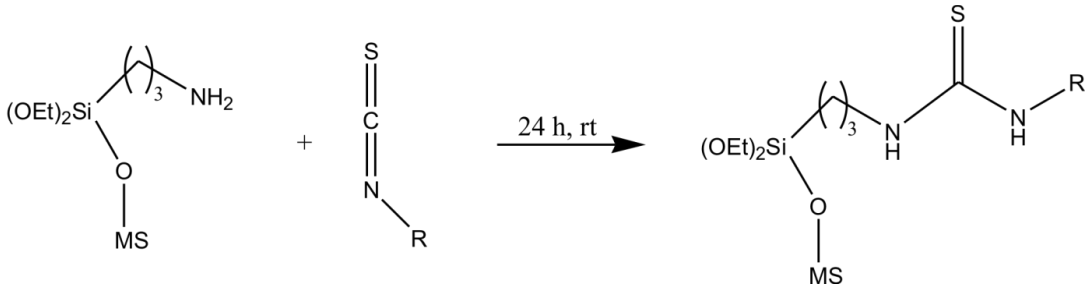

Fig. 9 Formation of a thiourea bond through the coupling of an amine and an isothiocyanate (MS = mesoporous silica).

Isothiocyanates and sulfonyl chlorides allow a fast and stable coupling to amines, forming a thiourea bond or a sulfonamide respectively (Fig. 9). The coupling yield of these reactions varies between 5 and 50 % depending on the pore size and the amount of amino groups on the surface.[40] Most often we introduce fluorescein isothiocyanate (FITC) (Fig. 10) as a label because of its high luminescence quantum yield, commercial availability and its sufficient photostability. For dual labeling, Texas Red (TR) is used as a second label. Due to the missing

spectral overlap between the emission of FITC and the absorption of TR, almost no energy transfer between these two labels occurs, thus minimizing the risk of measuring artifacts in CLSM.

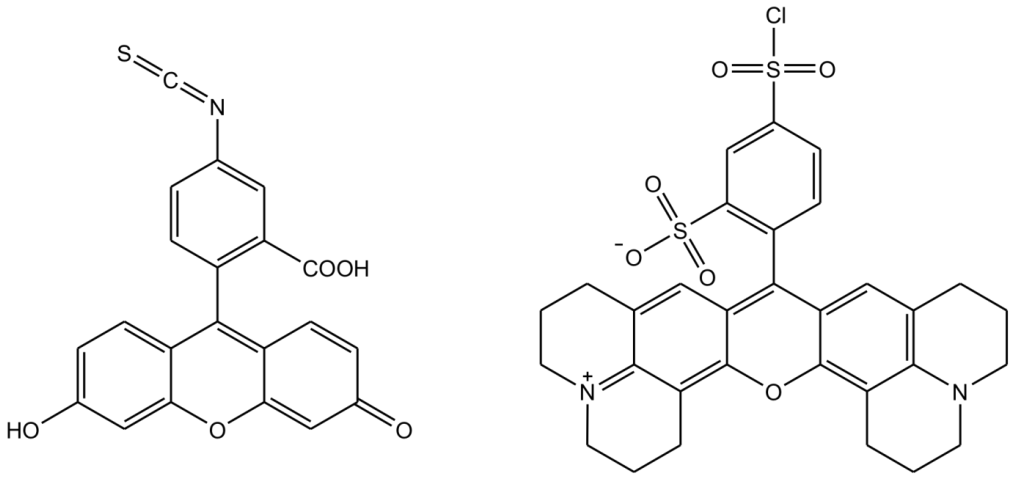

Fig. 10 Chemical structures of FITC (left) and TR (right).

2.3 Analysis

2.3.1 Determination of the amount of grafted aminosilane and coupled fluorescent label

An important analysis for the control of the functional group distribution is the analysis of the amount of functional groups that are covalently bound to the surface. This amount can be determined with sufficient precision by elemental analysis only for high degrees of functionalization.[41] For lower degrees of loading, an indirect method has to be applied, featuring the coupling of fluorescamine (Fig. 11).[42, 43] This method has been successfully applied on amine-functionalized mesoporous silica before.[27, 40] The mesoporous silica is dissolved in an alkaline solution and the amines are coupled to fluorescamine.

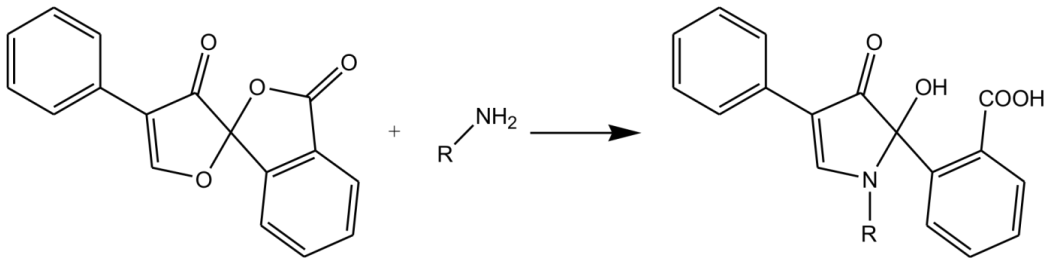

Fig. 11 Coupling of fluorescamine to an amine.

Upon coupling to a primary amine, the fluorescamine becomes luminescent. This luminescence is compared to the luminescence of a series of standard amine solutions treated with fluorescamine. From the obtained amount of amines and the originally employed amount of mesoporous silica for the measurement, the loading and therefore the grafting yield can be calculated. For low loadings up to 200 µmol/g, the grafting yields are typically in the range of 80 - 100 %.

After labeling the amines with a fluorophore such as FITC, the quantity of coupled fluorescein is determined using UV/vis absorption of the degraded sample. From the absorption and the extinction coefficient, which is 75'000 l/mol/cm for FITC in a degraded mesoporous silica solution,[40] the loading and the coupling yield can be calculated. Because of the sterical demand of the fluorophores, typical coupling yields for low loadings on ASNCs are around 30 %. For higher amine loadings this value decreases even more.

2.3.2 Confocal Laser Scanning Microscopy (CLSM)

CLSM is used to visualize the distribution of the labeled functional groups throughout the particle. In contrast to conventional microscopy, a true 3-dimensional resolution is obtained. This resolution is achieved by optical sectioning, the ability to acquire depth selective data from a sample. The depth selectivity is reached by the use of a confocal aperture in front of the detector. The luminescent sample is excited with a laser beam that is focused on the optically conjugated point to the confocal aperture. In this way all light, other than the light emitted from the focal point, is suppressed by the confocal aperture (Fig. 12).

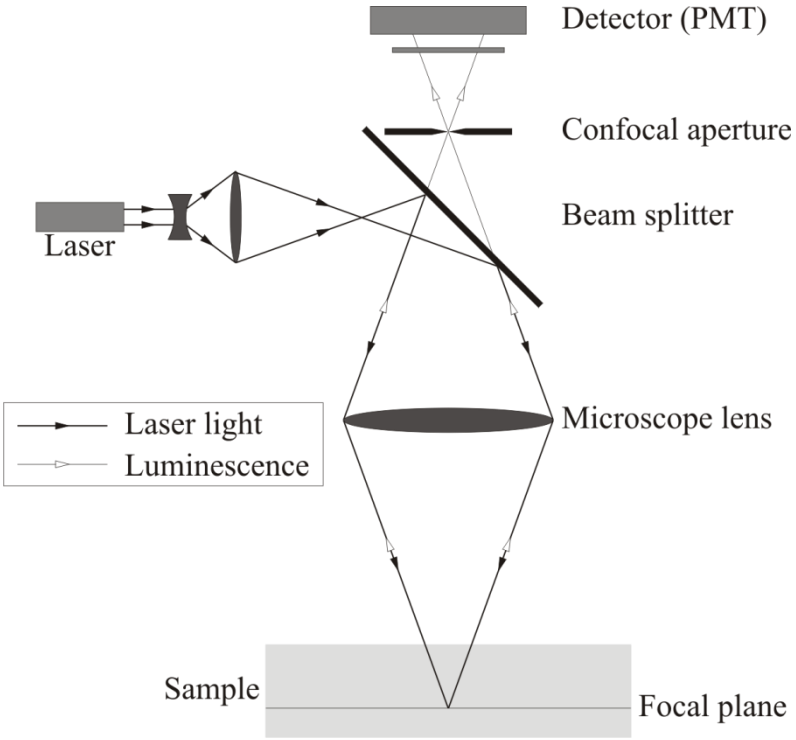

Fig. 12 Optical path in a CLS microscope (PMT = photo multiplier tube).

If the sample is not too opaque, the focal point can not only be chosen on the surface but also in the sample body. With an array of mirrors, the microscope now scans the fluorescence intensity over many points in the focal plane, and produces a 2-dimensional image out of these scans. A 3-dimensional image can be calculated from multiple scanned planes in different depths.

2.3.3 Scanning Electron Microscopy (SEM)

In SEM the specimen is scanned with a focused electron beam with an energy of 0.2 - 40 keV. The electron beam hitting the surface produces different effects such as backscattered electrons, secondary electrons and also X-rays. Most electron microscopes detect secondary electrons (inelastically backscattered electrons). These electrons lead to images with a similar contrast and interpretability as in optical microscopy.

2.3.4 Nitrogen Sorption

In the field of porous materials, gas adsorption, typically conducted with nitrogen, is one of the most important methods of characterization. It yields information about textural properties such as the size and shape and volume of the pores, the pore surface and the total surface. The amount of adsorbed/desorbed nitrogen is measured against the relative pressure at 77 K. This results in an adsorption/desorption isotherm. According to IUPAC there are 6 different types of isotherms (Fig. 13).[44]

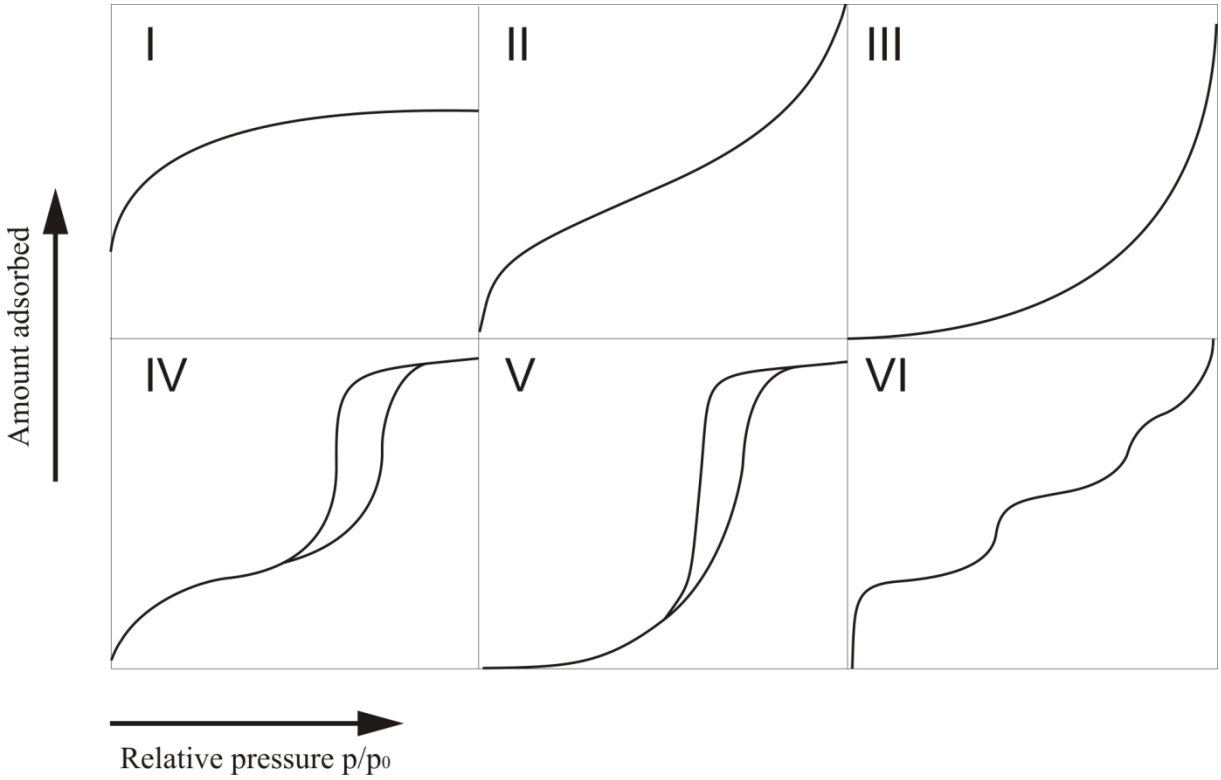

Fig. 13 Types of isotherms.

Type I isotherms are normally found for microporous samples with small external surface areas. Type II isotherms are obtained with macroporous or nonporous materials. A type III isotherm indicates a very weak interaction between adsorbate and adsorbent. Isotherms of type IV and V are typical for mesoporous specimen. Type V is an example of sorption on a mesoporous sample, where the interactions between sample and adsorbate are weak. Type VI isotherms rarely occur and indicate a layer-by-layer deposition.

For N_2-sorption on mesoporous silica, type IV isotherms are found exclusively. Oftentimes isotherms of mesoporous silica show a hysteresis loop between the adsorption branch and the desorption branch of the isotherm. Following the IUPAC recommendations, the hystereses are split into 4 categories (Fig. 14).[44]

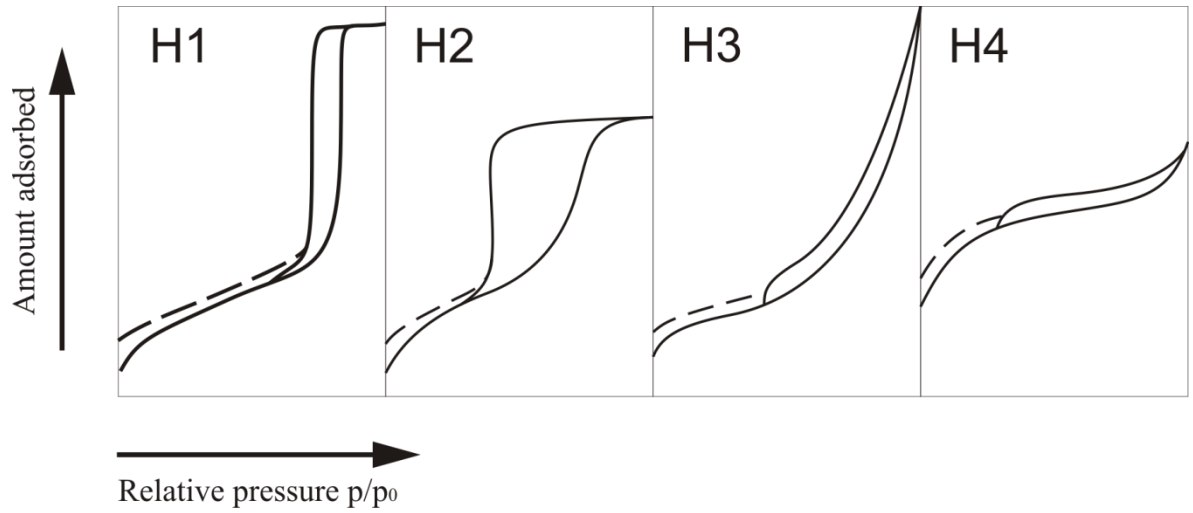

Fig. 14 Types of hysteresis loops.

Hystereses appear due to two main reasons. Firstly due to the formation of a metastable multilayer that leads to a delay in capillary condensation. Secondly due to the entrapment of condensate through network percolation that leads to a delay in the desorption process. The shape of the hysteresis reveals information about the shape of the pores. H1 type hystereses indicate uniform pores in a narrow size distribution as found in SBA-15. H2 hysteresis loops occur in specimen with interconnected pore networks and different pore sizes such as SBAs (Fig. 15). H3 and H4 are found in materials with slit or wedge shaped pores with H4 featuring primarily micropores.

The further analysis of these isotherms applies computational calculation. From the near-linear low pressure part of the isotherm the total surface is calculated by the method of Brunauer, Emmett and Teller.[45] This so-called BET equation relies on the model of monolayer-multilayer adsorption.

$$\frac{p}{n^a\left(p_0 - p\right)} = \frac{1}{n_m^a C} + \frac{\left(C-1\right)p}{n_m^a C p_0}$$

The variable n^a is the amount adsorbed at a certain relative pressure p/p_0, n^a_m is the monolayer capacity and C scales exponentially with the adsorption enthalpy of the first monolayer. For the monolayer calculation the average molecular area occupied by a N_2 molecule of 0.162 nm^2 is applied.

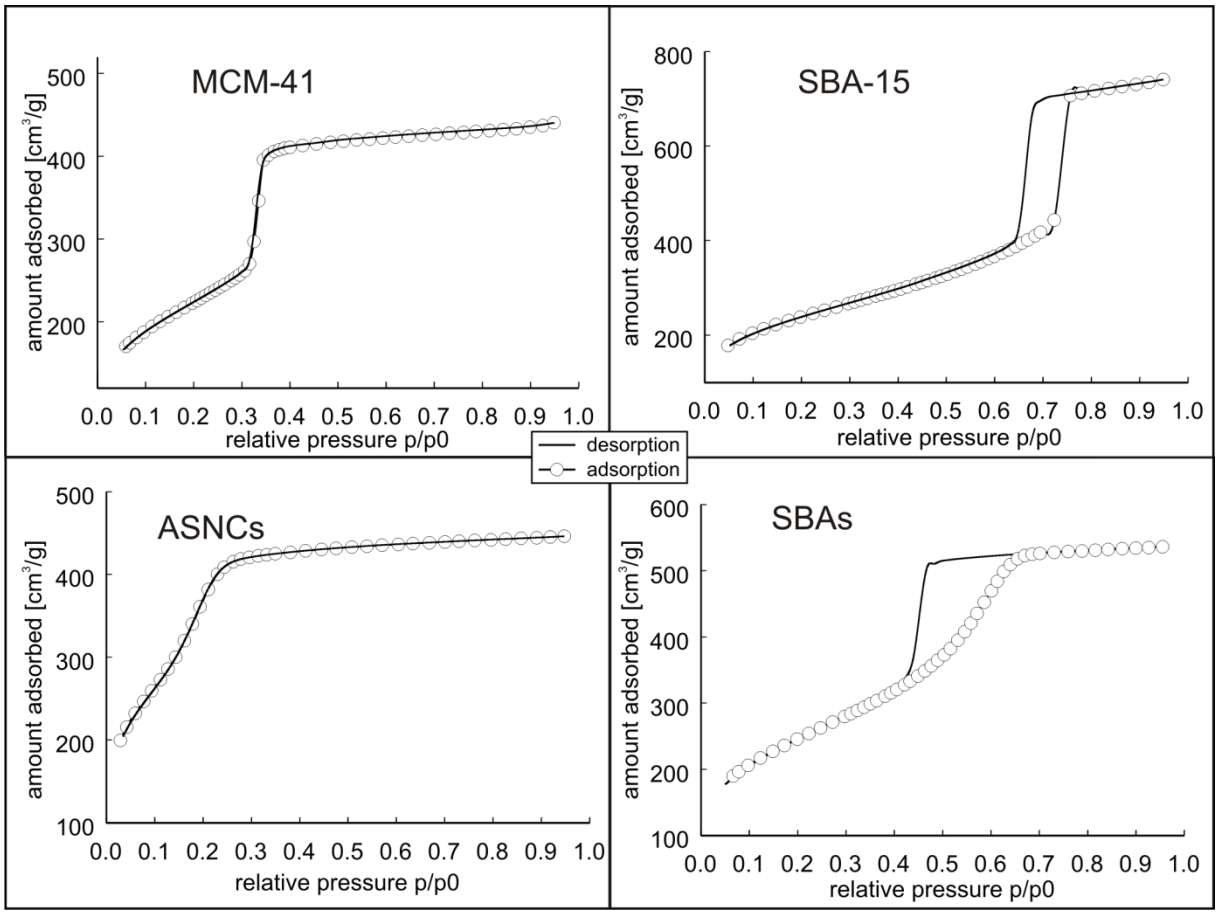

Fig. 15 Isotherms of different mesoporous samples.

Emanating from the relative pressure of pore condensation, the PSD can be calculated either by the Barrett-Joyner-Halenda (BJH) method[46] based on the Kelvin equation, or by density functional theory (DFT) calculation applying a fit to an ideal isotherm.

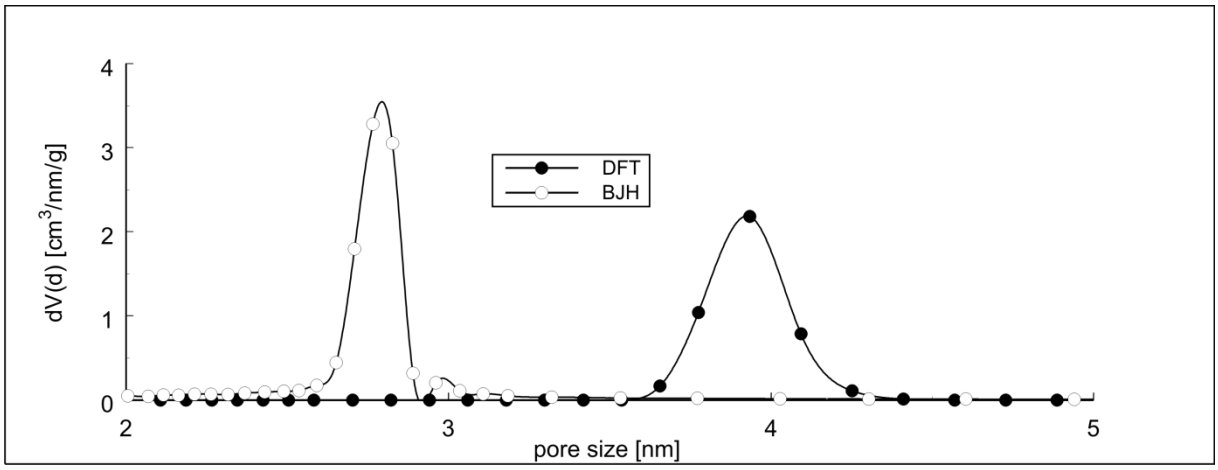

Fig. 16 PSD of MCM-41 calculated with DFT and BJH method from the adsorption branch.

It is known that the BJH method underestimates the pore size,[47, 48] whereas the DFT method might overestimate it slightly (Fig. 16).

From the high pressure linear part of the isotherm, the external surface can be calculated applying the α_s-plot method.[49, 50] In this method, it is assumed that the adsorption in the pores is the same as the adsorption on a nonporous reference material featuring similar surface properties. If this is true, the adsorption on the porous sample is proportional to the adsorption on the reference material.

$$\nu = \nu_p + \eta_2 \alpha_s$$

Where η_2 and ν_p are slope and intercept of the high pressure linear part of the isotherm and α_s is:

$$\alpha_s = \frac{\nu_{ref}(p)}{\nu_{ref,0.4}}$$

For values of $\alpha_s > 1$, the external surface is then calculated as follows:

$$S_{ex} = \frac{\eta_2 S_{BET,ref}}{\nu_{ref,0.4}}$$

$S_{BET,ref}$ is the BET surface of the reference and $\nu_{ref,0.4}$ is the amount adsorbed on the reference material at a relative pressure of 0.4.

The total pore volume is calculated from the amount of nitrogen adsorbed at a relative pressure of 0.95.

3. Results and Discussion

3.1 Mesoporous Materials

The first stage of this work focuses on the search for mesoporous model materials that are suited for analysis by CLSM, because the standard materials such as SBA-15 and MCM-41 do not feature regular morphologies. A material with a narrow pore size distribution and large regular particles would fulfill this condition. There are multiple reports of spherical and hexagonal mesoporous silica particles in the literature.[32, 51, 52] However, our first attempts to produce such spherical materials did only yield irregular or submicrometer sized particles (Fig. 17).

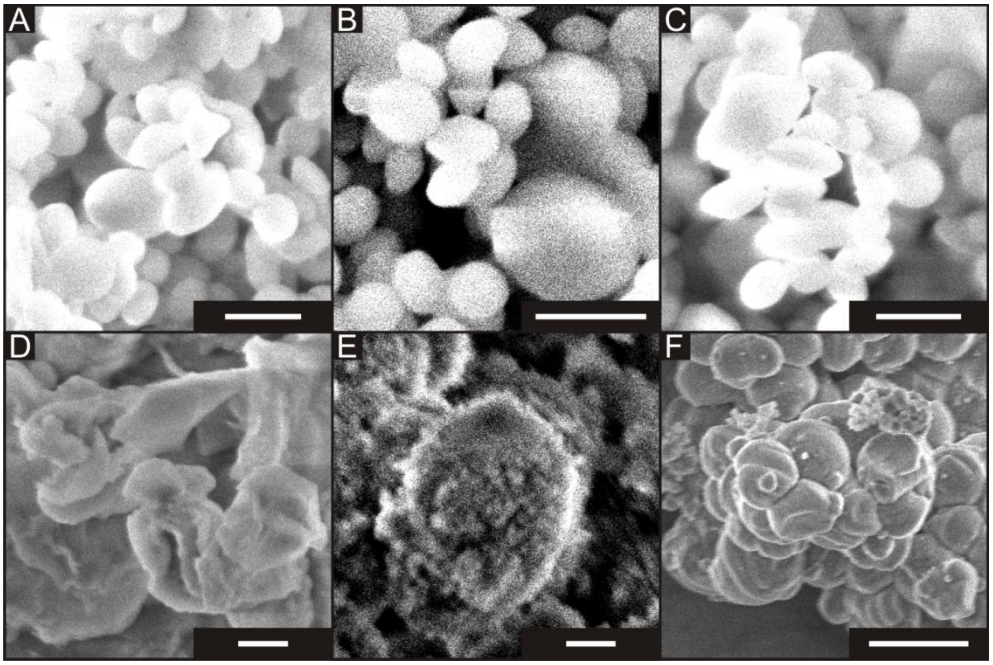

Fig. 17 SEM images of different mesoporous silica particles. Method of Cai et al.[51] (A) and variations with overnight curing (B), with less solvent (C) and applying tetrabutoxysilane (TBOS) (D). Furthermore, acid prepared mesoporous spheres according to Cheng and Landry[32] (E) and BI95 according to Mesa et al.[52] (F). Scale bar is 1 µm for A-E and 10 µm for F.

Finally, following the recipe of Katiyar and Pinto[16], a material was obtained that showed a smooth regular spherical morphology with a diameter of 4-10 µm (Fig. 18). This SBAs material was therefore used in our first experiments. However, SBAs exhibits a very broad PSD with a H2 hysteresis loop in nitrogen sorption, thus indicating an irregular pore network with interconnected pores.

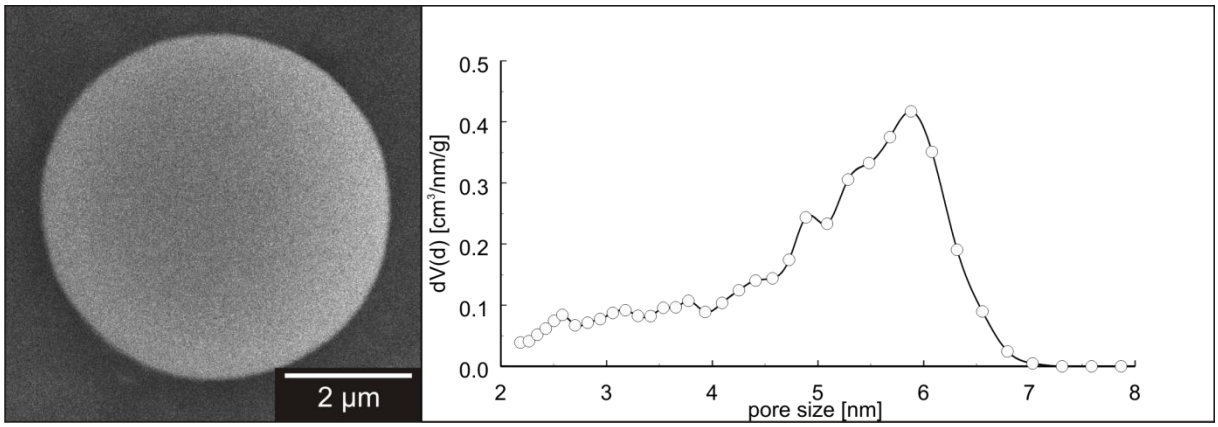

Fig. 18 SEM image (left) and PSD (right) (DFT adsorption branch) of SBAs.

It is known that the conditions that lead to spherical particles, such as high SDA dilution, high temperature and low acidity, enhance defect generation during the particle formation,[53] and therefore amplify disorder in the porous network. Due to this fact we chose not to continue working with SBAs, but instead focused on better ordered particles that were first reported by Kievsky and Sokolov.[19] This so-called ASNCs show a regular hexagonal rod-shaped morphology with a length of approximately 5 µm and width of approximately 2 µm and pore entrances located on top and bottom surface exclusively (Fig. 19). Nitrogen sorption experiments reveal a narrow PSD with an average pore diameter of 2.9 nm, a total BET surface area of 1120 m^2/g, an external surface area of only 37 m^2/g (3.4 % of the total surface area) and a total pore volume of 0.62 cm^3/g. These properties make ASNCs an ideal model system to visualize functional group distributions. Since the synthesis is not hydrothermal, one has to be careful if working with as-synthesized material, as the structure lacks stability. This fact can be avoided if the as-synthesized ASNCs are cured at 80 °C for 72 h before further use.

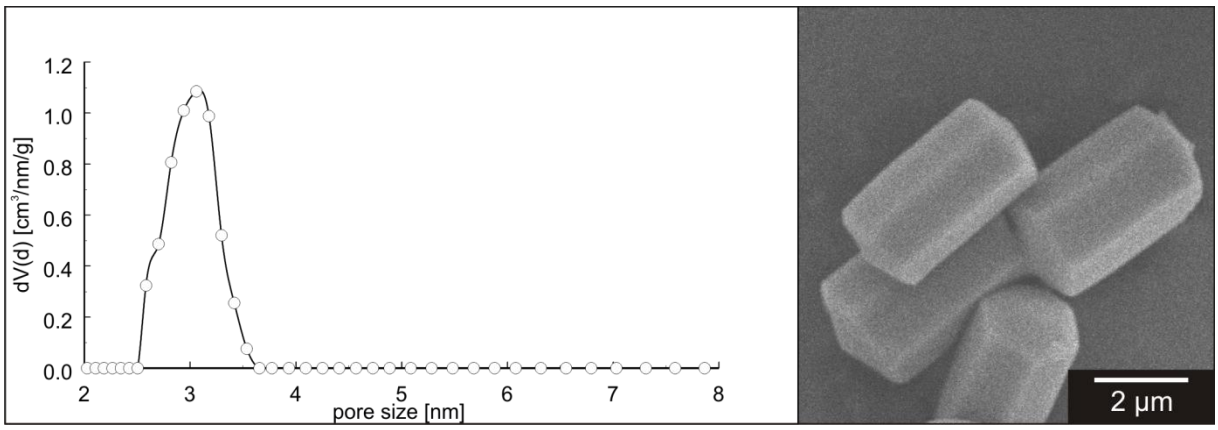

Fig. 19 SEM image (right) and PSD (left) (DFT adsorption branch) of ASNCs.

3.1.1 Experimental

Mesoporous micrometer sized spheres containing hexagonal oblates following the method of Cai et al.[51] (Fig. 17 A)

CTAB (1 g, 2.7 mmol, Fluka, ≥ 96 %) is dissolved in 25 % aqueous NH_3-solution (120 ml, Merck, p.a.) and deionized water (x = 160 ml) under slight heating. TEOS (5 ml, 22.4 mmol, Fluka, ≥ 99 %) is added dropwise under strong stirring. After 2 h of stirring, the product is collected by filtration, and dried overnight at room temperature. Calcination is performed by heating to 300 °C for 2 h and subsequent heating to 550 °C for 12 h at a heating rate of 2 °C/min.

Variations

- x = 210 ml ⟶ particles are not spherical anymore
- x = 110 ml ⟶ minor particle size decrease (Fig. 17 C)
- After 2 h of stirring, the reaction solution is left under quiescent conditions overnight ⟶ particles are not spherical anymore (Fig. 17 B)
- Reaction is performed at 0 °C ⟶ no reaction
- Reaction is done using TBOS (22.4 mmol, Fluka, ≥ 97 %) instead of TEOS ⟶ particles are not spherical anymore (Fig. 17 D)

Synthesis of acid-prepared mesoporous spheres following the procedure of Cheng and Landry.[32] (Fig. 17 E)

CTAB (1.2 g, 3.2 mmol, Fluka, ≥ 96 %) is dissolved in a mixture of deionized water (55.5 ml) and 32 % aqueous HCl (4.5 ml, Merck, p.a.). TEOS (6 ml, 26.9 mmol, Fluka, ≥ 99 %) is added slowly and the mixture is stirred for 1 h and then transferred to a Teflon-lined autoclave, followed by 40 min of heating at 150 °C. After cooling to room temperature, the precipitate is collected by filtration, washed and air dried.

Synthesis of BI95 spheres following the procedure of Mesa et al.[52] (Fig. 17 F)

CTAB (0.065 g, 175.5 µmol, Fluka, ≥ 96 %) and Pluronic P123 (triblock copolymer $EO_{20}PO_{70}EO_{20}$ / $HO(CH_2CH_2O)_{20}(CH_2CH(CH_3)O)_{70}(CH_2CH_2O)_{20}H$) (0.642 g, 110 µmol, Sigma-Aldrich) are dissolved in a mixture of deionized water (78 ml) and 32 % aqueous HCl (3 ml, Merck, p.a.). TEOS (2 ml, 9.0 mmol, Fluka, ≥ 99 %) is added slowly under strong stirring. The resulting solution is transferred into a Teflon-lined autoclave and heated to 95 °C for 120 h. After filtration the product is thoroughly washed with deionized water and dried in air at 80 °C.

Synthesis of SBAs following the procedure of Katiyar and Pinto.[16]

A solution of CTAB (0.465 g, 1.3 mmol, Fluka, ≥ 96 %) in ethanol (7.8 ml) and deionized water (20 ml) is added to a solution of Pluronic P123 (3.1 g, 0.5 mmol, Sigma-Aldrich) in 1.5 M aqueous HCl (46 ml, Merck, p.a.). TEOS (10 ml, 44.8 mmol, Fluka, ≥ 99 %) is added dropwise to this mixture. After 2 h of stirring the solution is transferred to a Teflon-lined

autoclave and heated to 78 °C for 72 h. After cooling to room temperature the product is obtained by filtration and washing. Calcination is performed at 500 °C for 16 h applying a heating rate of 1.2 °C/min.

Synthesis of ASNCs following the procedure of Kievsky and Sokolov.[19]

CTAC (4.85 g, 15.2 mmol, Acros, 99 %) is dissolved in doubly distilled water (76 ml) and 32 % aqueous HCl (60 ml, Merck, p.a.) under vigorous stirring. The solution is cooled to 0 °C in an ice bath for 15 min under quiescent conditions, followed by the dropwise addition of cooled TEOS (2 ml, 13.4 mmol, Aldrich, 99.999 %) under stirring. The reaction mixture is kept at 0 °C under quiescent conditions for 3 h. The product is filtered off and dried at room temperature. Calcination is performed by heating to 300 °C for 2 h and subsequent heating to 550 °C for 12 h at a heating rate of 2 °C/min.

3.2 Functional Group Distribution on Mesoporous Silica

Most applications of mesoporous silica require a postsynthetic functionalization with organic moieties, therefore the control and analysis of functional group distributions is very important. In our first experiments, we created multiple new methods to obtain a variety of different functional group distributions and also analyzed many procedures known from literature by applying CLSM. There are many synthetic pathways that assume e.g. homogeneous distribution or external surface functionalization, without providing solid analytic evidence. In our experiments an amine loading of 200 μmol/g is typically applied.

We first tried to achieve selective functionalization of the pore surface. This can be done only by passivation of the external surface. The highly reactive diphenyldichlorosilane is assumed to preferably react with accessible external surface sites and has therefore been used as a passivation agent.[33] The subsequently grafted APTES can now presumably only attach to the pore surface. The problem with selective pore surface modification arises upon analysis. Since only the functionalized part can be visualized by CLSM, the specimen appears the same as a slightly smaller particle with a total surface functionalization. We decreased our efforts in this field, because, unless mesoporous nanoparticles are considered, the external surface accounts for only 1 - 10 % of the total surface, and therefore the external surface modification can be neglected for uniformly functionalized samples with a low degree of functionalization.

To achieve a truly homogeneous distribution, co-condensation is the method of choice, but it is not readily applicable if mesoporous particles of certain sizes, morphologies or with a narrow PSD are required, since the co-condensed aminosilane influences the particle formation. It has for example so far not been possible to synthesize ASNCs by co-condensation with aminosilanes. Also, it cannot be excluded that the functional groups are partially included into the pore walls and are therefore unavailable for further modification. However, for many applications, a nearly homogeneous distribution is sufficient and such a modification can be achieved with postsynthetic grafting under the appropriate conditions. Our results show that the mobility of aminosilanes on silica surfaces strongly depends on the

aminosilane itself on the one hand, and on the solvent polarity on the other hand. Uniform distributions are achieved with polar solvents and APTES (Fig. 20).

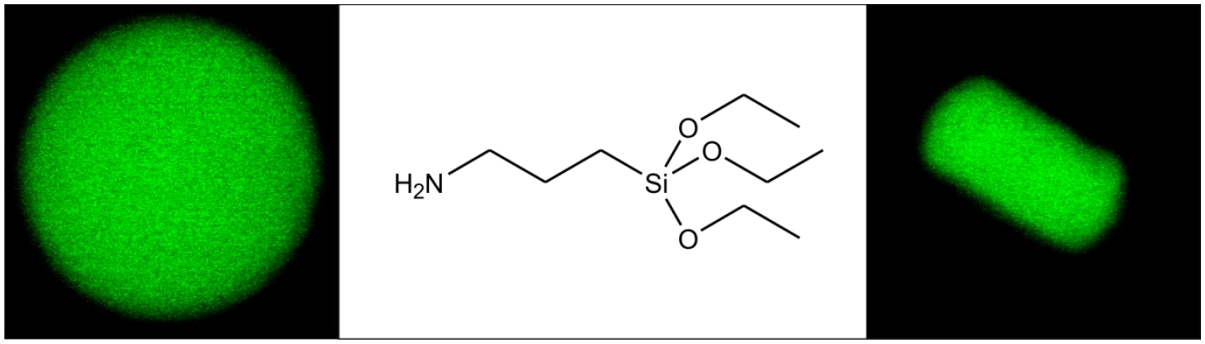

Fig. 20 Example of functional group distributions on SBAs (left) and ASNCs (right) after applying APTES in a polar solvent and subsequent labeling with FITC. The SBAs particle shown has a diameter of approximately 8 µm and the ASNCs particle has a length of approximately 5 µm.

The applied reaction conditions vary considerably in temperature and reaction time, but similar results were found. Temperatures from 20 °C up to 120 °C and reaction times from 10 min to 3 h were tested.

Our first approach to achieve the selective functionalization of the external surface was to imitate the external surface passivation method[33] using bromopropyltrichlorosilane instead of diphenyldichlorosilane. Analysis of the bromopropyl coupled fluoresceinamine with CLSM however did not show any selectivity towards the external surface. Another quite obvious approach for external surface selectivity is the use of as-synthesized mesoporous silica, still containing the SDA within the pores. APTES was grafted to the as-synthesized materials and the fluorescent label was attached. The SDA was removed afterwards by extraction. But even with the SDA inside the pores, the APTES was found to penetrate the pores to a considerable extent. Furthermore, we conducted the reaction with SDA containing materials in a non-polar solvent with a short reaction time following a procedure by Mal et al.[34, 35] Applying a non-polar solvent reduces the mobility of the aminosilanes on the silica surface and therefore should direct the functionalization towards the external surface. However, analysis by CLSM did not show any selectivity for the external surface (Fig. 21).

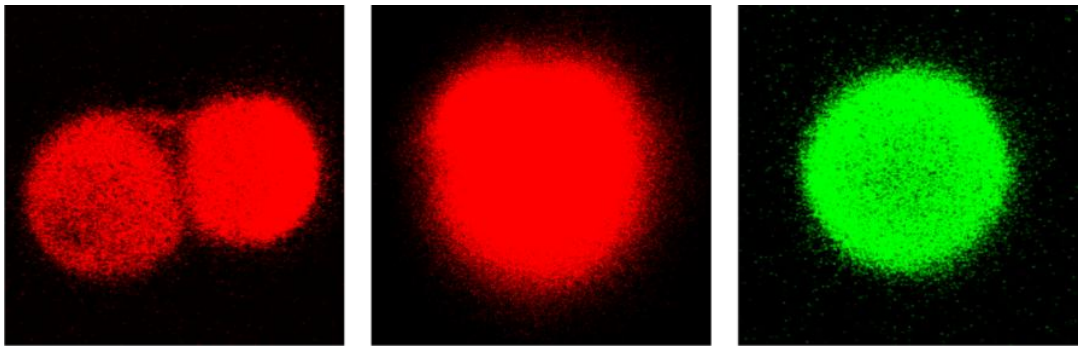

Fig. 21 CLSM images of SBAs functionalized with $Cl_3Si(CH_2)_3Br$ (left), with APTES on as-synthesized SBAs in a polar (middle) or non-polar (right) solvent. The diameter of the SBAs particles is 5 - 7 µm, the red samples are labeled with Rhodamin B isothiocyanate, the green sample is labeled with FITC.

The breakthrough in the selectivity for the external surface was the application of aminosilanes with reduced mobility on the mesoporous silica surface. Thin layer chromatography experiments showed that bis(triethoxysilyl)propylamine (BTESPA) and mainly 3-aminopropyltrimethoxyethoxyethoxysilane (APTMEES) are prominent candidates for external surface modification. Experiments in different solvents applying these two amines on either calcined or as-synthesized mesoporous materials proved that APTMEES in non-polar solvents provides an excellent selectivity for the external surface (Fig. 22).[38, 54] Experiments with Texas Red as a second label showed that no pore blocking occurs and that the pores are still accessible after APTMEES functionalization.

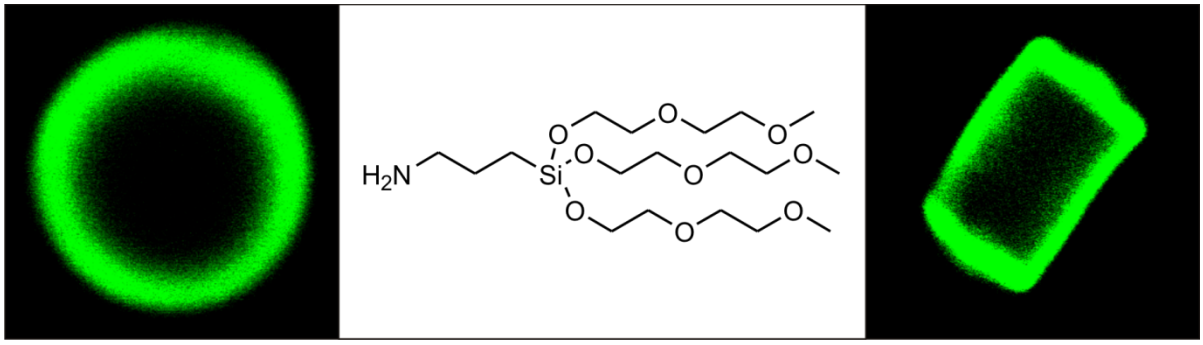

Fig. 22 Example of functional group distributions on SBAs (left) and ASNCs (right) after applying APTMEES in a non-polar solvent and subsequent labeling with FITC. The SBAs particle has a diameter of approximately 6 µm, the ASNCs particle a length of approximately 5 µm.

Results of this solvent and amine screening experiments revealed that APTES is suited best for achieving a homogeneous distribution, while APTMEES exhibits a high tendency to graft to the external surface. The use of BTESPA leads to inhomogeneous distributions but not selectively to an external surface functionalization (Fig. 23).

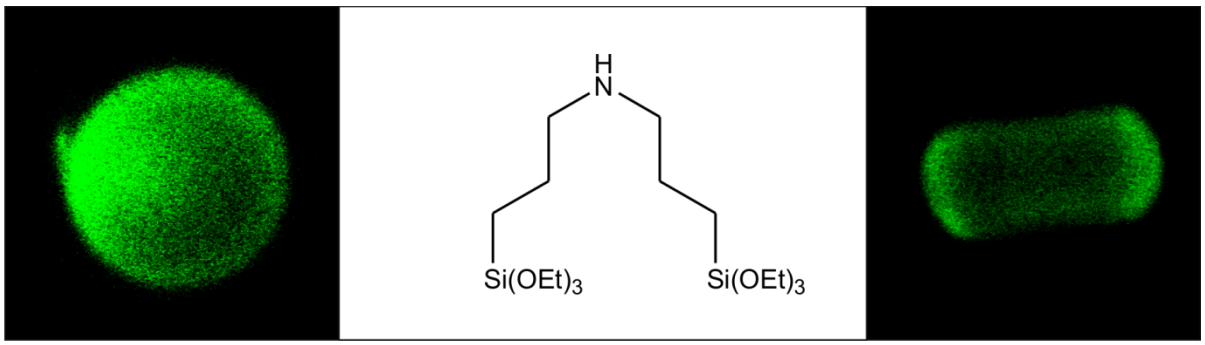

Fig. 23 Example of functional group distributions on SBAs (left) and ASNCs (right) after applying BTESPA in a non-polar solvent and subsequent labeling with FITC. The SBAs particle has a diameter of approximately 5 µm, the ASNCs particle a length of approximately 5 µm.

For an in-depth analysis of the spatial distributions of the luminescence, intensity profiles were calculated based on the CLSM images (Fig. 24).

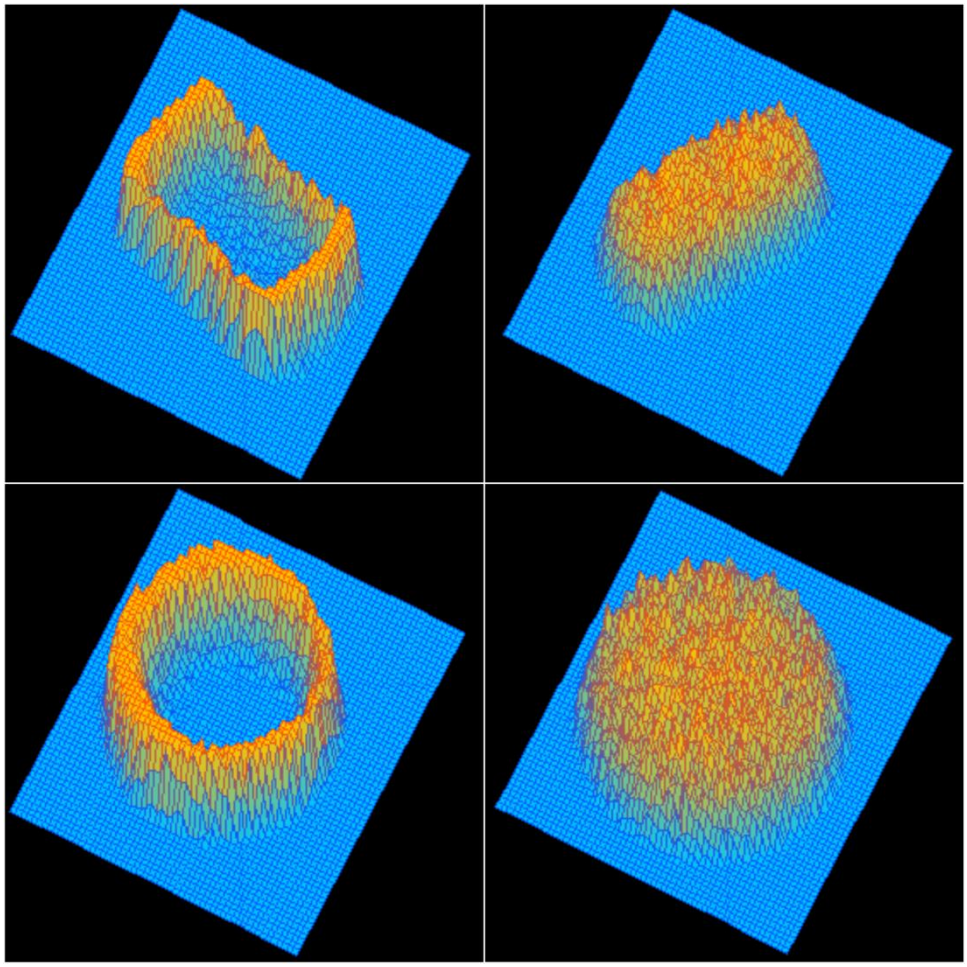

Fig. 24 Luminescence intensity profile of mesoporous samples, blue is low intensity, orange is high intensity. Top row: ASNCs, bottom row: SBAs, left column: functionalization with APTMEES, right column: functionalization with APTES. The ASNCs particles have a length of 5 µm, the SBAs a diameter of 6 - 8 µm.

In the solvent screening experiments, ethanol, acetone, THF, acetonitrile and toluene were investigated in addition to hexane. Results show that an increasing solvent polarity leads to increasingly uniform distributions.

The aminosilane/solvent combinations affect the FITC coupling yield. While the aminosilane grafting yield was always in the range of 80 - 100 %, independent of the solvent, the accessibility of the grafted amino groups was found to be affected. For small pores as in ASNCs (Tab. 1), a higher selectivity for the external surface also caused higher FITC coupling yields.

	as-synthesized	calcined
APTES	44	9
APTMEES	50	17
BTESPA	28	16

Tab. 1 FITC loadings on ASNCs after grafting with 100 µmol/g of the respective aminosilane in hexane. Values are given in µmol/g.

As-synthesized mesoporous silica features a higher surface silanol density than calcined mesoporous silica because of the condensation of silanol groups upon calcination.[21] Combined with the excellent accessibility of the amino groups on the external surface and at the pore entrances, this leads to the observed higher FITC coupling yields for as-synthesized samples.

Extraction of the as-synthesized materials was generally performed after FITC labeling. Extraction between grafting and FITC labeling did not alter the resulting FITC distribution.

For large pore materials such as SBAs (Tab. 2), the accessibility of the pore surface is generally better,[40] therefore the FITC coupling yields are larger for samples with homogeneously distributed amino groups. This is confirmed by our results for the calcined materials. For the as-synthesized materials, however the interactions between the SDA and the FITC play a major role, therefore these coupling yields are not representative for the aminosilane distribution

	as-synthesized	calcined
APTES	18	20
APTMEES	10	38
BTESPA	2	42

Tab. 2 FITC loadings on SBAs after grafting with 100 µmol/g of the respective aminosilane in hexane. Values are given in µmol/g.

Variation of the solvent used for grafting the aminosilane was performed on calcined ASNCs and shows trends in FITC loading (Tab. 3) similar to those found in the amine screening. Polar solvents lead to a more homogeneous amine distribution and therefore to a lower FITC coupling yield, whereas non-polar solvents lead to a higher degree of external surface functionalization and therefore to a higher FITC coupling yield.

solvent	acetone	ethanol	acetonitrile	THF	toluene
FITC	3	9	5	3	20

Tab. 3 FITC loadings on calcined ASNCs after grafting with 100 µmol/g of APTMEES in the respective solvent. Values are given in µmol/g.

Further results of aminosilane and solvent screening can be found in Chapter 5.1 and 5.2.

3.2.1 Experimental

Passivation of mesoporous silica surface with diphenyldichlorosilane[33] and further functionalization

MCM-41 (500 mg) is dried at 80 °C for 16 h and then dispersed in dry THF. Diphenyl-dichlorosilane (10 µl, 50 µmol, Fluka, ≥ 98.5 %) is added to the suspension. After stirring for 1 h, the mixture is cooled to -80 °C and a solution of APTES (9.3 µl, 40 µmol, Acros, 99 %) and FITC (30 mg, 77 µmol, Fluka, ≥ 97.5 %) in THF (5 ml) is added. The resulting mixture is stirred at -80 °C for 3 h and subsequently heated to 50 °C for 20 h. After cooling to room temperature the product is collected by filtration.

General method of postsynthetic FITC labeling

Amine-functionalized mesoporous silica is suspended in a solution of FITC (Fluka, ≥ 97.5 %) (1.5 - 2 eq with respect to the amine) in ethanol. After 24 h of stirring at room temperature, the labeled product is collected by filtration and washed thoroughly with ethanol and deionized water.

Co-condensation of APTES with SBAs

FITC (15.2 mg, 39 µmol) and APTES (9.6 µl, 41 µmol, Acros, 99 %) are dissolved in ethanol (7.8 ml) and stirred for 5 h. This solution is then added in the first step of the SBAs synthesis (see Chapter 3.1.1). The addition of FITC can also be omitted. If this is the case, FITC labeling is done postsynthetically.

Postsynthetically applied homogeneous distribution of amino groups

Mesoporous silica (ASNCs or SBAs) (100 mg) is dried at 80 °C for 1 h and subsequently dispersed in ethanol (20 ml). APTES (2.3 µl, 10 µmol, Acros, 99 %) is added to the solution and the mixture is subsequently heated to reflux for 3 h. After cooling to room temperature, the functionalized silica is collected by filtration and washed with ethanol.

Functionalization of SBAs with $Cl_3Si(CH_2)_3Br$ and coupling of fluoresceinamine

Calcined SBAs (150 mg) is dispersed in THF (15 ml) and $Cl_3Si(CH_2)_3Br$ (2.5 µl. 16 µmol) is added under strong magnetic stirring. The suspension is stirred for 15 min at room temperature. The product is thoroughly washed with THF (approx. 50 ml) and ethanol (approx. 50 ml). After drying at 80 °C, the white powder is dispersed in ethanol and fluoresceinamine (9.4 mg, 27 µmol, Aldrich) and triethylamine (3.8 µl, 279.5 mmol, Fluka, ≥ 99.5 %) are added. The mixture is stirred for 24 h followed by filtration and ethanol washing.

Functionalization according to the procedure of Mal et al.[34, 35]

As-synthesized mesoporous silica (ASNCs or SBAs) (100 mg) is dispersed in hexane (10 ml). APTES (2.3 µl, 10 µmol, Acros, 99 %) is added and the suspension is stirred for 15 min. After filtration the product is washed with a small amount of ethanol and deionized water and dried at 80 °C for 16 h prior to labeling with FITC and extraction (in case of as-synthesized material).

Solvent and amine screening experiments

Calcined or as-synthesized mesoporous silica (ASNCs or SBAs) (200 mg) is dispersed in the solvent (toluene, THF, acetone, acetonitrile or ethanol) (20 ml). Aminosilane (APTES (Acros, 99 %), BTESPA (ABCR, 95 %) or APTMEES (ABCR, 95 %)) (20 µmol) is added, and the suspension is stirred for 10 min. The product is collected by filtration, washed with a small amount of ethanol and deionized water and dried at 80 °C for 16 h followed by FITC labeling and extraction (in case of as-synthesized material).

SDA extraction of functionalized as-synthesized materials

The non-ionic SDA of SBAs is extracted by Soxhlet for 24 h with ethanol.[55] The ionic SDA of ASNCs is removed by ion exchange with NH_4NO_3 in ethanol.[56] Typically, ASNCs (200 mg) are dispersed in a solution of NH_4NO_3 (60 mg, 750 mmol, Merck, p.a.) in ethanol (30 ml). The suspension is heated to 60 °C under stirring for 15 min. The mesoporous material is recovered by filtration and washed with cold ethanol. The whole procedure is repeated twice.

3.3 Effect of Trace Water on the Distribution of Aminosilanes on Mesoporous Silica

The presence of trace water in grafting reactions largely influences the outcome. It is therefore important that grafting is performed under conditions with controlled water content. It has been shown that the presence of water leads to the polymerization of trialkoxysilanes on silica surfaces.[57, 58] The aminosilane clusters which form upon polymerization can cause pore blocking. Blocked pores are not accessible for functionalization, which can be observed by CLSM (Fig. 25). Materials with blocked pores also feature a non-functionalized pore body and therefore exhibit a larger pore size than homogeneously functionalized pores.

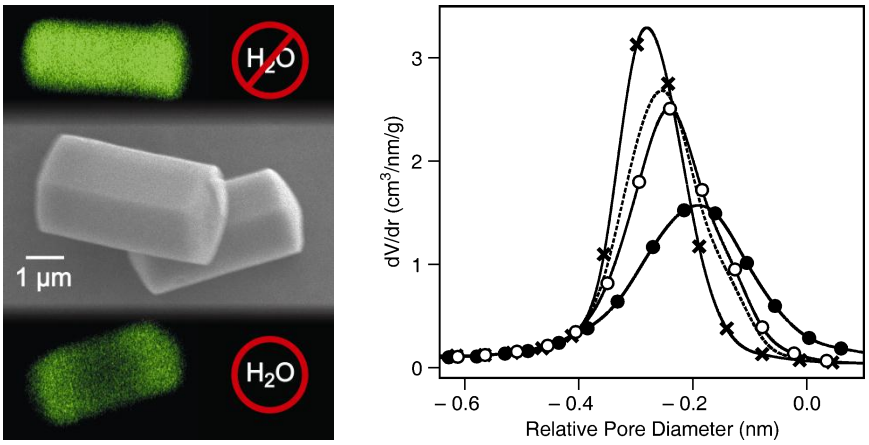

Fig. 25 SEM image of ASNCs with CLSM pictures of FITC labeled ASNCs grafted with APTES in water free and water containing solvent (left). PSDs of MCM-41 grafted with APTES without (crosses), with 0.5 monolayer (dashed line), 1 monolayer (empty circles), and 2 monolayers (full circles) of water relative to the silica surface. The pore diameter is given relative to the maximum of the pore size distribution of the unmodified material (right).

We investigated the changes in pore size and distribution that arise upon variation of the water content in the reaction, using CLSM and nitrogen sorption. The measurements were done with APTES grafted on mesoporous silica in solvents containing: no water, 0.5 monolayer of water, 1 monolayer of water or 2 monolayers of water. A monolayer refers to the amount of water needed to cover the total surface area of the mesoporous silica used in the reaction, based on the fact that 1 water molecule occupies 0.106 nm^2 in an adsorbed monolayer.[59] Nitrogen sorption allows tracking of the subtle differences that occur already upon the

addition of 0.5 monolayer of water (Fig. 25) if a material with a narrow PSD is used. Therefore the nitrogen sorption measurements were conducted with hydrothermally synthesized MCM-41 prepared according to the method of Brühwiler and Frei[60]. With CLSM however, only the more pronounced effects arising upon addition of at least 1 monolayer can be visualized. The results of the effect of water on the grafting of APTES on ASNCs in toluene can be found in the publication in Chapter 5.3

In addition to the investigation of the effect of water, we also analyzed the influence of different reaction parameters on this effect. The investigated parameters were: pore size, solvent, amount of aminosilane, and use of a non-polymerizing aminosilane.

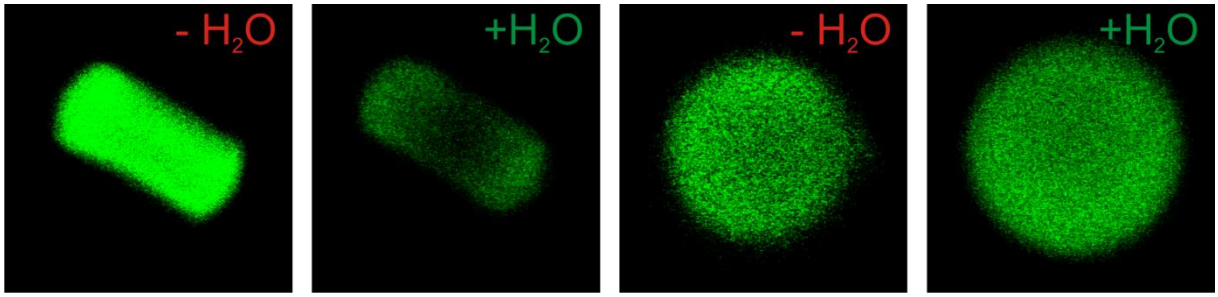

Fig. 26 CLSM images of ASNCs and SBAs grafted in toluene containing 0 or 2 monolayer(s) of water. ASNCs particles feature a length of approximately 5 µm, SBAs particles have a diameter of 5 - 7 µm.

CLSM analysis (Fig. 26) shows that the effect of water on the distribution of fluorescent labels is clearly visible for small pore diameters as in ASNCs. For large pore sizes as in SBAs, the effect disappears almost completely. This is most likely due to the APTES cluster formation and the resulting pore blocking, which is much more critical for mesoporous materials featuring small pores.

Different solvents were used to reveal potential solvent effects. Because of the boiling point of the different solvents, the reactions were conducted at lower temperature than the reactions in the other experiments (50 °C instead of 80 °C). The reference sample (toluene) showed no temperature depending effects.

The results (Fig. 27) illustrate that the effect of trace water on the aminosilane distribution is solvent independent for the investigated solvents. Trace water effects are therefore of potential relevance for grafting reactions in apolar, polar aprotic and polar protic solvents.

Experiments with different amounts of APTES were done to study the concentration-dependent effects on the cluster formation and subsequent pore blocking. Increasing pore blocking is expected to occur with increasing concentrations.

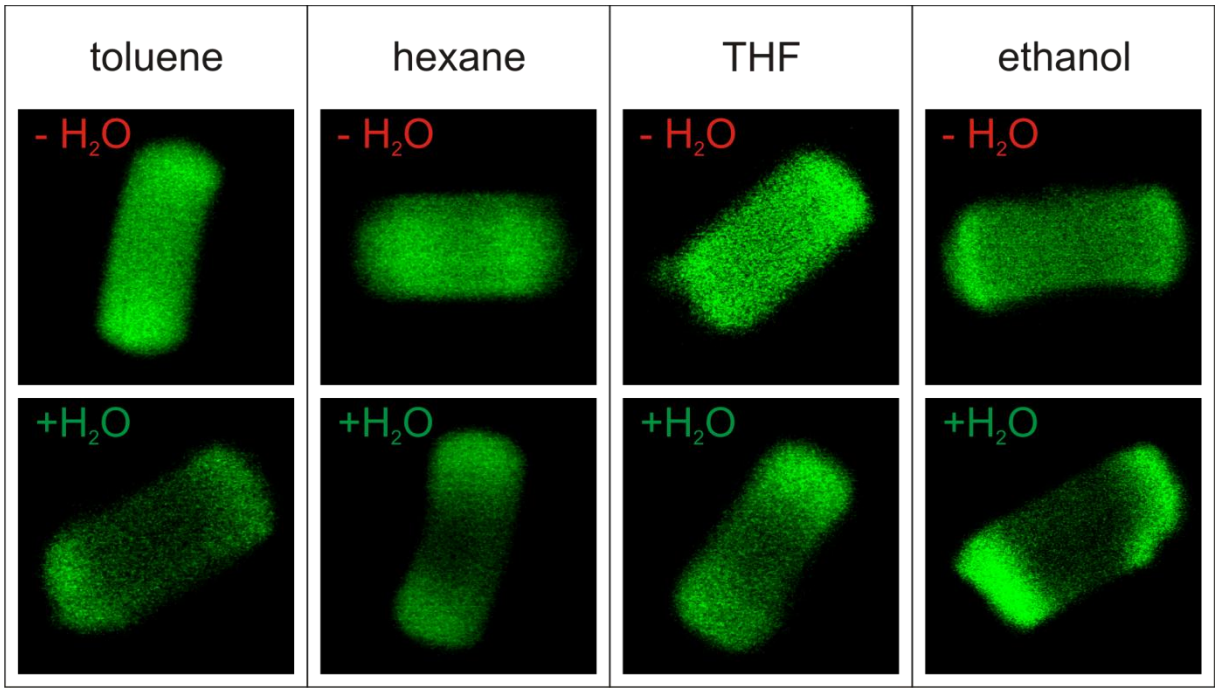

Fig. 27 CLSM images of ASNCs grafted with APTES in different solvents containing 0 or 2 monolayer(s) of water. The ASNCs particles feature a length of approximately 5 µm.

Indeed, for low APTES loading (100 µmol/g), no pore blocking occurs, indicating the formation of less or smaller clusters. For high loadings (800 µmol/g) pore blocking occurs even without any water present (Fig. 28). As a consequence of the high density of amines at the pore entrances, the fluorescent label (FITC) cannot easily penetrate the pores even in the absence of cluster formation.

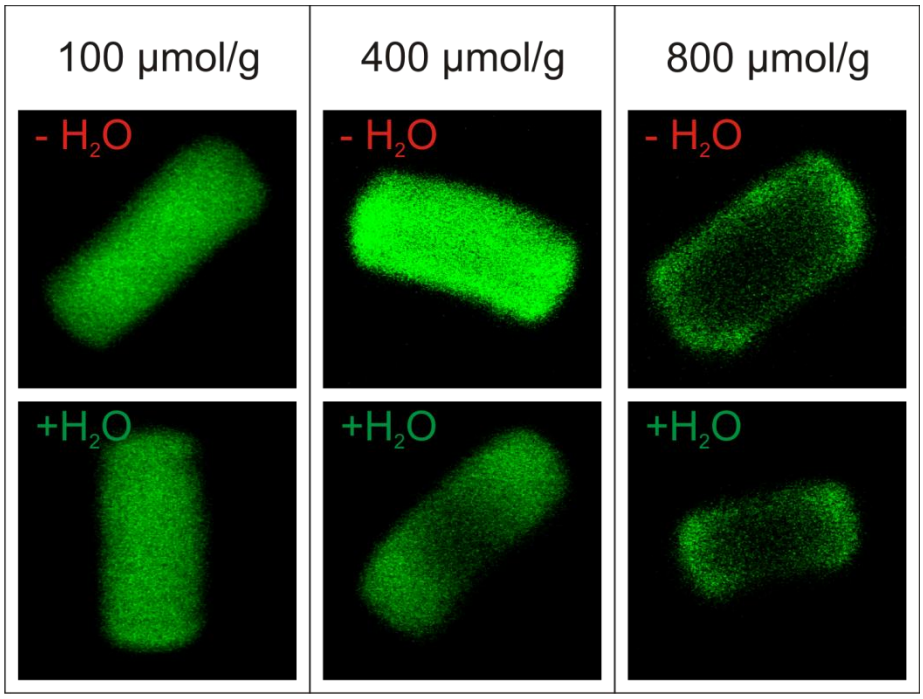

Fig. 28 CLSM images of ASNCs grafted with different amounts of APTES in toluene containing 0 or 2 monolayer(s) of water. The ASNCs particles feature an average length of approximately 5 µm.

To check whether the effects seen in the CLSM are based on cluster formation, a series of control experiments was conducted with an aminosilane unable to form clusters. 3-amino-propyldiisopropylethoxysilane (APDIPES) features only one alkoxysilane bond and can therefore only cross-link to form dimers.

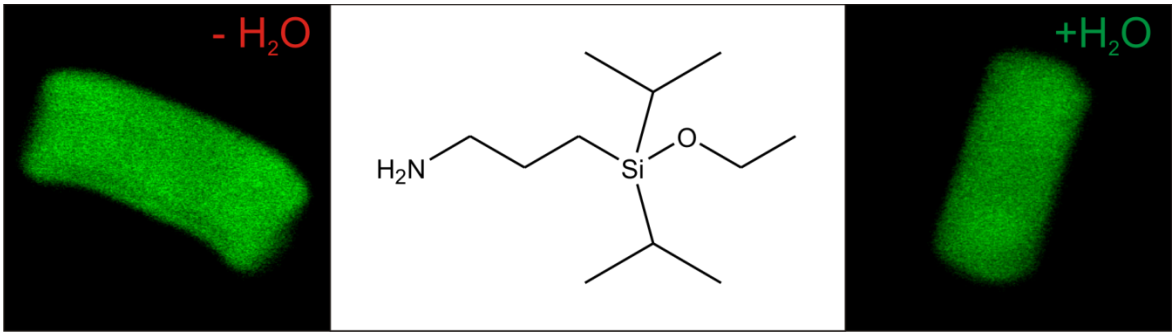

Fig. 29 CLSM images of ASNCs grafted with APDIPES in toluene containing 0 or 2 monolayer(s) of water. The ASNCs particles feature a length of approximately 5 µm.

The experiment shows that the addition of water has no effect on the distribution of APDIPES as was to be expected (Fig. 29). Experiments conducted in a later project (see Chapter 5.4) showed, however, that results achieved with APDIPES on mesoporous silica are not reliable and have to be studied carefully, because solutions containing APDIPES can partially degrade the mesoporous structure.

3.3.1 Experimental

General grafting procedure for water effect experiments

Calcined mesoporous silica (ASNCs or SBAs) (100 mg), stored at 80 °C is dispersed in dry toluene (10 ml, Sigma-Aldrich, $H_2O \leq 0.005$ %) and sonicated for a few seconds. Deionized water (0, 1 or 2 monolayer(s)) is added followed by another few seconds of ultrasonication. The suspension is stirred at room temperature for 1 h. APTES (9.3 µl, 40 µmol, Acros, 99 %) is added and the suspension is stirred at 80 °C for 3 h. The product is collected by filtration, washed with ethanol and dried in a vacuum. FITC coupling was performed in ethanol for 24 h.

Monolayer(s)

For SBAs, 1 monolayer equals 22.4 µl of water calculated for 100 mg of SBAs.

For ASNCs, 1 monolayer equals 31.6 µl of water calculated for 100 mg of ASNCs.

Alterations

- The second reaction step is done at 50 °C for solvent screening experiments
- 2.3 and 18.6 µl of APTES is added for 100 or 800 µmol/g loadings, respectively
- APDIPES (10 µl, 40 µmol, ABCR, 97 %) is used instead of APTES in the control experiments

3.4 Correlation between Nitrogen Sorption and Confocal Laser Scanning Microscopy

Emerging from our investigation of the trace water effect where we experienced what a powerful analysis the combination of nitrogen sorption and CLSM can be, we decided to do a series of experiments to show the value of this combination. While CLSM is a very potent tool to analyze the overall distribution of functional groups, it has some drawbacks. First, CLSM does not visualize the distribution of the functional groups, but only the distribution of the fluorescent label attached to it, and second, some different distributions cannot be distinguished by CLSM as the following examples will show (Fig. 30).

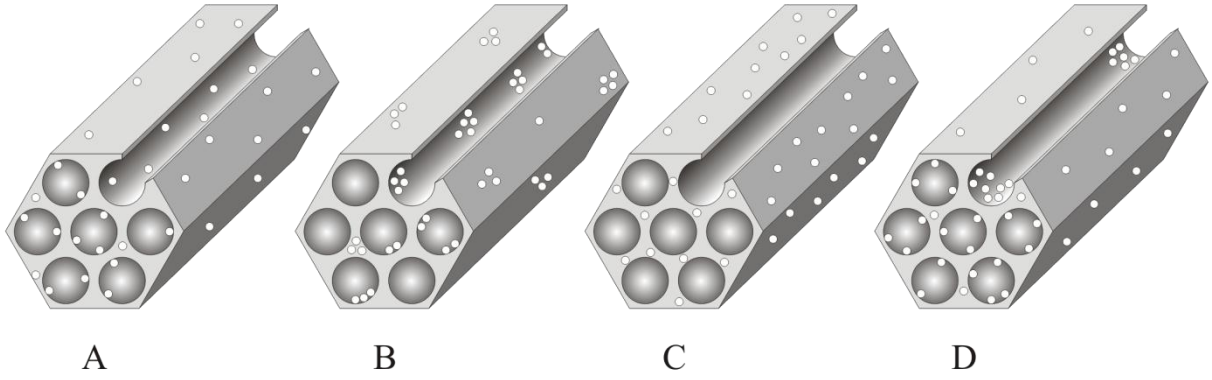

Fig. 30 Schematic representation of different examples of functional group distributions on mesoporous silica. A: homogeneous distribution, B: cluster formation, C: selective external surface functionalization, D: external surface functionalization with additional functionalization of pore entrances.

Due to lacking resolution in vertical direction (approximately 0.5 - 1 μm), CLSM always shows an overlay of hundreds of pores, therefore a sample featuring small clusters (Fig. 30 B) gives the same image in CLSM analysis as a homogeneously distributed one (Fig. 30 A). With nitrogen sorption, however, a smaller average pore size is measured for sample A than for B, with the same degree of functionalization, because the pores in B exhibit many subsections with almost no functionalization. A second example where CLSM analysis reaches its limit is the differentiation between exclusive external surface functionalization (Fig. 30 C) and external surface functionalization with a certain degree of functionalization at the pore entrances (Fig. 30 D). Again this differentiation can be measured with nitrogen sorption, due to the functional groups at the pore entrances, sample D features a smaller total pore volume than sample C.

These examples illustrate that it is important to support CLSM results with nitrogen sorption data. The experimental study on the correlation of nitrogen sorption and CLSM analysis can be found in Chapter 5.4.

3.5 Adjusting and Probing of Pore Size Distributions

Inspired by the dye/zeolite-based light harvesting and solar conversion systems,[61-64] we undertook efforts to build a similar system that is not restricted to a single pore size as small as the one of zeolite L, so that larger organic dyes could be integrated. Materials such as ASNCs are predestined for such an application, however, when we tried to align dye molecules in the channels, we recognized that although they show arrangement preferably in the direction along the channels, they are not strictly oriented in a unidirectional fashion (Fig. 31).

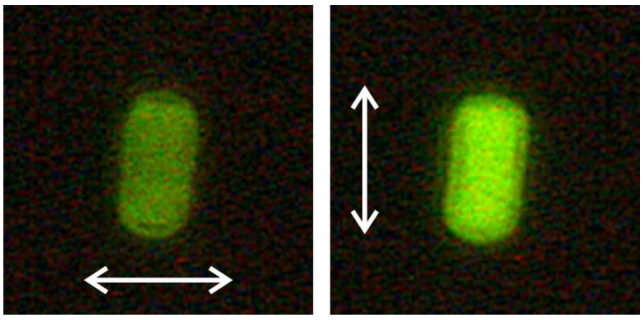

Fig. 31 Fluorescence microscopy image of PR 149, an organic perylene dye derivative, included in ASNCs. The images are acquired using a polarizer in front of the detector. The arrows indicate the polarization direction.

A possible solution to this problem is the tuning of the pore size of ASNCs. Our first approach was to modify the synthesis procedure. Swelling agents are used to enlarge the pore size of SBA materials,[25] most notably the addition of 1,3,5-trimethylbenzene (TMB) giving distinct pore sizes of up to 20 nm.[65] Unfortunately, the hexagonal morphology of the ASNCs is not retained upon the addition of TMB during the synthesis. We then focused our efforts on making ASNCs with smaller pore sizes. Applying dodecyltrimethylammonium chloride (C_{12}TAC) instead of CTAC (C_{16}TAC) as SDA leads to smaller micelles and therefore to a smaller pore diameter.[40] For ASNCs the pore size is reduced to values below 2 nm. The hexagonal morphology, however, is lost (Fig. 32).

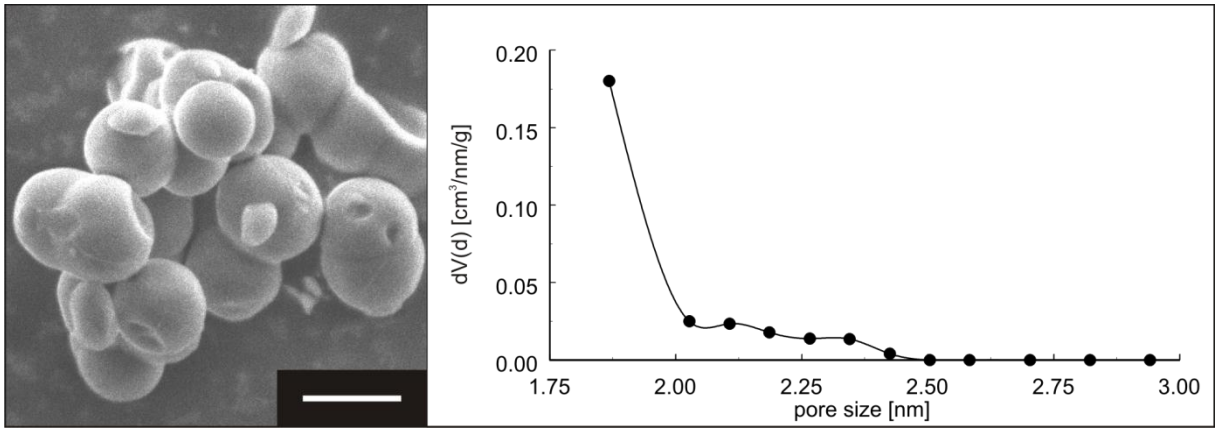

Fig. 32 SEM image (left) and PSD (right) of ASNCs synthesized using C_{12}TAC. SEM scale bar is 2 μm.

The experiments with TMB and C_{12}TAC show that the ASNCs synthesis procedure does not tolerate additional reactants, losing the well-defined morphology and pore structure.

Therefore we approached the problem in a different way, trying to modify the pore size post-synthetically. Our general idea for postsynthetic reduction of the pore size was a layer-by-layer deposition of silica from a precursor (Fig. 33).

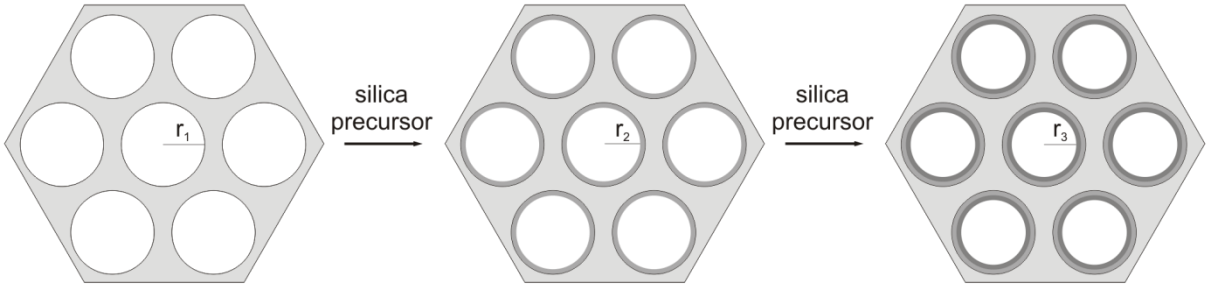

Fig. 33 Schematic representation of the layer-by-layer deposition method, where $r_1 > r_2 > r_3$.

The first and most obvious approach was to use TEOS as silica source for the additional layers. Based on the fact that mesoporous silica features 3 - 5 hydroxy groups per square nanometer,[21] we added an amount of TEOS that corresponds to 1 molecule per square nanometer. To remove the remaining surface alkoxy groups the material was dispersed in water and stirred for 20 min after TEOS grafting. The implementation of one layer of TEOS led to a remarkable reduction of pore size and pore volume, indicating a quite homogeneous grafting on the surface. Implementation of a second and third layer, however, resulted in almost no further reduction of the pore size (Fig. 34). The only reasonable explanation for this is a lack of accessible hydroxy groups on the surface.

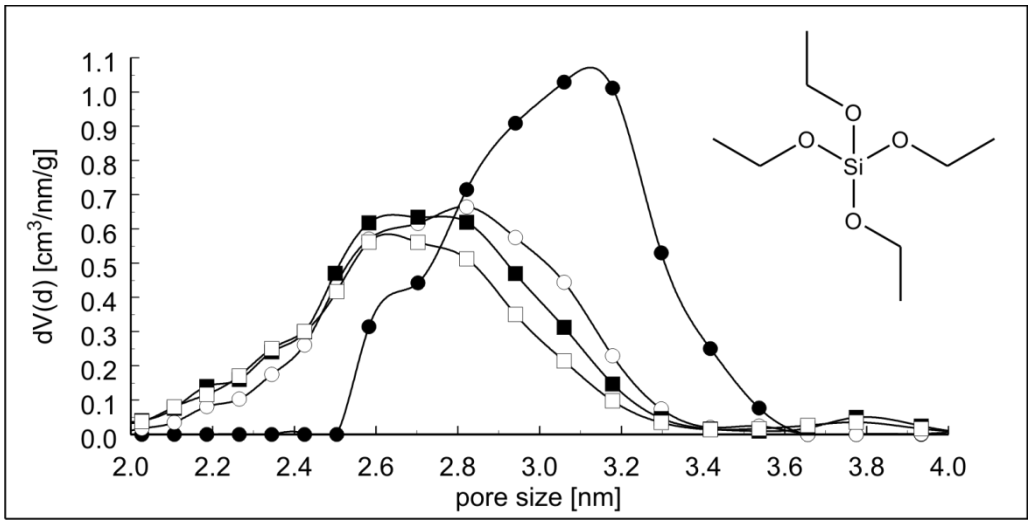

Fig. 34 PSDs of parent ASNCs (filled circles), grafted with one layer (empty circles), two layers (filled squares) or three layers (empty squares) of TEOS. PSDs were calculated by NLDFT from the adsorption branch of the nitrogen sorption isotherms.

To solve the problem of dealkoxylation and enhance the homogeneity of the layers we applied methyltrimethoxysilane (MTMS) as a silica source and removed the methyl groups by calcination in air. It can be seen (Fig. 35) that again the first step decreased both pore size and

pore volume considerably. However, as already experienced with TEOS, the subsequent steps had only a minor influence on the pore size and pore volume.

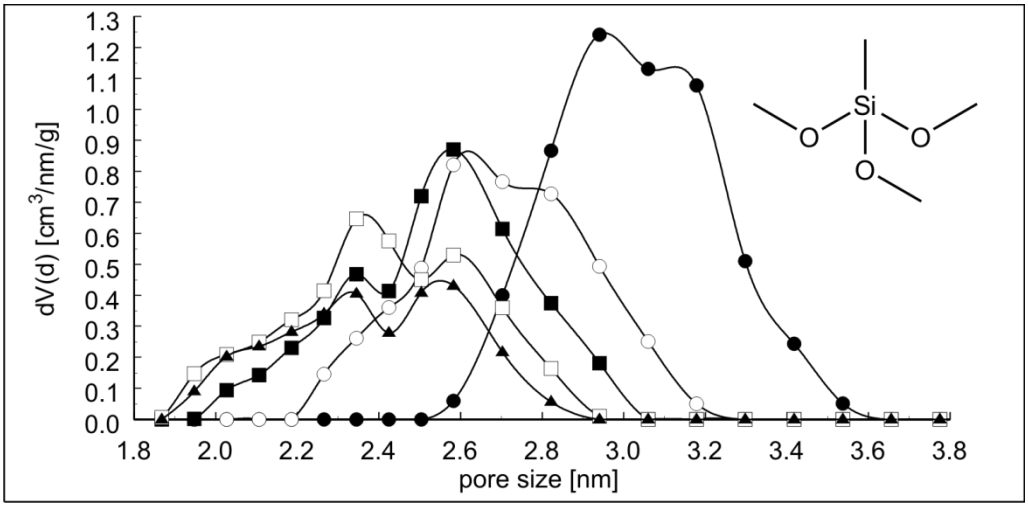

Fig. 35 PSDs of parent ASNCs (filled circles), grafted with one layer (empty circles), two layers (filled squares), three layers (empty squares) or four layers (filled triangles) of MTMS. PSDs were calculated by NLDFT from the adsorption branch of the nitrogen sorption isotherms.

Since the first step was successful in both experiments conducted so far, we came up with the idea to use larger siloxane molecules as precursors to form the layers. We applied octakis-(dimethylsiloxy)-t8-silsesquioxane (T8), a cluster, consisting of 16 oxygen bridged silicon atoms. T8 contains no alkoxysilanes and can therefore not be grafted to the surface in traditional fashion. T8 was added to a suspension of ASNCs in hexane, physisorbed on the surface by hexane evaporation, and calcined in air. The application of one layer of T8 resulted in complete occupation of the pores, reducing the pore volume to almost zero (Fig. 36).

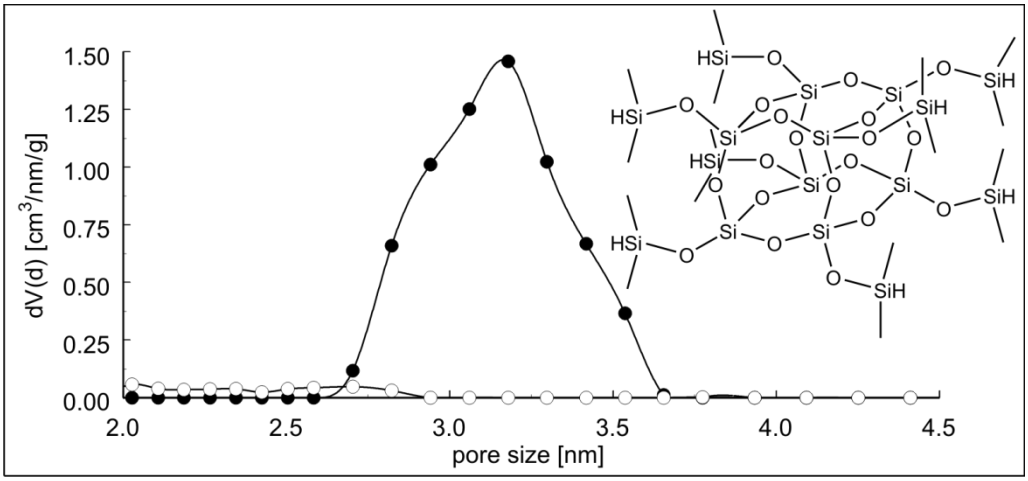

Fig. 36 PSDs of parent ASNCs (filled circles), grafted with one layer (empty circles) of T8. PSDs were calculated by NLDFT from the adsorption branch of the nitrogen sorption isotherms.

Deciding to make a compromise between the mono-silicon molecules and the large T8 cluster, we started experimenting with dodecamethylpentasiloxane (DMPS). Since DMPS is a pure alkylsiloxane without any alkoxysilyl groups, the same technique was applied for layer

adsorption as for T8. The nitrogen sorption results show that the adsorption of layers of DMPS leads to a continuous decrease in pore size and pore volume for every layer (Fig. 37), from a pore size of 3.2 nm down to 2.3 nm upon adsorption of three layers.

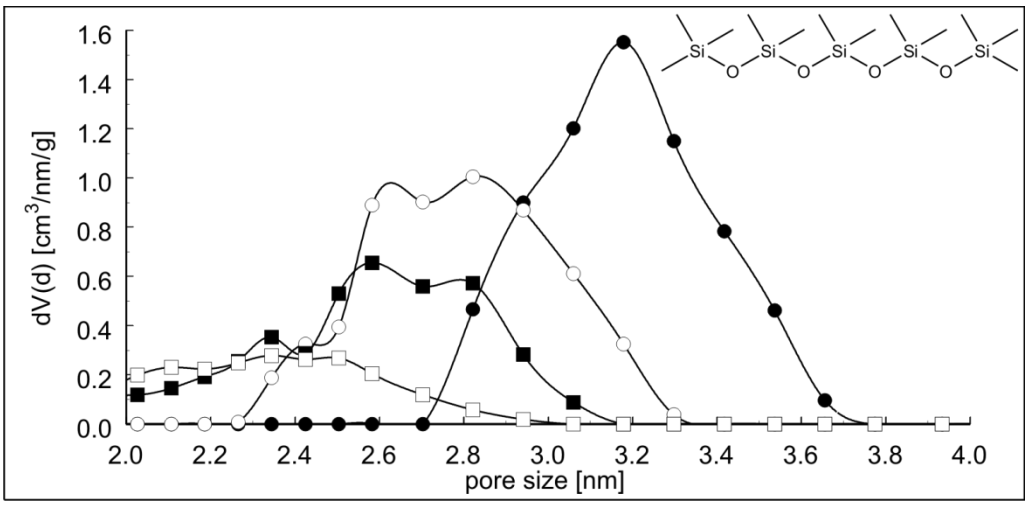

Fig. 37 PSDs of parent ASNCs (filled circles), grafted with one layer (empty circles), two layers (filled squares), and three layers (empty squares) of DMPS. PSDs were calculated by NLDFT from the adsorption branch of the nitrogen sorption isotherms.

To check if the pores are still fully accessible, pore size probing experiments were performed applying spatially demanding luminescent subphthalocyanines. Further results of DMPS adsorption and pore size probing can be found in the publication in Chapter 5.5.

3.5.1 Experimental

Pore swelling with TMB

TMB (x ml, Acros, 99 %) is added to the CTAC solution in the beginning of the ASNCs synthesis (see Chapter 3.1.1).

x = 2.1 (1 eq referring to CTAC), 1.05 (0.5 eq referring to CTAC) or 0.53 (0.25 eq referring to CTAC).

ASNCs synthesis with C_{12}TAC

ASNCs synthesis (see Chapter 3.1.1) is performed, using C_{12}TAC (x g, Aldrich, ≥ 99 %) instead of CTAC (Acros, 99 %).

x = 4.0 (1 eq referring to CTAC), 6.0 (1.5 eq referring to CTAC), 8.0 (2 eq referring to CTAC) or 6.67 g (same volume as CTAC, based on the following calculation).

Volume calculation for micelles with the same length l, based on the pore sizes of MCM-41(12)[40] and MCM-41(16).

Pore size: d(16) = 3.93 nm d(12) = 3.06 nm

Micelle volume: $V(16) = \left(\frac{3.93}{2}\right)^2 l\pi$ $V(12) = \left(\frac{3.06}{2}\right)^2 l\pi$

Ratio $\frac{V(16)}{V(12)}$: $\frac{V(16)}{V(12)} = \frac{3.93^2}{3.06^2} = 1.65$

Amount of C_{12}TAC: 1.65*Amount of CTAC (15 mmol) = 6.67 g (24.75 mmol)

Layer deposition of TEOS/MTMS

TEOS (55 µl, 246 µmol (1 molecule per nm^2), Fluka, ≥ 99 %) or MTMS (42 µl, 290 µmol, Aldrich, ≥ 98 %) is added to a suspension of calcined ASNCs (110 mg) in dry toluene (20 ml) and stirred for 1 h at 0 °C. Subsequently, the suspension is heated to 80 °C for 3 h. The ASNCs are recovered by filtration, washed with ethanol and deionized water, and redispersed in 40 ml of water. After stirring for 20 min at room temperature, the product is collected by filtration and dried at 80 °C.

The procedure is repeated once/twice for a second/third layer.

Layer deposition of T8/DMPS

T8 (70 mg, 69 µmol (approximately half a monolayer, if T8 is considered as a cube with an edge length of 1.2 nm), ABCR) or DMPS (53 µl, 122 µmol (1 molecule per 5 surface hydroxy groups), Sigma-Aldrich, 97 %) is dissolved in hexane (5 ml). ASNCs (100 mg) are added to the solution and the resulting suspension is stirred for 1 h. After evaporation of the solvent at room temperature, the material is calcined by heating to 300 °C for 2 h and subsequent heating to 550 °C for 12 h at a heating rate of 2 °C/min.

3.6 Adjusting Particle Size and Morphology

To achieve arrangements of molecules on a macroscopic scale, it is not only important to be able to align these molecules in the pores of ASNCs, but also to be able to align the ASNCs particles themselves. Although it is in principle possible to arrange such particles by introducing them into an suitable polymer foil, and stretching the latter,[66] the particles are oriented along the stretching direction and consequently have their channels running in parallel to a potential substrate. A very short hexagonal particle, however, could be oriented with the pores perpendicular to the surface with a high probability (Fig. 38). For a variety of optical applications, a channel orientation perpendicular to a substrate surface would be the arrangement of choice.[66]

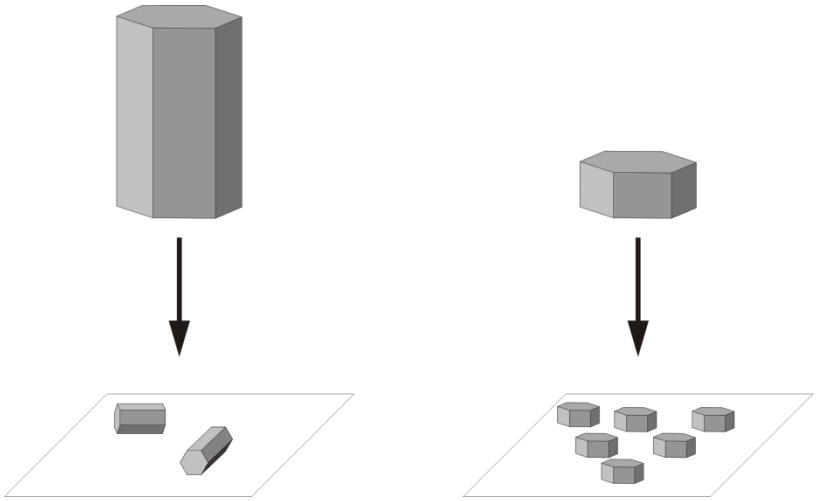

Fig. 38 Illustration of the orientation of long (left) and short (right) hexagonal rods on a surface.

Such particles have been reported by Chen et al. in 2008[67]. Unfortunately, the particles feature a large pore size of about 9 nm, and are often partly interwoven with each other (Fig. 39) and are therefore not suited for our field of application.

The platelet morphology of SBA-type materials is achieved by adding $ZrOCl_2$ to the reaction. Zr(IV) reagents interact with the triblock copolymers that serve as SDA and influence the micelles. However, materials that are synthesized with triblock copolymers exhibit large pore sizes. Experiments we conducted show that the synthesis of materials using CTAC as SDA are not influenced in the same manner by Zr(IV) reagents.

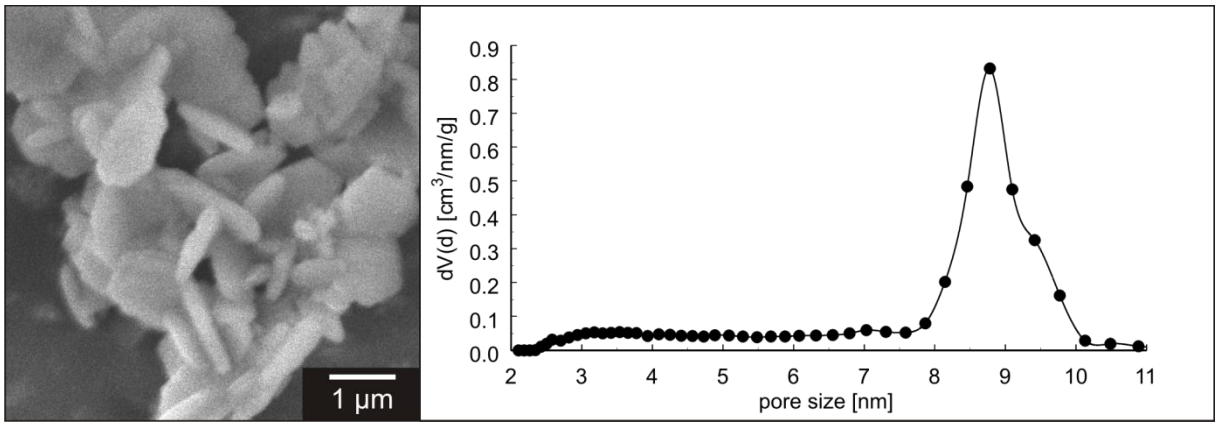

Fig. 39 SEM image (left) and PSD (right) (DFT equilibrium model) of SBA platelets synthesized according to the procedure of Chen et al.

Suzuki et al. found that applying Pluronic F127 (F127, $EO_{106}PO_{60}EO_{106}$) as a cosurfactant in the synthesis of MCM-41 leads to a dramatic decrease in particle size. F127 adsorbs onto the growing mesoporous silica particle, and in this way inhibits particle growth (Fig. 40). [68]

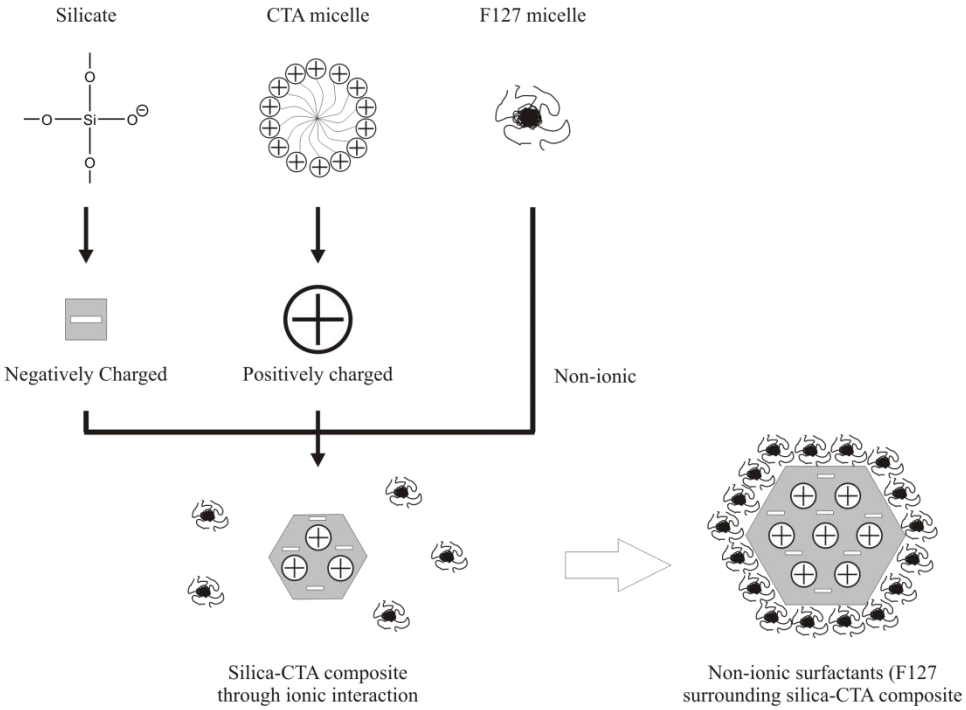

Fig. 40 Schematic representation of the functions of two surfactants.

Applying F127 in the synthesis of ASNCs showed that F127 preferentially adsorbs at the top and at the bottom surfaces, where the pore entrances are located and therefore leads to a smaller ratio of length to width (l:w ratio, smaller l:w ratio means shorter rods). However, F127 also causes a less pronounced hexagonal morphology. To investigate this effect we did a series of experiments with different amounts of F127 (Fig. 41). Since the exact average molecular weight is not known (presumably 12500 g/mol), the amount of F127 will be given in gram added to a ASNCs synthesis employing 2 ml of TEOS, 4.85 g of CTAC, and 136 ml of solvent.

Upon increase of the amount of F127 added to the synthesis, the resulting particles become shorter, but they also start featuring bulges on the top and bottom surfaces, therefore it is not possible to align them on a flat surface. Also, the reaction yield decreases from 250 - 300 mg without F127 to 20 - 50 mg with more than 3 g of F127. Upon addition of 3.7 g of F127 the reaction yielded no product.

An amount of 3.15 g proved to be a good compromise between short particles and curved top and bottom surfaces. However, further experiments showed that the degree of alignment of the particles on a flat surface is not sufficient.

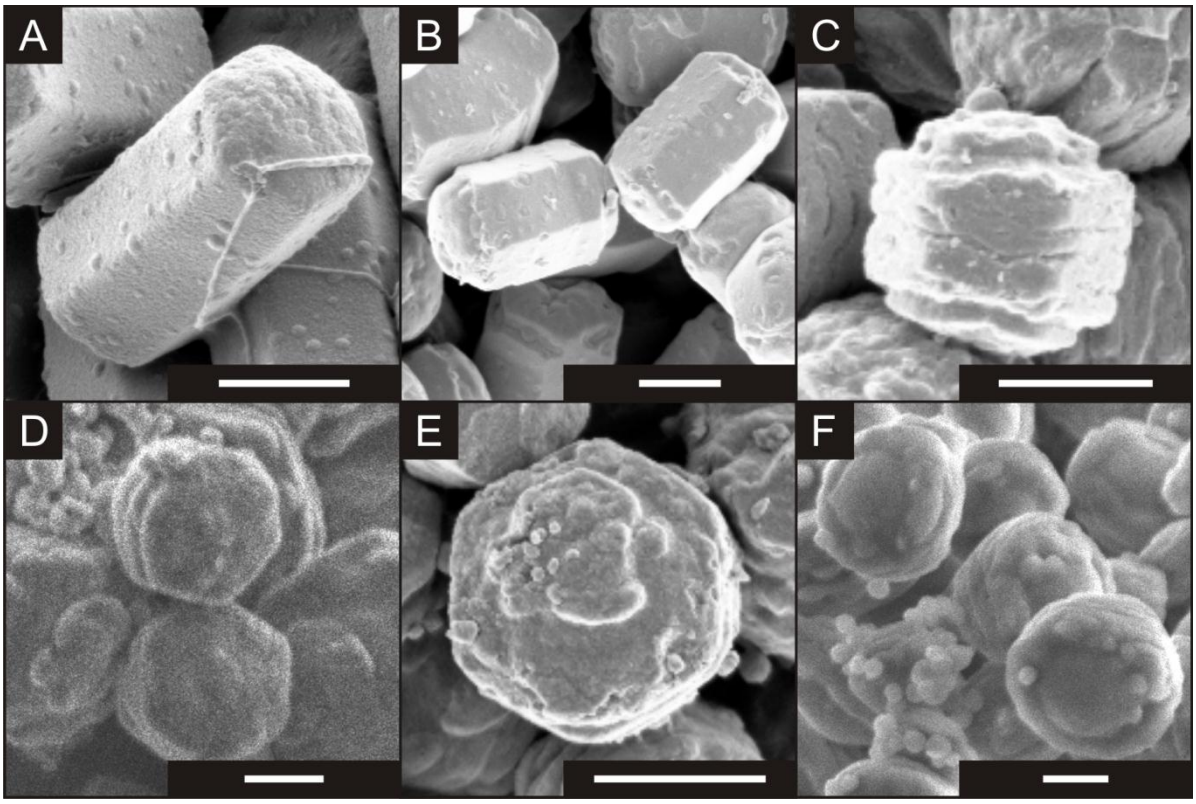

Fig. 41 ASNCs synthesized with different amounts of F127 as cosurfactant. Applied amounts were: 1 g (A), 2 g (B), 3 g (C), 3.15 g (D), 3.25 g (E), or 3.5 g (F). The scale bar is 1 µm for all samples.

To improve the particle morphology further, we changed the other reaction parameters, such as TEOS and CTAC concentration, temperature and reaction time. The change of the TEOS concentration had no visible effect on the outcome of the synthesis, whereas changes of the CTAC concentration yielded particles with undefined morphology.

Upon lowering the reaction temperature to - 5 °C, CTAC partially crystallized, and no product was formed. Increasing the temperature to 7 °C yielded long thin fibers (Fig. 42), the opposite of what we were looking for.

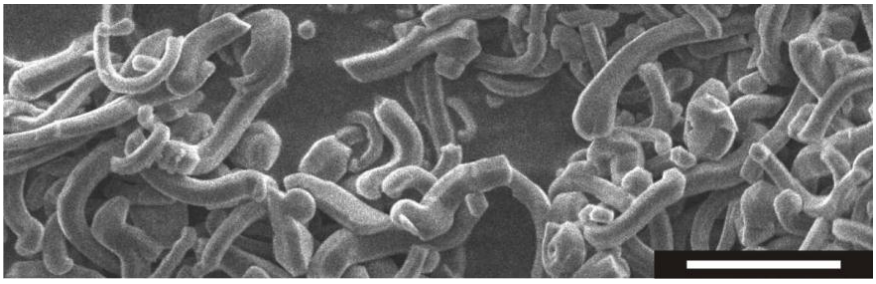

Fig. 42 SEM image of ASNCs synthesized at 7 °C. The scale bar is 10 µm.

After changing temperature and reactant concentrations gave no useful results, the reaction time remained the last parameter to vary for this reaction. Our results indicate (Fig. 43) that shorter reaction times in reactions containing F127 lead to particles with a slightly larger l:w ratio featuring a more distinct hexagonal morphology, whereas longer reaction times lead to

particles with a lower l:w ratio with a less defined morphology. Unfortunately, shorter reaction times also decrease the yield of the ASNCs synthesis.

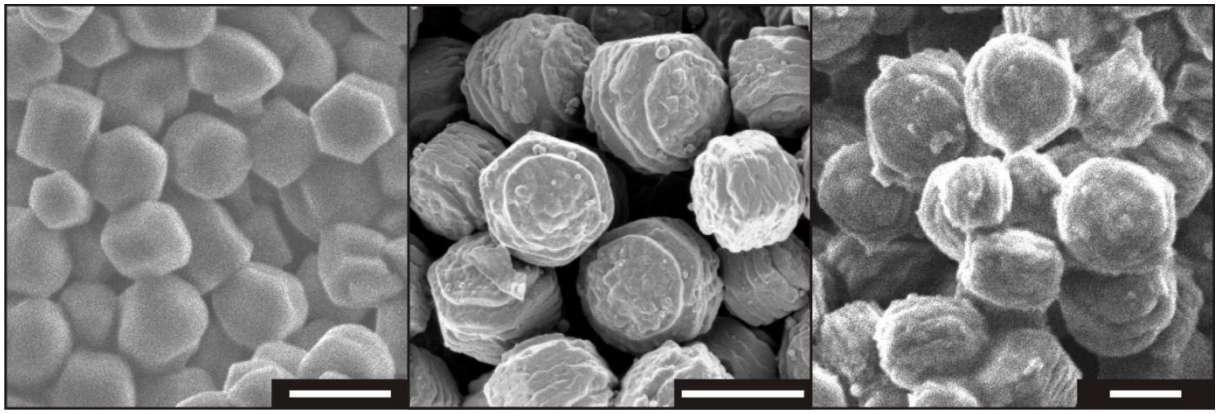

Fig. 43 ASNCs synthesized in a reaction containing 3 g of F127. The reaction time was 1 h 30 min (left), 3 h (middle) or 4 h (right). The scale bar is 2 µm.

Based on the knowledge we gained about the influence of F127 and the reaction time, we should be able to get the desired particles by application of a certain amount of F127 and the right reaction time, because we are able to control the length of the particles by controlling the amount of F127 and the quality of the particle morphology by shortening of the reaction times. Due to the fact that shorter reaction times also lead to larger l:w ratio, amounts of F127 larger than 3.15 g have to be applied. The biggest problem that arises with this amount of F127 and a reaction time below 2 h is that almost no product can be collected from the synthesis anymore. Our best results so far were achieved using 3.20 g and 3.25 g of F127 with a reaction time of 1.5 h (Fig. 44). In these reactions, particles with the desired morphologies are found. However, the yield is low and the particle morphology is not homogeneous enough for further application.

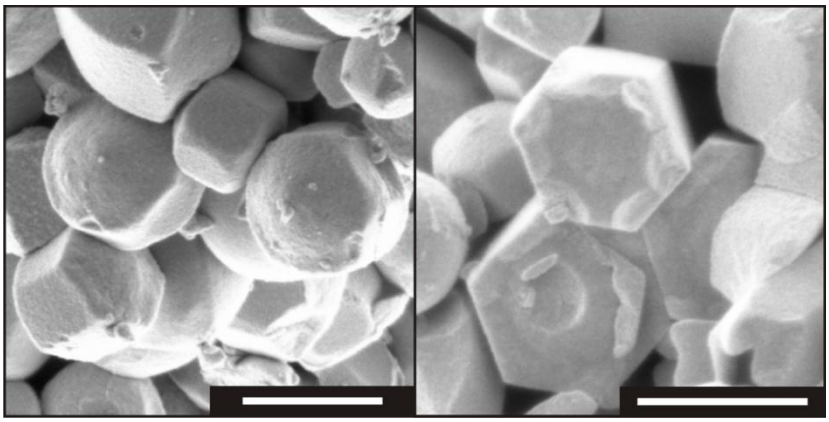

Fig. 44 ASNCs synthesized in a reaction containing 3.20 g (left) or 3.25 g (right) of F127. The reaction time was 1 h 30 min. The scale bar is 1 µm.

3.6.1 Outlook

Considering the fact that the addition of a cosurfactant during the synthesis significantly alters the l:w ratio of the resulting ASNCs, the next step will be the application of different cosurfactants. We already tried syntheses with multiple commercially available triblock copolymers with different EO:PO ratios which did not result in hexagonal particles. For an ideal cosurfactant, polymers with subtle differences to F127 have to be synthesized and investigated.

3.6.2 Experimental

SBA-platelets following the procedure of Chen et al.[67]

P123 (1 g, 172 µmol, Sigma-Aldrich) and $ZrOCl_2$•8 H_2O (162.5 mg, 504 µmol, Merck, p.a.) are dissolved in 2 M aqueous HCl (40 g). After subsequent addition of TEOS (2.25 ml, 10.1 mmol, Fluka, ≥ 99 %) the solution is stirred at 35 °C for 24 h. The mixture is then transferred to a Teflon-lined autoclave and heated to 90 °C for another 24 h under static conditions. The product is collected by filtration, washed with deionized water (100 ml) and dried at 80 °C. Calcination is performed at 500 °C for 16 h applying a heating rate of 1.2 °C/min.

ASNCs synthesis with Zr(IV)

CTAC (4.85 g, 15.2 mmol, Acros, 99 %) and $ZrOCl_2$•8 H_2O (144 mg, 447 µmol, Merck, p.a.) are dissolved in a mixture of doubly distilled water (76 ml) and 32 % aqueous HCl (60 ml). The solution is cooled in an ice bath for 15 min, followed by the addition of cooled TEOS (2 ml, 9 mmol, Sigma-Aldrich, 99.999 %). After 3 h of aging at 0 °C under static condition, the product is recovered by filtration, washed with deionized water (150 ml) and dried at 80 °C. Calcination is performed by heating to 300 °C for 2 h and subsequent heating to 550 °C for 12 h at a heating rate of 2 °C/min.

ASNCs synthesis with F127

CTAC (4.85 g, 15.2 mmol, Acros, 99 %) and F127 (w = 3 g, Sigma) are dissolved in a mixture of doubly distilled water (76 ml) and 32 % aqueous HCl (60 ml). The solution is cooled in an ice bath for 15 min, followed by the addition of cooled TEOS (x = 2 ml, 9 mmol, Sigma-Aldrich, 99.999 %). The developing slurry is kept at y = 0 °C under static conditions for z = 3 h. After filtration, the collected product is washed with deionized water and dried at 80 °C. Calcination is performed by heating to 300 °C for 2 h and subsequent heating to 550 °C for 12 h at a heating rate of 2 °C/min.

Variations

- experiments with x = 1.5 and x = 3
- experiments with y = -5 and y = 7
- experiments with variation of w from 1 to 3.7 and simultaneously of z from 1.5 to 4

4. References

[1] C. T. Kresge, M. E. Leonowicz, W. J. Roth, J. C. Vartuli, J. S. Beck, *Nature* **1992**, *359*, 710.

[2] J. S. Beck, J. C. Vartuli, W. J. Roth, M. E. Leonowicz, C. T. Kresge, K. D. Schmitt, C. T. W. Chu, D. H. Olson, E. W. Sheppard, S. B. McCullen, J. B. Higgins, J. L. Schlenker, *Journal of the American Chemical Society* **1992**, *114*, 10834.

[3] Y. Wan, D. Y. Zhao, *Chemical Reviews* **2007**, *107*, 2821.

[4] A. Taguchi, F. Schüth, *Microporous and Mesoporous Materials* **2005**, *77*, 1.

[5] M. Hartmann, *Chemistry of Materials* **2005**, *17*, 4577.

[6] J. H. Clark, D. J. Macquarrie, S. J. Tavener, *Dalton Transactions* **2006**, 4297.

[7] A. Galarneau, J. Lapichella, D. Brunel, F. Fajula, Z. Bayram-Hahn, K. Unger, G. Puy, C. Demesmay, J. L. Rocca, *Journal of Separation Science* **2006**, *29*, 844.

[8] I. I. Slowing, B. G. Trewyn, S. Giri, V. S. Y. Lin, *Advanced Functional Materials* **2007**, *17*, 1225.

[9] H. Yoshitake, *New Journal of Chemistry* **2005**, *29*, 1107.

[10] G. E. Fryxell, S. V. Mattigod, Y. H. Lin, H. Wu, S. Fiskum, K. Parker, F. Zheng, W. Yantasee, T. S. Zemanian, R. S. Addleman, J. Liu, K. Kemner, S. Kelly, X. D. Feng, *Journal of Materials Chemistry* **2007**, *17*, 2863.

[11] M. Vallet-Regì, F. Balas, D. Arcos, *Angewandte Chemie-International Edition* **2007**, *46*, 7548.

[12] I. I. Slowing, J. L. Vivero-Escoto, C. W. Wu, V. S. Y. Lin, *Advanced Drug Delivery Reviews* **2008**, *60*, 1278.

[13] M. Liong, J. Lu, M. Kovochich, T. Xia, S. G. Ruehm, A. E. Nel, F. Tamanoi, J. I. Zink, *ACS Nano* **2008**, *2*, 889.

[14] G. Begum, S. Singh, N. Rangaraj, G. Srinivas, R. K. Rana, *Journal of Materials Chemistry* **2010**, *20*, 8563.

[15] N. Gartmann, D. Brühwiler, *Materials* **2011**, *4*, 1096.

[16] A. Katiyar, N. G. Pinto, *Small* **2006**, *2*, 644.

[17] Y. R. Ma, L. M. Qi, J. M. Ma, Y. Q. Wu, O. Liu, H. M. Cheng, *Colloids and Surfaces A-Physicochemical and Engineering Aspects* **2003**, *229*, 1.

[18] A. Katiyar, S. Yadav, P. G. Smirniotis, N. G. Pinto, *Journal of Chromatography A* **2006**, *1122*, 13.

[19] Y. Kievsky, I. Sokolov, *IEEE Transactions on Nanotechnology* **2005**, *4*, 490.

[20] J. Rouquerol, D. Avnir, C. W. Fairbridge, D. H. Everett, J. H. Haynes, N. Pernicone, J. D. F. Ramsay, K. S. W. Sing, K. K. Unger, *Pure and Applied Chemistry* **1994**, *66*, 1739.

[21] I. G. Shenderovich, G. Buntkowsky, A. Schreiber, E. Gedat, S. Sharif, J. Albrecht, N. S. Golubev, G. H. Findenegg, H. H. Limbach, *Journal of Physical Chemistry B* **2003**, *107*, 11924.

[22] F. Hoffmann, M. Cornelius, J. Morell, M. Fröba, *Angewandte Chemie-International Edition* **2006**, *45*, 3216.

[23] Q. S. Huo, D. I. Margolese, U. Ciesla, D. G. Demuth, P. Y. Feng, T. E. Gier, P. Sieger, A. Firouzi, B. F. Chmelka, F. Schüth, G. D. Stucky, *Chemistry of Materials* **1994**, *6*, 1176.

[24] Q. S. Huo, D. I. Margolese, U. Ciesla, P. Y. Feng, T. E. Gier, P. Sieger, R. Leon, P. M. Petroff, F. Schüth, G. D. Stucky, *Nature* **1994**, *368*, 317.

[25] D. Y. Zhao, J. L. Feng, Q. S. Huo, N. Melosh, G. H. Fredrickson, B. F. Chmelka, G. D. Stucky, *Science* **1998**, *279*, 548.

[26] D. Y. Zhao, Q. S. Huo, J. L. Feng, B. F. Chmelka, G. D. Stucky, *Journal of the American Chemical Society* **1998**, *120*, 6024.
[27] H. Ritter, M. Nieminen, M. Karppinen, D. Brühwiler, *Microporous and Mesoporous Materials* **2009**, *121*, 79.
[28] A. Galarneau, N. Cambon, F. Di Renzo, R. Ryoo, M. Choi, F. Fajula, *New Journal of Chemistry* **2003**, *27*, 73.
[29] S. Jun, S. H. Joo, R. Ryoo, M. Kruk, M. Jaroniec, Z. Liu, T. Ohsuna, O. Terasaki, *Journal of the American Chemical Society* **2000**, *122*, 10712.
[30] P. I. Ravikovitch, A. V. Neimark, *Journal of Physical Chemistry B* **2001**, *105*, 6817.
[31] A. Galarneau, H. Cambon, F. Di Renzo, F. Fajula, *Langmuir* **2001**, *17*, 8328.
[32] K. Cheng, C. C. Landry, *Journal of the American Chemical Society* **2007**, *129*, 9674.
[33] D. S. Shephard, W. Z. Zhou, T. Maschmeyer, J. M. Matters, C. L. Roper, S. Parsons, B. F. G. Johnson, M. J. Duer, *Angewandte Chemie-International Edition* **1998**, *37*, 2719.
[34] N. K. Mal, M. Fujiwara, Y. Tanaka, *Nature* **2003**, *421*, 350.
[35] N. K. Mal, M. Fujiwara, Y. Tanaka, T. Taguchi, M. Matsukata, *Chemistry of Materials* **2003**, *15*, 3385.
[36] H. Salmio, D. Brühwiler, *Journal of Physical Chemistry C* **2007**, *111*, 923.
[37] K. K. Sharma, A. Anan, R. P. Buckley, W. Ouellette, T. Asefa, *Journal of the American Chemical Society* **2008**, *130*, 218.
[38] N. Gartmann, D. Brühwiler, *Angewandte Chemie-International Edition* **2009**, *48*, 6354.
[39] N. Gartmann, C. Schütze, H. Ritter, D. Brühwiler, *Journal of Physical Chemistry Letters* **2010**, *1*, 379.
[40] H. Ritter, D. Brühwiler, *Journal of Physical Chemistry C* **2009**, *113*, 10667.
[41] S. Ek, E. I. Iiskola, L. Niinisto, J. Vaittinen, T. T. Pakkanen, J. Keranen, A. Auroux, *Langmuir* **2003**, *19*, 10601.
[42] S. Udenfriend, S. Stein, P. Bohlen, W. Dairman, *Science* **1972**, *178*, 871.
[43] M. Weigele, J. P. Tengi, W. Leimgruber, S. l. Debernar, *Journal of the American Chemical Society* **1972**, *94*, 5927.
[44] K. S. W. Sing, D. H. Everett, R. A. W. Haul, L. Moscou, R. A. Pierotti, J. Rouquerol, T. Siemieniewska, *Pure and Applied Chemistry* **1985**, *57*, 603.
[45] S. Brunauer, P. H. Emmett, E. Teller, *Journal of the American Chemical Society* **1938**, *60*, 309.
[46] E. P. Barrett, L. G. Joyner, P. P. Halenda, *Journal of the American Chemical Society* **1951**, *73*, 373.
[47] C. Lastoskie, K. E. Gubbins, N. Quirke, *Journal of Physical Chemistry* **1993**, *97*, 4786.
[48] P. I. Ravikovitch, S. C. O'Domhnaill, A. V. Neimark, F. Schüth, K. K. Unger, *Langmuir* **1995**, *11*, 4765.
[49] M. Kruk, M. Jaroniec, R. Ryoo, J. M. Kim, *Microporous Materials* **1997**, *12*, 93.
[50] A. Sayari, P. Liu, M. Kruk, M. Jaroniec, *Chemistry of Materials* **1997**, *9*, 2499.
[51] Q. Cai, Z. S. Luo, W. Q. Pang, Y. W. Fan, X. H. Chen, F. Z. Cui, *Chemistry of Materials* **2001**, *13*, 258.
[52] M. Mesa, L. Sierra, B. Lopez, A. Ramirez, J. L. Guth, *Solid State Sciences* **2003**, *5*, 1303.
[53] L. Sierra, B. Lopez, J. L. Guth, *Microporous and Mesoporous Materials* **2000**, *39*, 519.
[54] N. Gartmann, D. Brühwiler, *Chimia* **2011**, *65*, 250.
[55] J. A. Melero, G. D. Stucky, R. van Grieken, G. Morales, *Journal of Materials Chemistry* **2002**, *12*, 1664.
[56] N. Lang, A. Tuel, *Chemistry of Materials* **2004**, *16*, 1961.

[57] K. M. R. Kallury, P. M. Macdonald, M. Thompson, *Langmuir* **1994**, *10*, 492.
[58] K. C. Vrancken, P. Van der Voort, I. Gillis-D'Hamers, E. F. Vansant, P. Grobet, *Journal of the Chemical Society-Faraday Transactions* **1992**, *88*, 3197.
[59] F. S. Baker, K. S. W. Sing, *Journal of Colloid and Interface Science* **1976**, *55*, 605.
[60] D. Brühwiler, H. Frei, *Journal of Physical Chemistry B* **2003**, *107*, 8547.
[61] D. Brühwiler, L. Q. Dieu, G. Calzaferri, *Chimia* **2007**, *61*, 820.
[62] G. Calzaferri, H. Li, D. Brühwiler, *Chemistry-A European Journal* **2008**, *14*, 7442.
[63] T. Dienel, C. Bauer, I. Dolamic, D. Brühwiler, *Solar Energy* **2010**, *84*, 1366.
[64] G. Calzaferri, R. Meallet-Renault, D. Brühwiler, R. Pansu, I. Dolamic, T. Dienel, P. Adler, H. Li, A. Kunzmann, *ChemPhysChem* **2011**, *12*, 580.
[65] L. N. Wang, T. Qi, Y. Zhang, J. L. Chu, *Microporous and Mesoporous Materials* **2006**, *91*, 156.
[66] D. Brühwiler, G. Calzaferri, T. Torres, J. H. Ramm, N. Gartmann, L. Q. Dieu, I. Lopez-Duarte, M. V. Martinez-Diaz, *Journal of Materials Chemistry* **2009**, *19*, 8040.
[67] S. Y. Chen, C. Y. Tang, W. T. Chuang, J. J. Lee, Y. L. Tsai, J. C. C. Chan, C. Y. Lin, Y. C. Liu, S. F. Cheng, *Chemistry of Materials* **2008**, *20*, 3906.
[68] K. Suzuki, K. Ikari, H. Imai, *Journal of the American Chemical Society* **2004**, *126*, 462.

5. Publications

5.1 Controlling and Imaging the Functional-Group Distribution on Mesoporous Silica

Nando Gartmann and Dominik Brühwiler*

Institute of Inorganic Chemistry, University of Zurich, Winterthurerstrasse 190, 8057 Zurich, Switzerland

Angewandte Chemie International Edition **2009**, 40, 6354-6356

Angewandte Chemie **2009**, 121, 6472-6475

In, out, shake it all about: The distribution of fluorescence-labeled amino groups on mesoporous silica is imaged by confocal laser scanning microscopy. The mobility of the aminosilane precursor determines the degree of external vs. pore surface functionalization. This observation was used to develop a simple and general method for the modification of external mesoporous silica surfaces.

The control of the distribution of functional groups on mesoporous silica is essential for applications of these materials in various fields including catalysis,[1] drug delivery,[2] and sensing.[3] In order to define the interaction of the mesoporous silica particles with their surrounding medium, the selective modification of the external surface is of particular importance. Externally grafted functional groups can for example regulate the cellular uptake[4] or provide targeting ability[5] of mesoporous silica based drug delivery systems.

The introduction of functional groups by grafting to a preformed mesoporous material (often referred to as *postsynthetic functionalization*) is a versatile modification method, as the desired pore size distribution, pore system dimensionality, particle size, and particle morphology can be obtained in a straightforward manner. However, the control of the functional group distribution poses a particular challenge. A recently reported concept employs fmoc-modified organosilanes which are grafted to the external and internal (pore) surfaces of mesoporous silica. Under certain reaction conditions, the external surface groups can be deprotected selectively and subsequently functionalized further, whereas the groups located on the pore surface remain fmoc-protected.[6] A frequently used general method of postsynthetic external surface modification is based on the reaction of chloro-, methoxy-, or ethoxysilanes with as-synthesized mesoporous silica, i.e., mesoporous silica still containing the structure-directing agent (SDA). We will show that considerable grafting to the pore surface can occur despite the presence of the SDA, and describe a convenient postsynthetic functionalization method with a high selectivity for the external surface.

Confocal laser scanning microscopy (CLSM) has been used to visualize the spatial distribution of fluorescent guests in mesoporous and microporous host materials.[7] The distribution of functional groups covalently bound to mesoporous silica can be similarly imaged after coupling with appropriate fluorescent labels. Large particles of defined morphology are ideal for this purpose. We have been working with hexagonal particles, also known as arrays of silica nanochannels (ASNCs),[8] as well as with spherical particles of the SBA-15 type (SBA-s)[9] featuring a less ordered pore system and a larger average pore size than the ASNCs (Figure 1, Table 1). In both cases, functionalization reactions were carried out either before or after removal of the SDA.

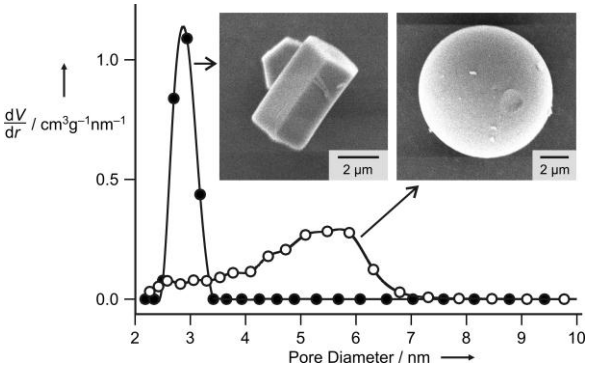

Table 1. Textural properties of the parent ASNCs and SBA-s.

	ASNCs	SBA-s
Average Pore Diameter [nm]	2.9	ca. 5.5
BET Surface Area [m^2/g]	1120	795
External Surface Area [m^2/g]	37	10
Total Pore Volume [cm^3/g]	0.62	0.74

Figure 1. Pore size distribution of ASNCs (solid circles) and SBA-s (empty circles). The well-defined morphology of the particles is illustrated by the corresponding electron micrographs. The image of the ASNCs shows two particles (one particle is standing on its hexagonal base).

Apart from the frequently employed 3-aminopropyltriethoxysilane (APTES), 3-aminopropyltris(methoxyethoxyethoxy)silane (APTMEES) and bis(triethoxysilylpropyl)-

amine (BTESPA) were used as reactants (Figure 2). The surface-grafted amino groups were subsequently labeled with fluorescein isothiocyanate (FITC) or Texas Red sulfonyl chloride (TR). Room temperature deposition of the silanes from hexane and curing at 80 °C led to the remarkably different distributions shown in Figure 2. The following can be concluded from these results: (1) Due to the comparatively large pore diameter, reaction with calcined SBA-s leads to a high degree of pore surface grafting for all investigated silanes. The uniformity of the functional group distribution decreases in the series APTES > BTESPA > APTMEES. As a consequence of the narrower channels, this tendency is more pronounced when grafting to calcined ASNCs. In the case of APTMEES, an excellent selectivity for the external surface is obtained. The observation that BTESPA produces a less uniform distribution than APTES is in agreement with results obtained from a systematic study of the pore size distributions and luminescence intensities of respective FITC coupled, MCM-41 based samples.[10] (2) Despite the presence of the SDA, grafting of APTES to as-synthesized SBA-s and ASNCs leads to significant pore surface derivatization. The reaction of APTES with as-synthesized mesoporous materials of the MCM-41 (alkyltrimethyl-ammonium ions as SDA) and SBA-15 type (poly(alkylene oxide) block copolymer as SDA) is a frequently used procedure for the functionalization of the external surface. Our results show, however, that this method is not ideal. A similar result is obtained with BTESPA, despite its larger size and higher reactivity. The ability of ethoxy-, methoxy-, and chlorosilanes to displace the SDA from MCM-41 type materials can in fact be exploited to accomplish pore surface functionalization.[11] (3) High selectivity for the external surface is observed upon grafting of APTMEES to as-synthesized materials.

Analysis of the amount of surface-grafted amino groups by the fluorogenic derivatization reaction with fluorescamine[12] revealed quantitative adsorption of the respective silanes on calcined ASNCs and SBA-s. Exclusive grafting to the external surface would therefore give rise to an amino group density of 1.6 nm^{-2} for ASNCs and 6.0 nm^{-2} for SBA-s.

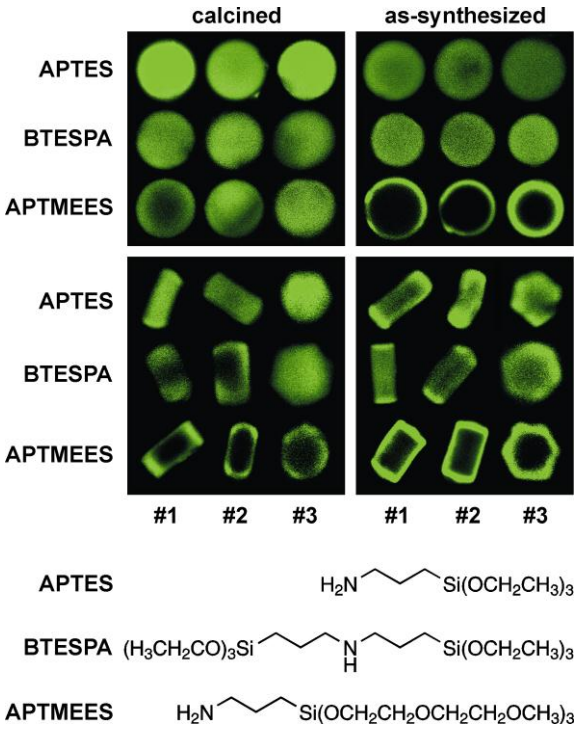

Figure 2. CLSM images (after FITC labeling) of SBA-s (top panels) and ASNCs (bottom panels) functionalized with APTES, BTESPA, or APTMEES, showing three particles for each silane/silica combination. In the case of the as-synthesized samples, the SDA was extracted after FITC labeling. Particles of ASNCs depicted in columns #3 are standing on their hexagonal base.

As such high densities are unlikely, we assume that partial grafting to the pore surface occurs even in the case of APTMEES, although apparently predominantly at sites close to the pore entrances.

The question remains whether the pronounced tendency of APTMEES to graft to the external surface is a consequence of pore blocking. To exclude this possibility, we have conducted the following experiment. As-synthesized SBA-s and ASNCs were functionalized with APTMEES as described above. After FITC labeling and extraction of the SDA, APTES was deposited from ethanol (3 h, RT), coupled to TR, and cured at 80 °C. The samples were washed repeatedly until the washing solution became colorless. Figure 3 shows that the bulky TR labels have entered the channels despite the presence of FITC labeled amino groups on the external surface. This indicates that the pores are indeed accessible after external surface functionalization with APTMEES.

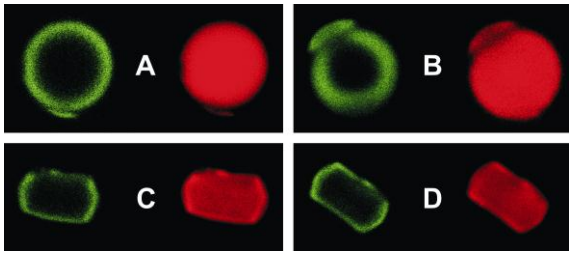

Figure 3. CLSM images of SBA-s (A and B) and ASNCs (C and D) after external surface functionalization with APTMEES and labeling with FITC, followed by reaction with APTES in ethanol and labeling with TR. The left (green) images of each panel show the luminescence of the coupled FITC labels, whereas the right (red) images are obtained upon selective excitation of the TR labels.

Deposition of aminopropylalkoxysilanes on silica at room temperature results in the formation of hydrogen bonds between the amino groups and the surface silanols. There is evidence in the case of APTES that this adsorption step reaches an equilibrium within 1 min (in toluene).[13] Deprotonation of silanol groups by the amines can lead to electrostatic interactions. The formation of siloxane bonds prior to the curing step has been observed in the APTES/silica system.[13] The distribution of a given aminosilane is determined by its mobility on the mesoporous silica surface, and, in the case of as-synthesized materials, its ability to penetrate the SDA-filled channels. Our results suggest that APTMEES is significantly less mobile than BTESPA and APTES.

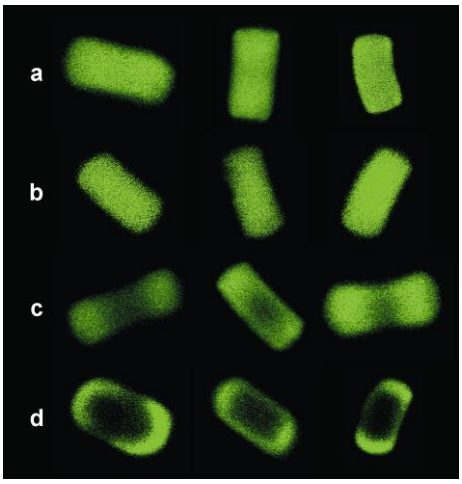

Figure 4. CLSM images of calcined ASNCs after functionalization with APTMEES in ethanol (a), acetone (b), THF (c), toluene (d), and subsequent FITC labeling. The amino contents of the samples are close to 100 µmol/g.

It is reasonable to assume that polar solvents lead to increased mobility. This concept has previously been used to control the site isolation of amino groups on mesoporous silica.[10,14] The combination of APTMEES deposition and CLSM imaging allows to

directly visualize the effect of the solvent on the functional group distribution. As can be seen in Figure 4, the uniformity of the functional group distribution increases in the series toluene (≈hexane) < THF < acetone ≈ ethanol.

In summary, we have shown that the deposition of APTMEES from hexane leads to excellent selectivity for the external surface of mesoporous silica. In case of small mesopore sizes, a high degree of external surface modification is obtained even for calcined samples. When working with as-synthesized samples, APTMEES is superior to the frequently used APTES in terms of its tendency to graft to the external particle surface. The mesopores remain accessible after external surface functionalization with APTMEES.

Experimental Section

Spherical SBA-15 particles (SBA-s) were synthesized as follows:[9] A solution of 0.465 g of hexadecyltrimethylammonium bromide (Fluka) in 20 ml of H_2O was added to a solution of 3.10 g of Pluronic P123 ($EO_{20}PO_{70}EO_{20}$, m_{av} = 5800, Aldrich) in 45.9 ml of 1.5 M aqueous HCl. After the addition of 7.8 ml of ethanol, the mixture was stirred vigorously and 10 ml of tetraethoxysilane (TEOS, Fluka) was added dropwise. Following further stirring for 2 h at RT, the mixture was transferred to a Teflon lined autoclave and kept at 78 °C for 72 h. The product was obtained by filtration, washed with 50 ml of H_2O, and dried at RT. Calcination was performed at 500 °C for 16 h with a heating rate of 1.2 °C/min. As an alternative to calcination, the structure directing agent (SDA) was removed by Soxhlet extraction with ethanol during 24 h.[15]

ASNCs were prepared by a procedure similar to the one reported by Kievsky and Sokolov.[8] An amount of 4.85 g of hexadecyltrimethylammonium chloride (Acros) was dissolved in 76 ml of double distilled H_2O and 60 ml of 32 % aqueous HCl by stirring for 1 min at ca. 1000 rpm in a polypropylene beaker. The solution was subsequently cooled to 0 °C for 15 min without stirring, followed by the slow addition of 2 ml of cold TEOS (Aldrich, 99.999 %) and further stirring for 30 s. The resulting mixture was kept at 0 °C under quiescent conditions for 3 h. The product was collected by filtration and washed with 250 ml of H_2O. The SDA was removed by first heating at 300 °C for 2 h and calcining at 550 °C for 12 h. Heating rates of 2 °C/min were applied. Alternatively, the SDA was extracted by dispersing 200 mg of the as-synthesized ASNCs in a solution of 90 mg of ammonium nitrate in 45 ml of ethanol, and stirring the mixture at 60 °C for 15 min. For complete extraction, this step was repeated twice.[16] For both ASNCs and SBA-s, removal of the SDA by extraction was performed after aminosilane grafting and FITC coupling. Extraction of the SDA before FITC coupling led to the same results in terms of the distribution of the labels.

Amino groups were grafted to the mesoporous silica materials as follows: 200 mg of calcined or as-synthesized ASNCs or SBA-s was dispersed in 10 ml of hexane and 20 µmol of APTES, APTMEES, or BTESPA (ABCR GmbH & Co.) was added. After stirring the mixture for 10 min, the functionalized mesoporous silica was

recovered by filtration and cured in an oven at 80 °C for 16 h.

The samples were labeled by stirring in ethanol containing 3 equivalents (relative to the amount of the respective silane) of FITC (fluorescein 5-isothiocyanate, isomer I, Fluka) or TR (Texas Red sulfonyl chloride, mixed isomers, Molecular Probes) for 16 h at RT. The labeled samples were washed repeatedly with ethanol until the washing solution became colorless.

Nitrogen sorption isotherms were collected at 77 K using a Quantachrome NOVA 2200. Samples were vacuum-degassed at 80 °C for 3 h. The total surface area was calculated by the BET method, whereas the external surface area was determined from the high pressure linear part of the α_S-plot ($\alpha_S > 1$).[17] Mesopore size distributions were evaluated by the NLDFT method developed for silica exhibiting cylindrical pore geometry (NOVAWin2 software, Version 2.2, Quantachrome Instruments).[18] The adsorption branch of the respective isotherm was used for the calculations. The total pore volume was determined by the amount of adsorbed nitrogen at a relative pressure of 0.95. Scanning electron microscopy images were acquired on a JEOL JSM-6060. The CLSM setup consisted of a Olympus BX 60 microscope equipped with a FluoView detector and lasers operating at 488 and 543.5 nm. Optical slices in the center of the particles were selected.

[1] A. Taguchi, F. Schüth, *Microporous Mesoporous Mater.* **2004**, *77*, 1.
[2] M. Vallet-Regí, F. Balas, D. Arcos, *Angew. Chem. Int. Ed.* **2007**, *46*, 7548; *Angew. Chem.* **2007**, *119*, 7692.
[3] I. I. Slowing, B. G. Trewyn, S. Giri, V. S.-Y. Lin, *Adv. Funct. Mater.* **2007**, *17*, 1225.
[4] I. I. Slowing, B. G. Trewyn, V. S.-Y. Lin, *J. Am. Chem. Soc.* **2006**, *128*, 14792.
[5] M. Liong, J. Lu, M. Kovochich, T. Xia, S. G. Ruehm, A. E. Nel, F. Tamanoi, J. I. Zink, *ACS Nano* **2008**, *2*, 889.
[6] K. Cheng, C. C. Landry, *J. Am. Chem. Soc.* **2007**, *129*, 9674.
[7] a) S. Megelski, A. Lieb, M. Pauchard, A. Drechsler, S. Glaus, C. Debus, A. J. Meixner, G. Calzaferri, *J. Phys. Chem. B* **2001**, *105*, 25; b) M. Pauchard, S. Huber, R. Méallet-Renault, H. Maas, R. Pansu, G. Calzaferri, *Angew. Chem. Int. Ed.* **2001**, *40*, 2839; *Angew. Chem.* **2001**, *113*, 2921; c) C. Seebacher, J. Rau, F.-W. Deeg, C. Bräuchle, S. Altmaier, R. Jäger, P. Behrens, *Adv. Mater.* **2001**, *13*, 1374; d) G. Calzaferri, S. Huber, H. Maas, C. Minkowski, *Angew. Chem. Int. Ed.* **2003**, *42*, 3732; *Angew. Chem.* **2003**, *115*, 3860.
[8] Y. Kievsky, I. Sokolov, *IEEE Trans. Nanotechnol.* **2005**, *4*, 490.
[9] a) Y. Ma, L. Qi, J. Ma, Y. Wu, O. Liu, H. Cheng, *Colloids Surf. A* **2003**, *229*, 1; b) A. Katiyar, N. G. Pinto, *Small* **2006**, *2*, 644.
[10] H. Salmio, D. Brühwiler, *J. Phys. Chem. C* **2007**, *111*, 923.
[11] a) V. Antochshuk, M. Jaroniec, *Chem. Commun.* **1999**, 2373; b) V. Antochshuk, M. Jaroniec, *Chem. Mater.* **2000**, *12*, 2496.
[12] H. Ritter, M. Nieminen, M. Karppinen, D. Brühwiler, M*icroporous Mesoporous Mater.* **2009**, *121*, 79.
[13] K. C. Vrancken, K. Possemiers, P. Van Der Voort, E. F. Vansant, *Colloids Surf. A* **1995**, *98*, 235.
[14] K. K. Sharma, A. Anan, R. P. Buckley, W. Ouellette, T. Asefa, *J. Am. Chem. Soc.* **2008**, *130*, 218.
[15] C. A. Melero, G. D. Stucky, R. van Grieken, G. Morales, *J. Mater. Chem.* **2002**, *12*, 1664.
[16] N. Lang, A. Tuel, *Chem. Mater.* **2004**, *16*, 1961.
[17] A. Sayari, P. Liu, M. Kruk, M. Jaroniec, *Chem. Mater.* **1997**, *9*, 2499.
[18] P. I. Ravikovitch, S. C. O. Domhnaill, A. V. Neimark, F. Schüth, K. K. Unger, *Langmuir* **1995**, *11*, 4765.

5.2 Functional Group Distributions on Mesoporous Silica

Nando Gartmann and Dominik Brühwiler

Institute of Inorganic Chemistry, University of Zurich, Winterthurerstrasse 190, 8057 Zurich, Switzerland

Chimia **2011**, 65, 250-252 (Laureates Issue)

Abstract

Most applications of mesoporous silica require some degree of functionalization. The surface of porous materials can be divided into external and internal (pore) surfaces, and in many cases, a selective functionalization of these surface subsections is desired. This short review outlines our recent work in this field and focuses on the postsynthetic functionalization of mesoporous silica with aminopropylalkoxysilanes and on the analysis of the respective functional group distributions by confocal laser scanning microscopy. Methods to obtain an amino-functionalized external surface and functional group gradients on the pore surface are reported. Arrays of silica nanochannels (ASNCs) serve as a model system for mesoporous silica.

1. Introduction

Since its discovery in the early 1990s,[1] mesoporous silica with ordered pores has quickly developed into an important class of materials with wide-spread applications in fields such as catalysis,[2] drug delivery,[3] sensing,[4] imaging,[5] and adsorption.[6] Most of these applications require functionalization of the mesoporous silica surface. Mesoporous silica particles for drug delivery are a particularly illustrative example for the need of modification techniques that enable a controlled placement of functional groups on specific parts of the very large surface of these materials. Functional groups on the external particle surface define the interaction with the surrounding medium, solving different tasks, such as targeting, avoiding detection by the immune system, or preventing particle aggregation. In addition to the modification of the external surface, the pore surface needs to be functionalized independently with moieties for the optimization of drug adsorption. An ideal drug delivery system should further be equipped with stimuli-responsive gates ensuring zero release before reaching the target. The concept of opening and closing mesoporous silica channels by a physical or chemical stimulus has recently gained substantial interest.[7]

A key issue in the characterization of functionalized mesoporous silica is the identification of the functional group distribution. Unfortunately, in many reports, particularly in the field of catalysis, this issue is not well addressed. As a result, conclusions regarding structure-activity relationships are often based on incomplete data and do not contribute to advance the understanding of the respective systems. To investigate the parameters that affect the functional group distribution, we have been mainly focusing on amines, as they are among the most frequently employed groups for the modification of mesoporous silica surfaces. Once the amines are anchored, a further moiety can be coupled by means of amine-reactive derivatives such as isothiocyanates or sulfonyl chlorides. This concept is especially helpful for the analysis of the amino group distributions, because it allows the attachment of labels which amplify the presence of the amino groups in the pores by reducing the pore volume and, in certain cases, the pore diameter.[8,9] The use of fluorescent labels opens further possibilities for characterizing the functional group distributions by confocal laser scanning microscopy (CLSM).[10-12] However, CLSM requires relatively large mesoporous silica particles with defined morphology. Most procedures for the synthesis of mesoporous silica yield materials with irregular morphology but often extremely narrow pore size distributions (Figure 1).

Despite their slightly broader pore size distribution, arrays of silica nanochannels (ASNCs) are ideal for CLSM,[10] as the entrances of the hexagonally arranged channels are exclusively located on the base surfaces of the well-defined particles.[13] Selective external surface functionalization, accumulation at the pore entrances, or uniform distributions of functional groups can therefore immediately be identified.

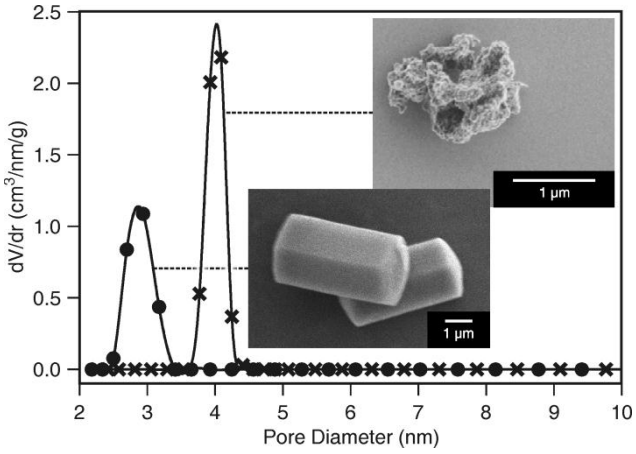

Fig. 1. Pore size distributions and scanning electron microscopy images of mesoporous silica MCM-41 (crosses) and arrays of silica nanochannels (ASNCs, dots).

2. Functionalization of the External Surface

The synthesis of mesoporous silica employs structure-directing agents (SDAs) to generate an ordered pore system.[14] Grafting of 3-aminopropyltrialkoxysilanes, typically 3-aminopropyltriethoxysilane (APTES), to mesoporous silica before removing the SDA is regarded as a straightforward method for external surface modification. Intuitively, one would assume that the SDA blocks the pores and thus prevents the silane molecules from reacting with silanol groups on the pore surface. Following this approach, we found that the degree of pore surface grafting strongly depends on the organosilane. In case of the frequently used APTES, significant derivatization of the pore surface was found despite the presence of the SDA in the pores, whereas 3-aminopropyltris(methoxyethoxyethoxy)silane (APTMEES) grafted preferentially to external surface sites, most likely as a consequence of the higher steric hindrance and lower surface mobility (Figure 2).

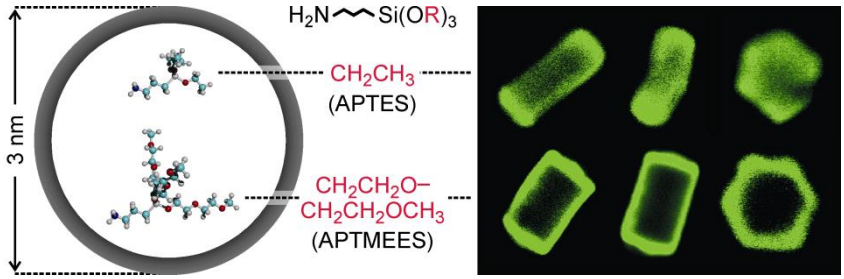

Fig. 2. Functionalization of as-synthesized mesoporous silica with a 3-aminopropyltrialkoxysilane. ASNCs were used to enable imaging of the functional group distribution by means of CLSM. The grafted amino groups were labeled with fluorescein isothiocyanate (FITC) and optical slices in the center of the particles were selected. Each row of CLSM images shows three particles, with the outermost right particle standing on its hexagonal base. The top row of the CLSM images indicates the distribution of the amino groups in the case of the frequently used precursor APTES (R = CH_2CH_3). Note that a significant amount of pore surface functionalization occurs. Selective functionalization of the external surface is obtained with APTMEES (R = $CH_2CH_2OCH_2CH_2OCH_3$), as apparent from the bottom row of CLSM images. The scheme on the left compares the size of the silanes with the pore size of the ASNCs.

The mesopores remained fully accessible for further modification after functionalization of the external surface with APTMEES (Figure 3). This method also works well for materials with pores larger than those of the ASNCs and has been tested for hexadecyltrimethyl-ammonium and block copolymer SDAs.[10]

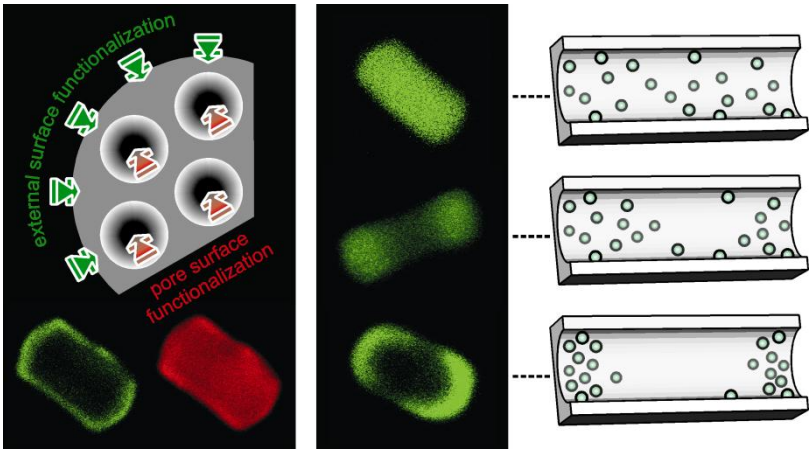

Fig. 3. Left: CLSM images of ASNCs after external surface functionalization with APTMEES and labeling with FITC, followed by reaction with APTES in ethanol and labeling with Texas Red (TR). The green image shows the luminescence of the FITC labels, whereas the red image was obtained upon excitation of the TR labels, indicating the excellent accessibility of the channels after external surface functionalization. Right: CLSM images of calcined ASNCs after functionalization with APTMEES in acetone, THF, toluene (top to bottom, particles are FITC-labeled) and schematic representation of the corresponding functional group distribution in the silica nanochannels. Note that the channels are in fact much longer (ca. 5 µm) compared to the pore diameter (3 nm). One particle contains approximately 200'000 nanochannels.

The technique of grafting to as-synthesized mesoporous silica (still containing the SDA) suffers from the disadvantage that the preferred method of SDA removal, i.e., calcination at temperatures around 500 °C, cannot be employed. The SDA needs to be extracted to conserve the functional groups, which often requires several steps to obtain a material that is free of residual SDA. We found that grafting of APTMEES from non-polar solvents produces a high degree of external surface functionalization even in the case of calcined materials with fully accessible pores. However, in contrast to grafting to as-synthesized mesoporous silica, the degree of external surface functionalization strongly depends on the pore diameter. Large pore diameters increase the degree of pore surface functionalization.[10]

3. Functionalization of the Pore Surface

Obtaining uniform distributions of functional groups by a postsynthetic approach is challenging. Co-condensation techniques are typically employed to achieve a homogeneous distribution over the entire mesoporous silica surface.[15] This requires a condensable precursor, often silanes of the type R'-Si$(OR)_3$, with the functionality R' being stable under the conditions of the mesoporous silica synthesis. The addition of organoalkoxysilanes to the synthesis mixture can have a pronounced effect on the pore structure and morphology of the

resulting mesoporous material. High functionalization degrees lead to decreasing mesoscopic order. Postsynthetic functionalization, on the other hand, offers possibilities for functional group placement and high surface concentration without compromising the mesoscopic order.[16] A simple procedure for conducting postsynthetic functionalization is the reaction of an organotrialkoxysilane R'-Si(OR)$_3$ with the surface silanol groups of the calcined mesoporous silica. Such reactions are typically performed in an organic solvent, often at elevated temperatures. Trace water needs to be avoided if a high uniformity of the functional group distribution is desired. We have observed that clustering of the silanes is promoted by the presence of water, leading to non-uniform distributions of the grafted amino groups with higher concentrations at the pore entrances. The accumulation of functional groups at the pore entrances in combination with cross-linking of the silanes eventually causes pore blocking. As a consequence, the central part of the channels (the pore body) becomes inaccessible.[11]
Particularly in the case of amino-functionalized silanes, it is reasonable to assume that polar solvents lead to increased mobility of the molecules on the mesoporous silica surface. This concept can for example be applied to control the site isolation of amino groups on mesoporous silica.[9,17] Using the deposition of APTMEES on ASNCs, we have investigated the influence of solvent polarity on the functional group distribution. The uniformity of the pore surface functionalization was found to increase with increasing solvent polarity. Interestingly, grafting of APTMEES from non-polar solvents led to external surface functionalization accompanied by an accumulation of functional groups on the pore surface close to the pore entrances. This feature is of particular interest for the installation of pore entrance gates.

4. Conclusions

For many applications of mesoporous silica, a controlled functional group placement is crucial. The functionalization of specific regions of the mesoporous silica surface (external surface, pore surface, pore entrances) forms an integral part of the concept of using these materials as drug delivery devices, sensors, or advanced adsorbents. CLSM is an ideal method to analyze the spatial distribution of functional groups on mesoporous silica and has allowed us to devise procedures for grafting to surface subsections or for producing functional group gradients. Considering the variety of pore and particle sizes in the mesopore range, it is obvious that the development of generally applicable methods for the selective functionalization of mesoporous silica surfaces remains a challenge. This is particularly true for mesoporous nanoparticles, where the differences in the accessibility of pore surface vs. external surface can become negligibly small.

Acknowledgment. This work has been financially supported by the Swiss National Science Foundation (Project 200020-117591) and by the European Commission through the Human Potential Programme (Marie-Curie RTN Nanomatch, Grant No. MRTN-CT-2006-035884).

References

[1] a) T. Yanagisawa, T. Shimizu, K. Kuroda, C. Kato, *Bull. Chem. Soc. Jpn.* **1990**, *63*, 988; b) C. T. Kresge, M. E. Leonowicz, W. J. Roth, J. C. Vartuli, J. S. Beck, *Nature* **1992**, *359*, 710; c) J. S. Beck, J. C. Vartuli, W. J. Roth, M. E. Leonowicz, C. T. Kresge, K. D. Schmitt, C. T.-W. Chu, D. H. Olson, E. W. Sheppard, S. B. McCullen, J. B. Higgins, J. L. Schlenker, *J. Am. Chem. Soc.* **1992**, *114*, 10834.

[2] a) A. Taguchi, F. Schüth, M*icroporous Mesoporous Mater.* **2005**, *77*, 1; b) J. H. Clark, D. J. Macquarrie, S. J. Tavener, *Dalton Trans.* **2006**, 4297.

[3] a) M. Vallet-Regí, F. Balas, D. Arcos, *Angew. Chem. Int. Ed.* **2007**, *46*, 7548; b) I. I. Slowing, J. L. Vivero-Escoto, C.-W. Wu, V. S.-Y. Lin, *Adv. Drug Deliv. Rev.* **2008**, *60*, 1278; c) K. T. Kim, S. A. Meeuwissen, R. J. M. Nolte, J. C. M. van Hest, *Nanoscale* **2010**, *2*, 844; d) M. Manzano, M. Vallet-Regí, *J. Mater. Chem.* **2010**, *20*, 5593.

[4] I. I. Slowing, B. G. Trewyn, S. Giri, V. S.-Y. Lin, *Adv. Funct. Mater.* **2007**, *17*, 1225.

[5] a) Y. Yang, X. Yan, Y. Cui, Q. He, D. Li, A. Wang, J. Fei, J. Li, *J. Mater. Chem.* **2008**, *18*, 5731; b) C.-P. Tsai, Y. Hung, Y.-H. Chou, D.-M. Huang, J.-K. Hsiao, C. Chang, Y.-C. Chen, C.-Y. Mou, *Small* **2008**, *4*, 186.

[6] a) G. E. Fryxell, S. V. Mattigod, Y. Lin, H. Wu, S. Fiskum, K. Parker, F. Zheng, W. Yantasee, T. S. Zemanian, R. S. Addleman, J. Liu, K. Kemner, S. Kelly, X. Feng, *J. Mater. Chem.* **2007**, *17*, 2863; b) H. Yoshitake, *J. Mater. Chem.* **2010**, *20*, 4537.

[7] a) N. K. Mal, M. Fujiwara, Y. Tanaka, *Nature* **2003**, *421*, 350; b) Q. Yang, S. Wang, P. Fan, L. Wang, Y. Di, K. Lin, F.-S. Xiao, *Chem. Mater.* **2005**, *17*, 5999; c) T. D. Nguyen, Y. Liu, S. Saha, K. C.-F. Leung, J. F. Stoddart, J. I. Zink, *J. Am. Chem. Soc.* **2007**, *129*, 626; d) M. Liong, S. Angelos, E. Choi, K. Patel, J. F. Stoddart, J. I. Zink, *J. Mater. Chem.* **2009**, *19*, 6251.

[8] H. Ritter, D. Brühwiler, *J. Phys. Chem. C* **2009**, *113*, 10667.

[9] H. Salmio, D. Brühwiler, *J. Phys. Chem. C* **2007**, *111*, 923.

[10] N. Gartmann, D. Brühwiler, *Angew. Chem. Int. Ed.* **2009**, *48*, 6354.

[11] N. Gartmann, C. Schütze, H. Ritter, D. Brühwiler, *J. Phys. Chem. Lett.* **2010**, *1*, 379.

[12] J. H. Ramm, N. Gartmann, D. Brühwiler, *J. Colloid Interf. Sci.* **2010**, *345*, 200.

[13] Y. Y. Kievsky, B. Carey, S. Naik, N. Mangan, D. ben-Avraham, I. Sokolov, *J. Chem. Phys.* **2008**, *128*, 151102.

[14] Y. Wan, D. Zhao, *Chem. Rev.* **2007**, *107*, 2821.

[15] F. Hoffmann, M. Cornelius, J. Morell, M. Fröba, *Angew. Chem. Int. Ed.* **2006**, *45*, 3216.

[16] a) D. Brühwiler, *Nanoscale* **2010**, *2*, 887; b) I. I. Slowing, J. L. Vivero-Escoto, B. G. Trewyn, V. S.-Y. Lin, *J. Mater. Chem.* **2010**, *20*, 7924.

[17] K. K. Sharma, A. Anan, R. P. Buckley, W. Ouellette, T. Asefa, *J. Am. Chem. Soc.* **2008**, *130*, 218.

5.3 The Effect of Water on the Functionalization of Mesoporous Silica with 3-Aminopropyltriethoxysilane

Nando Gartmann, Christina Schütze, Hanna Ritter, Dominik Brühwiler*

Institute of Inorganic Chemistry, University of Zurich, Winterthurerstrasse 190, 8057 Zurich, Switzerland

Journal of Physical Chemistry Letters **2010**, 1, 379-382

Abstract

The effect of water on the reaction of 3-aminopropyltriethoxysilane (APTES) with mesoporous silica is investigated on two model systems. A MCM-41 type material with a well-defined pore size is used to investigate changes in the pore size distribution upon reaction with APTES in toluene containing various amounts of water. It is found that with increasing amount of water, clustering of APTES occurs, leading to a non-uniform distribution of the grafted amino groups and a scarcely functionalized pore body. A second model system with defined particle morphology and one-dimensional channels is employed to visualize the distribution of the grafted amino groups by fluorescent labeling and confocal laser scanning microscopy. The combination of nitrogen sorption and confocal laser scanning microscopy provides valuable insights concerning the role of trace water in the functionalization of mesoporous silica with alkoxysilanes.

Postsynthetic functionalization by grafting of substituted trialkoxysilanes is one of the most popular methods for the modification of mesoporous silica. Aminopropylalkoxysilanes are frequently employed for this purpose, allowing subsequent reaction with a variety of functional groups, such as isothiocyanate or sulfonyl chloride. Amino-functionalized mesoporous silicas have further been investigated in terms of their potential applications in drug delivery,[1] catalysis,[2-6] and adsorption.[7,8] The identification of the parameters that control the distribution of the grafted amino groups has been the topic of recent publications. It has been shown that the polarity of the solvent used in the reaction of aminoalkyl-substituted alkoxysilanes with mesoporous silica has a pronounced influence on the distribution of the surface-anchored amino groups.[2,9] Water has been identified as one of the most important parameters in the reaction of trialkoxysilanes with silica surfaces. Excellent work has been carried out to identify possible binding modes of 3-aminopropyltriethoxysilane (APTES) on silica gel in dependence of surface water, leading to the conclusion that polymerization of APTES takes place on the silica surface after adsorption of the silane molecules.[10,11] In the case of mesoporous silica, one can assume that the polymerization of APTES on the pore surface affects the diffusion of further silane molecules and therefore determines the final distribution of the grafted functional groups.

Acquiring information on the distribution of functional groups on mesoporous silica is challenging and generally requires a comparative investigation of the nitrogen sorption isotherms.[12,13] Inspired by results obtained from the analysis of the spatial distribution of fluorescent guests in zeolites,[14,15] we have combined the nitrogen sorption based analysis with confocal laser scanning microscopy (CLSM).

The investigation of the functional group distribution by means of nitrogen sorption requires a starting material with a pore size distribution that is as narrow as possible, allowing the identification of subtle differences in the sorption isotherms upon functionalization. Our MCM-41 sample fulfils this condition and we have previously used this type of material for the study of functional group distributions.[12] However, the morphology of this particular MCM-41 sample is irregular and therefore not suitable for CLSM, which requires relatively large particles of defined morphology. Hexagonal particles (arrays of silica nanochannels, ASNCs)[16] are ideal for this purpose (Figure 1, Table 1).

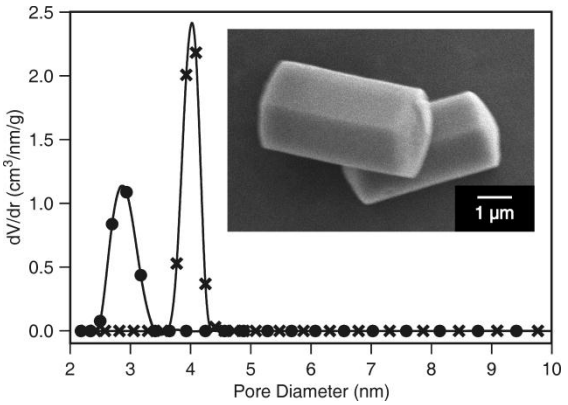

Figure 1. Pore size distributions of MCM-41 (crosses) and ASNCs (circles). The inset shows a scanning electron microscopy image of ASNCs.

Table 1. Structural properties of the parent materials.

sample	d_{NLDFT} [a] [nm]	S_{BET} [b] [m^2/g]	S_{Ext} [c] [m^2/g]	V_{tot} [d] [cm^3/g]
MCM-41	4.1	1014	78	0.86
ASNCs	2.9	1120	37	0.62

[a] pore diameter calculated by NLDFT
[b] total BET surface area
[c] external particle surface area
[d] total pore volume

Starting from calcined MCM-41, we have prepared amino-functionalized samples by grafting APTES in toluene containing different amounts of water (Table 2). Amounts of water corresponding to 0.5, 1, and 2 theoretical monolayer(s) were used, taking into account that one water molecule occupies 0.106 nm^2 in an adsorbed monolayer.[17] A comparison of the pore size distribution and the amino group content of the products provides insight into the effect of water on the grafting behavior. While the amount of grafted amino groups is largely independent of the amount of water in the reaction mixture, the pore size distribution is clearly affected (Figure 2). As expected, the sample prepared in dry toluene, M-0, features a narrow and symmetrical pore size distribution. Samples prepared with additional water, on the other hand, feature an increasing contribution of larger pores, suggesting a less uniform distribution of the amino groups.

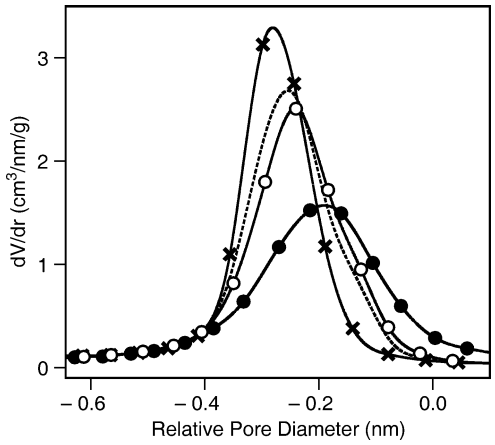

Figure 2. Pore size distributions of M-0 (crosses), M-0.5 (dashed line), M-1 (empty circles), and M-2 (full circles). The pore diameter is given relative to the maximum of the pore size distribution of the unmodified material.

Table 2. Amino-functionalized materials.

sample	silica	APTES [mmol/g]	H_2O [monolayer]	$-NH_2$ [a] [mmol/g]	FITC [b] [mmol/g]
M-0	MCM-41	0.40	0	0.36	-
M-0.5	MCM-41	0.40	0.5	0.36	-
M-1	MCM-41	0.40	1	0.35	-
M-2	MCM-41	0.40	2	0.34	-
A-0	ASNCs	0.40	0	0.36	0.11
A-1	ASNCs	0.40	1	0.37	0.11
A-2	ASNCs	0.40	2	0.36	0.08
A-0.1-2	ASNCs	0.10	2	0.10	0.02

[a] experimentally determined amount of grafted amino groups

[b] experimentally determined amount of coupled FITC

From studies of the reaction of APTES with silica gel it is known that surface water promotes the interaction of the amino groups with the surface, partially by proton transfer from the surface silanols to the amino moieties and subsequent electrostatic interaction.[18] The resulting orientation of the amino groups towards the silica surface provides accessible triethoxysilyl moieties for cross-linking, ultimately leading to the formation of clusters. The presence of such clusters can render pores partially inaccessible for additional APTES molecules, thus resulting in a non-uniform distribution of the grafted amino groups. It should be noted that despite APTES clustering, the pores are still accessible for nitrogen molecules, leading to the detection of larger pores in materials functionalized in the presence of water. Pore volumes of the amino-functionalized materials were found to be largely independent of the presence of water in the reaction mixture. This is in agreement with the almost equal amounts of surface-anchored amino groups in the functionalized MCM-41 samples (Table 2).

The distribution of amino groups on mesoporous silica can be imaged by CLSM after fluorescent labeling, provided that the particles are large and of well defined morphology.[9] ASNCs are ideal for this purpose. The pore openings of the ASNCs are located at the hexagonal bases and the channels run parallel to the long axis of the particles.[19] Figure 3 shows CLSM images of APTES-functionalized ASNCs after labeling with fluorescein isothiocyanate (FITC). Particles functionalized in the presence of an amount of water equivalent to one monolayer show only minor differences compared to particles prepared under dry conditions. Despite the fact that particles with spatially non-uniform luminescence can be found (e.g. particle #3 of A-1, Figure 3), clustering of APTES is obviously not sufficiently severe to cause inhomogeneities that are detectable with our CLSM setup. However, increasing the amount of water to two monolayers clearly causes an accumulation of labeled amino groups at the pore entrances. We can conclude that in this case, clustering of APTES in the channels leads to pore blocking. It should be noted that based on the CLSM images of A-2, we cannot exclude the presence of amino groups in the center of the channels, as they might have been rendered inaccessible for FITC labeling. However, taking into consideration the results of the analysis by nitrogen sorption, there is evidence for a pronounced gradient of the density of grafted amino groups, with higher density at the channel entrances and scarcely functionalized channel centers. The observation that A-2 binds less FITC than A-1 and A-0 (Table 2) can be explained by the presence of closely spaced amino groups and partial pore blocking in A-2.

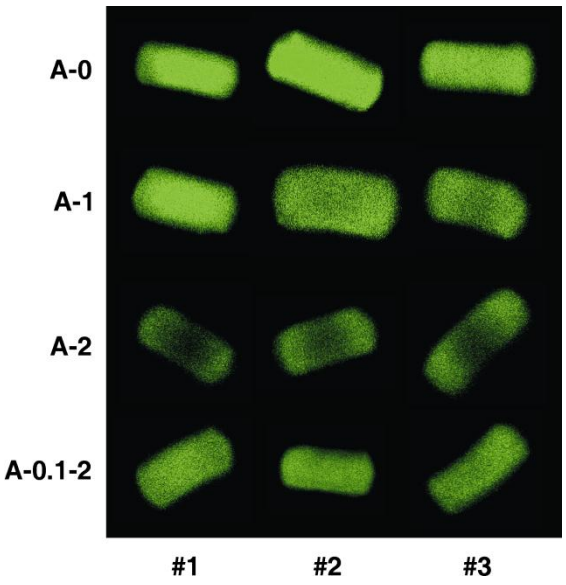

Figure 3. CLSM images of ASNCs after functionalization with APTES in toluene under dry conditions (A-0), and in the presence of water equivalent to one (A-1) or two (A-2) monolayers. Sample A-0.1-2 was prepared in the presence of an amount of water equivalent to two monolayers, but with a four times lower amino content. Three particles are shown for each reaction condition. Optical slices in the center of the particles were selected. The length of the particles is approximately 5 µm.

An interesting question that needs to be considered is whether water adsorbed in the channels could hinder the penetration of APTES. Assuming that this would be the case, we would expect to see a non-uniform distribution of labeled amino groups even for low amino contents. However, Figure 3 (sample A-0.1-2) shows that a reduction of the amino content leads to an uniform distribution of the coupled FITC labels, even in the presence of water. In fact, it seems that at this low APTES concentration, clusters cannot grow large enough to significantly affect the diffusion of FITC through the channels.

Based on the CLSM images given for samples A-0, A-1, and A-2, one could further speculate that an increased reactivity of APTES in the presence of water leads to preferential grafting to the most accessible sites, namely those on the external particle surface and on the pore surface close to the channel entrances. Such a hypothesis is largely based on the observation that the silanol groups of the hydrolyzed silanes react faster with the silica surface than the alkoxysilane groups.[20,21] Considering the uniform functional group distribution obtained for sample A-0.1-2, we can, however, exclude this possibility.

The combination of nitrogen sorption and CLSM imaging for the analysis of fluorescence-labeled functionalized mesoporous silica provides insights into the parameters that govern the distribution of the grafted functional groups. While we have focused on the role of water in the deposition of APTES from toluene, a variety of further parameters, such as solvent polarity, temperature, or the presence of co-adsorbed species other than water, can be thought of in terms of their influence on the grafting process. From the present study, we can conclude that clustering of APTES in mesopores is promoted by the presence of water and eventually leads to pore blocking and non-uniform distributions of functional groups with higher grafting densities at the pore entrances. Clustering of organosilanes on the pore surface close to the pore openings is a process that is not desirable for most applications of functionalized mesoporous silica. There are, however, instances where a high local concentration of cross-linked organosilanes at the pore entrances might in fact be useful. mesoporous silica based drug delivery devices often require the functionalization of the pore entrances to install a gating mechanism.[22-24] Having multiple, closely spaced anchoring points with some degree of vertical polymerization might facilitate the stable attachment of the gatekeepers.

Experimental Methods

MCM-41 was synthesized as described in reference 12. Arrays of silica nanochannels (ASNCs) were prepared according to a method reported by Kievsky and Sokolov.[16] Samples were stored at 80 °C after calcination. Postsynthetic modify-cation was performed as follows: Calcined mesoporous silica was dispersed in dry toluene (containing less than 0.005 % of H_2O, Fluka, puriss., absolute, stored over molecular sieve). After a few seconds of ultrasonication, a calculated amount of de-ionized H_2O was added and the suspen-sion was again briefly ultrasonicated be-fore being stirred for 1 h at room tempera-ture. Finally, 0.10 or 0.40 mmol of 3 ami-nopropyltriethoxysilane (APTES, Fluka,

≥ 98.0 %) per gram of silica was added, and the mixture was stirred for 3 h at 80 °C. The product was recovered by filtration, washed with ethanol, and dried in a vacuum. Labeling with fluorescein 5-isothiocyanate (FITC, Fluka, ≥ 97.5 %) was carried out according to reference 12, with a coupling time of 24 h at room temperature (in absolute ethanol).

The amount of surface-grafted amino groups was analyzed by the fluorogenic derivatization reaction with fluorescamine.[25] In the investigated range of amino contents, the average relative error of this analysis method is typically below 10 %.[13] The amount of coupled fluorescein was determined by dissolving the sample in a 0.2 M aqueous solution of NaOH and measuring the UV-vis absorption spectrum of the resulting clear solution. An extinction coefficient of 75000 $M^{-1}cm^{-1}$ (at λ_{max} = 490 nm) was used for the calculations.[13] Nitrogen sorption isotherms were collected at 77 K using a Quantachrome NOVA 2200. Samples were vacuum-degassed at 80 °C for 3 h. The total surface area S_{BET} was obtained using the standard BET method for adsorption data in a relative pressure range from 0.05 to 0.20.[26] The total pore volume V_{tot} was calculated from the amount of nitrogen adsorbed at a relative pressure of 0.95. The external surface area S_{Ext} was determined from the linear part of the α_S-plot (α_S > 1).[27] Mesopore size distributions of the functionalized samples were evaluated from the desorption branches of the nitrogen isotherms by means of the BJH method.[28] All MCM-41 samples exhibited type IV isotherms, and condensation in the primary mesopores was not accompanied by hysteresis. The average pore diameter and pore size distribution of the parent materials was calculated from the respective adsorption isotherms by means of a NLDFT model developed for silica exhibiting cylindrical pore geometry (NOVAWin2 software, Version 2.2, Quantachrome Instruments).[29] Scanning electron microscopy images were acquired on a JEOL JSM-6060. The CLSM setup consisted of a Olympus BX 60 microscope with a FluoView confocal unit. The FITC-labeled samples were excited at 488 nm.

Acknowledgment. Financial support was provided by the European Commission through the Human Potential Program (Marie-Curie RTN Nanomatch, Grant No. MRTN-CT-2006-035884) and by the Swiss National Science Foundation (Project 200020-117591).

References

1. Balas, F.; Manzano, M.; Horcajada, P.; Vallet-Regi, M. Confinement and Controlled Release of Bisphosphonates on Ordered Mesoporous Silica-Based Materials. *J. Am. Chem. Soc.* **2006**, *128*, 8116-8117.

2. Sharma, K. K.; Anan, A.; Buckley, R. P.; Ouellette, W.; Asefa, T. Toward Efficient Nanoporous Catalysts: Controlling Site-Isolation and Concentration of Grafted Catalytic Sites on Nanoporous Materials with Solvents and Colorimetric Elucidation of Their Site-Isolation. *J. Am. Chem. Soc.* **2008**, *130*, 218-228.

3. Sharma, K. K.; Asefa, T. Efficient Bifunctional Nanocatalysts by Simple Postgrafting of Spatially Isolated Catalytic Groups on Mesoporous Materials. *Angew. Chem. Int. Ed.* **2007**, *46*, 2879-2882.

4. Wang, X.; Lin, K. S. K.; Chan, J. C. C.; Cheng, S. Direct Synthesis and Catalytic Applications of Ordered Large Pore

Aminopropyl-Functionalized SBA-15 Mesoporous Materials. *J. Phys. Chem. B* **2005**, *109*, 1763-1769.

5. Macquarrie, D. J.; Jackson, D. B. Aminopropylated MCMs as Base Catalysts: A Comparison with Aminopropylated Silica. *Chem. Commun.* **1997**, 1781-1782.

6. Cauvel, A.; Renard, G.; Brunel, D. Monoglyceride Synthesis by Heterogeneous Catalysis Using MCM-41 Type Silicas Functionalized with Amino Groups. *J. Org. Chem.* **1997**, *62*, 749-751.

7. Liu, A. M.; Hidajat, K.; Kawi, S.; Zhao, D. Y. A New Class of Hybrid Mesoporous Materials with Functionalized Organic Monolayers for Selective Adsorption of Heavy Metal Ions. *Chem. Commun.* **2000**, 1145-1146.

8. Han, Y.-J.; Stucky, G. D.; Butler, A. Mesoporous Silicate Sequestration and Release of Proteins. *J. Am. Chem. Soc.* **1999**, *121*, 9897-9898.

9. Gartmann, N.; Brühwiler, D. Controlling and Imaging the Functional-Group Distribution on Mesoporous Silica. *Angew. Chem. Int. Ed.* **2009**, *48*, 6354-6356.

10. Vrancken, K. C.; Van Der Voort, P.; Gillis-D'Hamers, I.; Vansant, E. F.; Grobet, P. Influence of Water in the Reaction of γ-aminopropyltriethoxysilane with Silica Gel. A Fourier-Transform Infrared and Cross-Polarisation Magic-Angle-Spinning Nuclear Magnetic Resonance Study. *J. Chem. Soc., Faraday Trans.* **1992**, *88*, 3197-3200.

11. Kallury, K. M. R.; Macdonald, P. M.; Thompson, M. Effect of Surface Water and Base Catalysis on the Silanization of Silica by (Aminopropyl)alkoxysilanes Studied by X-ray Photoelectron Spectroscopy and ^{13}C Cross-Polarization/Magic Angle Spinning Nuclear Magnetic Resonance. *Langmuir* **1994**, *10*, 492-499.

12. Salmio, H.; Brühwiler, D. Distribution of Amino Groups on a Mesoporous Silica Surface after Submonolayer Deposition of Aminopropylsilanes from an Anhydrous Liquid Phase. *J. Phys. Chem. C* **2007**, *111*, 923-929.

13. Ritter, H.; Brühwiler, D. Accessibility of Amino Groups in Postsynthetically Modified Mesoporous Silica. *J. Phys. Chem. C* **2009**, *113*, 10667-10674.

14. Megelski, S.; Lieb, A.; Pauchard, M.; Drechsler, A.; Glaus, S.; Debus, C.; Meixner, A. J.; Calzaferri, G. Orientation of Fluorescent Dyes in the Nano Channels of Zeolite L. *J. Phys. Chem. B* **2001**, *105*, 25-35.

15. Pauchard, M.; Huber, S.; Méallet-Renault, R.; Maas, H.; Pansu, R.; Calzaferri, G. Time- and Space-Resolved Luminescence of a Photonic Dye-Zeolite Antenna. *Angew. Chem. Int. Ed.* **2001**, *40*, 2839-2842.

16. Kievsky, Y.; Sokolov, I. Self-Assembly of Uniform Nanoporous Silica Fibers. *IEEE Trans. Nanotechnol.* **2005**, *4*, 490-494.

17. Baker, F. S.; Sing, K. S. W. Specificity in the Adsorption of Nitrogen and Water on Hydroxylated and Dehydroxylated Silicas. *J. Colloid Interface Sci.* **1976**, *55*, 605-613.

18. Caravajal, G. S.; Leyden, D. E.; Quinting, G. R.; Maciel, G. E. Structural Characterization of (3-Aminopropyl)triethoxysilane-Modified Silicas by Silicon-29 and Carbon-13 Nuclear Magnetic Resonance. *Anal. Chem.* **1988**, *60*, 1776-1786.

19. Kievsky, Y. Y.; Carey, B.; Naik, S.; Mangan, N.; ben-Avraham, D.; Sokolov, I. Dynamics of Molecular Diffusion of Rhodamine 6G in Silica Nanochannels. *J. Chem. Phys.* **2008**, *128*, 151102.

20. Assink, R. A.; Kay, B. D. Sol-Gel Kinetics. I. Functional Group Kinetics. *J. Non-Cryst. Sol.* **1988**, *99*, 359-370.

21. Luechinger, M.; Prins, R.; Pirngruber, G. D. Functionalization of Silica Surfaces with Mixtures of 3-aminopropyl and Methyl Groups. M*icroporous Mesoporous Mater.* **2005**, *85*, 111-118.

22. Mal, N. K.; Fujiwara, M.; Tanaka, Y. Photocontrolled Reversible Release of Guest Molecules from Coumarin-modified Mesoporous Silica. *Nature* **2003**, *421*, 350-353.

23. Lai, C.-Y.; Trewyn, B. G.; Jeftinija, D. M.; Jeftinija, K.; Xu, S.; Jeftinija, S.; Lin, V. S.-Y. A Mesoporous Silica Nanosphere-Based Carrier System with Chemically Removable CdS Nanoparticle Caps for Stimuli-Responsive Controlled Release of Neurotransmitters and Drug Molecules. *J. Am. Chem. Soc.* **2003**, *125*, 4451-4459.

24. Hernandez, R.; Tseng, H.-R.; Wong, J. W.; Stoddart, J. F.; Zink, J. I. An Operational Supramolecular Nanovalve. *J. Am. Chem. Soc.* **2004**, *126*, 3370-3371.

25. Ritter, H.; Nieminen, M.; Karppinen, M.; Brühwiler, D. A Comparative Study of the Functionalization of Mesoporous Silica MCM-41 by Deposition of 3-aminopropyl-trimethoxysilane from Toluene and from the Vapor Phase. M*icroporous Mesoporous Mater.* **2009**, *121*, 79-83.

26. Brunauer, S.; Emmett, P. H.; Teller, E. Adsorption of Gases in Multimolecular Layers. *J. Am. Chem. Soc.* **1938**, *60*, 309-319.

27. Kruk, M.; Jaroniec, M.; Ryoo, R.; Kim, J. M. Monitoring of the Structure of Siliceous Mesoporous Molecular Sieves Tailored Using Different Synthesis Conditions. M*icroporous Mater.* **1997**, *12*, 93-106.

28. Barrett, E. P.; Joyner, L. G.; Halenda, P. P. The Determination of Pore Volume and Area Distributions in Porous Substances. I. Computations from Nitrogen Isotherms. *J. Am. Chem. Soc.* **1951**, *73*, 373-380.

29. Ravikovitch, P. I.; Domhnaill, S. C. O.; Neimark, A. V.; Schüth, F.; Unger, K. K. Capillary Hysteresis in Nanopores: Theoretical and Experimental Studies of Nitrogen Adsorption on MCM-41. *Langmuir* **1995**, *11*, 4765-4772.

5.4 Correlation of Nitrogen Sorption and Confocal Laser Scanning Microscopy for the Analysis of Amino Group Distributions on Mesoporous Silica

Nando Gartmann and Dominik Brühwiler*

Institute of Inorganic Chemistry, University of Zurich, Winterthurerstrasse 190, 8057 Zurich, Switzerland

Materials **2011**, 4, 1096-1103

Abstract

Aminopropylalkoxysilanes are frequently used for the functionalization of mesoporous silica. The analysis of amino group distributions on arrays of silica nanochannels by a combination of nitrogen sorption and confocal laser scanning microscopy provides valuable insight into the mechanisms underlying the interaction of these silanes with mesoporous silica surfaces. Tendencies towards external surface functionalization, non-uniform distribution in the pores, and hydrolysis of the silica framework are shown to depend to a large extent on the mobility of the aminopropylalkoxysilane molecules, which can be adjusted by the number and type of alkoxy groups.

1. Introduction

In the early 1990s, the synthesis of highly ordered mesoporous silica was first reported [1-3]. The following years saw further development towards providing a wide range of pore sizes and morphologies. Progress has been remarkable, leading to a rich palette of structure-directing agents (SDAs) and synthetic pathways [4,5]. The number of scientific publications on the topic of mesoporous silica literally exploded, mainly due to potential applications of these materials in fields as diverse as drug delivery [6,7] and catalysis [8]. Many of these applications require functionalization of the mesoporous silica, which is often conducted postsynthetically, for example by reaction with an alkoxysilane. In this context, interesting questions concerning the location of the functional groups on the mesoporous silica surface arise [9-11].

To investigate the parameters that affect the distribution of functional groups on mesoporous silica, we have been focusing on aminopropylalkoxysilanes, as they are among the most frequently employed reagents for the modification of mesoporous silica. Once the amines are anchored, a further moiety can be coupled by means of amine-reactive derivatives. This concept is especially useful for the visualization of functional group distributions by confocal laser scanning microscopy (CLSM), as it opens possibilities for fluorescent labeling [12-14]. Arrays of silica nanochannels (ASNCs) [15] fulfill the conditions required for the analysis of functional group distributions by CLSM and by nitrogen sorption, as the large, regularly shaped particles feature a comparatively narrow pore size distribution. The combined analysis by CLSM (single particle) and nitrogen sorption (ensemble) is particularly instructive concerning the interpretation of changes in pore size and pore volume upon surface functionalization. Not less importantly, it shows that an exclusive characterization by one of these two methods might lead to conclusions that are misleading.

2. Results and Discussion

ASNCs are hexagonally shaped fibers, each consisting of approximately 200'000 parallel nanochannels that run along the entire length of the particles [16]. As a consequence, the mesopore structure of ASNCs can be considered as a set of open-ended, non-intersecting cylinders. Calculation of the pore diameter from the adsorption isotherm by means of the BJH method [17] gives an average value of 2.02 nm. Whereas the standard BJH analysis is known to underestimate the pore size [18], a more reliable value of 3.06 nm is obtained by employing a non-local density functional theory (NLDFT) model (Figure 1) [19]. As the NLDFT kernel is not strictly valid for organo-functionalized silica surfaces, BJH was used to investigate the relative pore size changes upon grafting of the aminopropylalkoxysilanes. It should be noted that the structural properties of ASNCs (BET surface area, pore volume, pore diameter) show slight variation from batch to batch. For comparative studies such as the present one, it is therefore crucial to perform experiments with the same parent material.

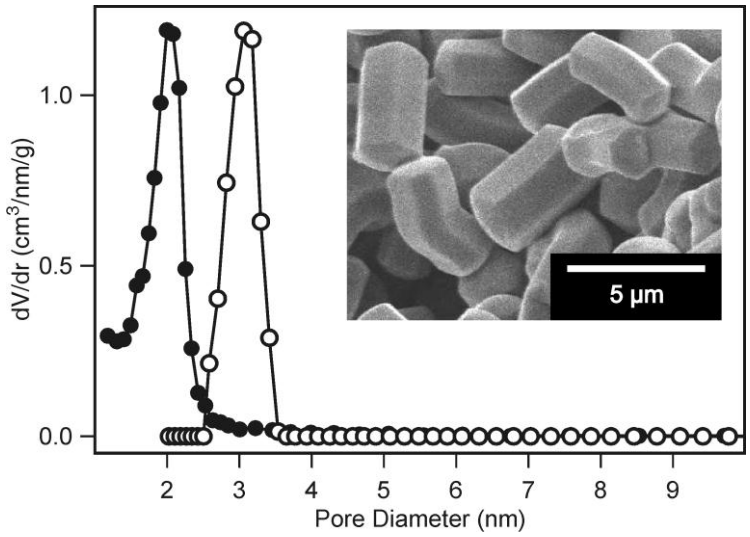

Figure 1. Pore size distributions of ASNCs calculated from the nitrogen adsorption isotherm by BJH (●) and NLDFT (○). The inset shows a SEM image of calcined ASNCs.

We have compared the grafting behavior of various aminopropylalkoxysilanes (Figure 2) by depositing an identical molar amount of each silane onto ASNCs from toluene at room temperature. The samples were labeled with fluorescein isothiocyanate (FITC) and imaged by CLSM. Structural properties of the materials are given in Table 1. CLSM images of the FITC-labeled materials along with the pore size distributions of the amino-functionalized samples are shown in Figure 3. In all experiments, the grafting behavior of APDIPES was found to be very similar to that of APDMMS. For brevity, only the results for APDMMS are shown.

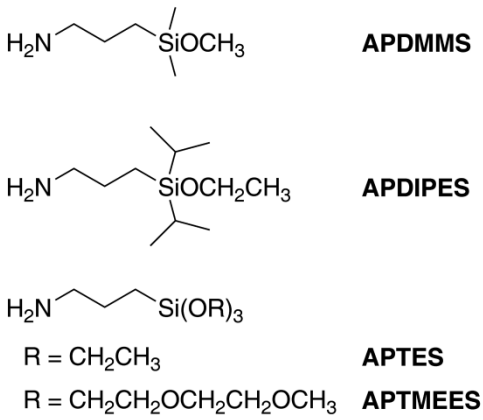

Figure 2. Structures and abbreviations of the employed aminopropylalkoxysilanes: 3-aminopropyldimethyl-methoxysilane (APDMMS), 3-aminopropyldiisopropylethoxysilane (APDIPES), 3-aminopropyltriethoxysilane (APTES), and 3-aminopropyltris(methoxyethoxyethoxy)silane (APTMEES).

	S_{BET} [m^2/g]	V_{tot} [cm^3/g]
parent	1170	0.72
APDMMS	865	0.44
APTES	987	0.61
APTMEES	1115	0.69

Table 1. BET surface area (S_{BET}) and pore volume (V_{tot}) of parent and amino-functionalized ASNCs

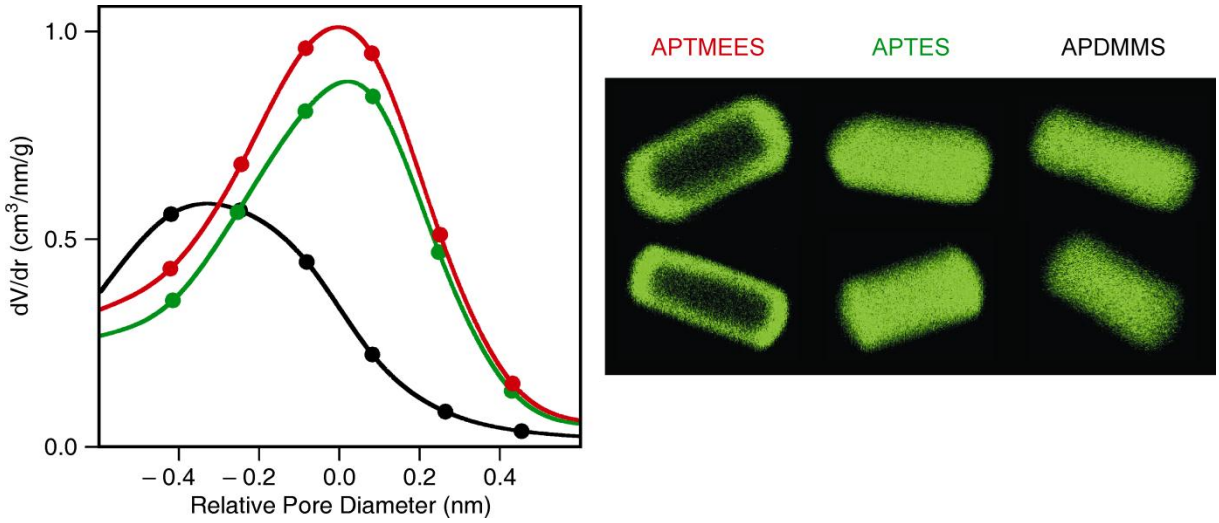

Figure 3. Representative CLSM images (after FITC labeling) of ASNCs functionalized with different aminopropylalkoxysilanes and the pore size distributions of the respective amino-functionalized materials relative to the pore diameter of the parent material: APTMEES (red), APTES (green), and APDMMS (black). The length of the particles in the CLSM images is in the order of 5 µm. Two particles are shown for each silane. Optical slices in the center of the particles were selected.

Deposition of APTMEES causes only a minor decrease of the pore volume, pore diameter, and BET surface area (Table 1, Figure 3). This is commonly interpreted as being a consequence of external surface functionalization. Indeed, CLSM images of the fluorescent-labeled samples confirm this interpretation and are in agreement with previously reported results [12].

In the case of APTES, pore volume and BET surface area are significantly reduced upon deposition, suggesting derivatization of the pore surface. The corresponding CLSM images support this conclusion by showing fluorescence over the entire length of the particles. It is interesting to note that the maximum of the pore size distribution of the APTES-functionalized sample remains at a pore size value similar to that of the parent material. This typically indicates a non-uniform distribution of the grafted moieties in the pores, with the pore body having a lower functionalization degree than the pore surface close to the pore entrances. For APTES, however, this effect does not seem to be pronounced enough to become visible in the CLSM images.

To our surprise, deposition of APDMMS strongly reduced the BET surface area, pore volume, and pore diameter. This could be interpreted as a homogeneous distribution of the grafted amino groups over the entire pore surface. While such an assumption is supported by the corresponding CLSM images, as well as by the fact that monoalkoxysilanes are known to produce more uniform distributions than trialkoxysilanes [20], the effect is rather large for the comparatively low grafting densities investigated in this work. Fluorescamine analysis yielded an amino content of 50 µmol/g after deposition of APDMMS. This corresponds roughly to 1200 amino groups per nanochannel or 0.025 amino groups per nm^2.

To gain insight into the mechanisms leading to the pronounced pore size reduction observed for APDMMS, we conducted blind experiments by replacing APDMMS with n-hexylamine. This allowed us to focus on possible effects of the amino group in the absence of covalent bond formation. As expected, the final product only contained negligible amounts of amino groups (less than 2 µmol/g) after washing with ethanol and 0.4 M aqueous HCl to remove the electrostatically adsorbed n-hexylamine molecules. Surprisingly, despite being a non-functionalized product, the pore size distribution after removal of n-hexylamine is shifted towards smaller pore size (Figure 4), indicating a partial hydrolysis of the silica framework. The fact that this effect was only observed for n-hexylamine, APDIPES, and APDMMS, points to the important role of the mobility of the respective amine. Our samples most likely contained a certain amount of trace water. When depositing silanes from solution, trace water is generally difficult to eliminate, as silica behaves as an efficient drying agent, adsorbing even minute quantities of water [21]. Under our conditions used for grafting, we can expect these adsorbed water molecules to be immobile and localized [22,23]. Hydrolysis of the silica framework is therefore only promoted if the amine is sufficiently mobile. APTMEES molecules react with silanol groups on the external surface and are quickly immobilized, leaving the mesoporous silica framework intact. From this set of experiments we can conclude that the high mobility of APDMMS and APDIPES leads to uniform distributions of grafted amino groups, but also causes partial hydrolysis of the silica framework.

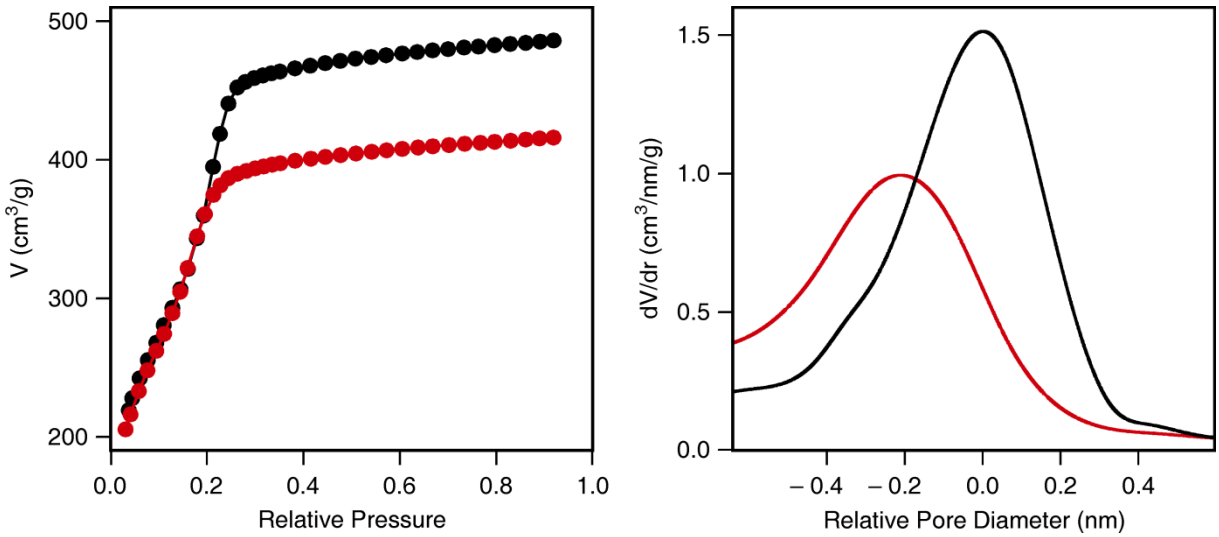

Figure 4. Nitrogen adsorption isotherms (left) and corresponding pore size distributions (right) of ASNCs before (black) and after deposition and removal of n-hexylamine (red).

3. Experimental Section

3.1. Arrays of Silica Nanochannels

ASNCs were synthesized according to a published procedure [15]. However, as our comparative studies require larger batches of starting material, the procedure was upscaled by a factor of 3. Briefly, an amount of 14.55 g of hexadecyltrimethylammonium chloride (Acros, 99 %) was dissolved in 228 ml of double distilled H_2O and 180 ml of 32 % aqueous HCl by stirring for 1 min at ca. 1000 rpm in a polypropylene beaker. The solution was subsequently

cooled to 0 °C for 15 min without stirring, followed by the slow addition of 6 ml of cold tetraethoxysilane (Aldrich, 99.999 %) and further stirring for 30 s. The resulting mixture was kept at 0 °C under quiescent conditions for 3 h. The product was collected by filtration and washed with H_2O. The SDA was removed by first heating at 300 °C for 2 h and calcining at 550 °C for 12 h. Heating rates of 2 °C/min were applied.

3.2. Functionalization

Reactions of aminopropylalkoxysilanes with ASNCs were conducted by dispersing 200 mg of ASNCs in 10 ml of dry toluene and subsequently adding 20 µmol of the respective silane. After the mixture had been stirred for 10 min at room temperature, the functionalized ASNCs were recovered by filtration and cured in an oven at 80 °C for 16 h.

3.3. Characterization

Labeling with fluorescein 5-isothiocyanate (FITC, Fluka, ≥ 97.5 %) was carried out according to reference 20, with a coupling time of 24 h at room temperature (in absolute ethanol). The amount of surface-grafted amino groups was analyzed by the fluorogenic derivatization reaction with fluorescamine [24]. Nitrogen sorption isotherms were collected at 77 K using a Quantachrome NOVA 2200. Samples were vacuum-degassed at 80 °C for 3 h. The total surface area S_{BET} was obtained using the standard BET method for adsorption data in a relative pressure range from 0.05 to 0.10 [25]. The total pore volume V_{tot} was calculated from the amount of nitrogen adsorbed at a relative pressure of 0.95. The relative changes of the mesopore size distributions upon functionalization were evaluated by analyzing the adsorption isotherms by means of the BJH model [17]. A NLDFT model developed for silica exhibiting cylindrical pore geometry (NOVAWin2 software, Version 2.2, Quantachrome Instruments) was employed to characterize the parent materials [19]. Scanning electron microscopy images were acquired on a JEOL JSM-6060. The CLSM setup consisted of a Olympus BX 60 microscope with a FluoView confocal unit. The FITC-labeled samples were excited at 488 nm. Optical slices in the center of the particles were selected.

4. Conclusions

The characterization of porous materials by nitrogen sorption is a standard technique to obtain information on BET surface area, pore volume, and pore diameter. When investigating the outcome of grafting reactions, the interpretation of the respective data in terms of the location of the grafted moieties is often difficult and results tend to be ambiguous. We have shown that complementing nitrogen sorption with CLSM imaging greatly facilitates the interpretation of pore structure data. The combination of nitrogen sorption and CLSM paints a comprehensive picture of the distribution of the amino groups on ASNCs after functionalization with various aminopropylalkoxysilanes. Tendencies towards external surface functionalization, non-uniform distribution in the pores, and hydrolysis of the silica framework can be identified and were shown to depend to a large extent on the mobility of the respective aminopropylalkoxysilane molecules.

Acknowledgments

Financial support was provided by the European Commission through the Human Potential Program (Marie-Curie RTN Nanomatch, Grant No. MRTN-CT-2006-035884) and by the Swiss National Science Foundation (Project 200020-117591).

References and Notes

1. Beck, J.S.; Vartuli, J.C.; Roth, W.J.; Leonowicz, M.E.; Kresge, C.T.; Schmitt, K.D.; Chu, C.T.-W.; Olson, D.H.; Sheppard, E.W.; McCullen, S.B.; Higgins, J.B.; Schlenker, J.L. A new family of mesoporous molecular sieves prepared with liquid crystal templates. *J. Am. Chem. Soc.* **1992**, *114*, 10834-10843.
2. Kresge, C.T.; Leonowicz, M.E.; Roth, W.J.; Vartuli, J.C.; Beck, J.S. Ordered mesoporous molecular sieves synthesized by a liquid-crystal template mechanism. *Nature* **1992**, *359*, 710-712.
3. Yanagisawa, T.; Shimizu, T.; Kuroda, K.; Kato, C. The preparation of alkyltrimethylammonium-kanemite complexes and their conversion to microporous materials. *Bull. Chem. Soc. Jpn.* **1990**, *63*, 988-992.
4. Wan, Y.; Zhao, D. On the controllable soft-templating approach to mesoporous silicates. *Chem. Rev.* **2007**, *107*, 2821-2860.
5. Meynen, V.; Cool, P.; Vansant, E.F. Verified syntheses of mesoporous materials. *Microporous Mesoporous Mater.* **2009**, *125*, 170-223.
6. Vallet-Regí, M.; Balas, F.; Arcos, D. Mesoporous materials for drug delivery. *Angew. Chem. Int. Ed.* **2007**, *46*, 7548-7558.
7. Slowing, I.I.; Vivero-Escoto, J.L.; Wu, C.-W.; Lin, V.S.-Y. Mesoporous silica nanoparticles as controlled release drug delivery and gene transfection carriers. *Adv. Drug Delivery Rev.* **2008**, *60*, 1278-1288.
8. Taguchi, A.; Schüth, F. Ordered mesoporous materials in catalysis. *Microporous Mesoporous Mater.* **2005**, 77, 1-45.
9. Brühwiler, D. Postsynthetic functionalization of mesoporous silica. *Nanoscale* **2010**, *2*, 887-892.
10. Yoshitake, H. Design of functionalization and structural analysis of organically-modified siliceous oxides with periodic structures for the development of sorbents for hazardous substances. *J. Mater. Chem.* **2010**, *20*, 4537-4550.
11. Gartmann, N.; Brühwiler, D. Functional group distributions on mesoporous silica. *Chimia* **2011**, *65*, 250-252.
12. Gartmann, N.; Brühwiler, D. Controlling and imaging the functional-group distribution on mesoporous silica. *Angew. Chem. Int. Ed.* **2009**, *48*, 6354-6356.
13. Blum, C.; Cesa, Y.; Escalante, M.; Subramaniam, V. Multimode microscopy: spectral and lifetime imaging. *J. R. Soc. Interface* **2009**, *6*, S35-S43.
14. Pauchard, M.; Huber, S.; Méallet-Renault, R.; Maas, H.; Pansu, R.; Calzaferri, G. Time- and space-resolved luminescence of a photonic dye-zeolite antenna. *Angew. Chem. Int. Ed.* **2001**, *40*, 2839-2842.
15. Kievsky, Y.; Sokolov, I. Self-assembly of uniform nanoporous silica fibers. *IEEE Trans. Nanotechnol.* **2005**, *4*, 490-494.
16. Kievsky, Y.; Carey, B.; Naik, S.; Mangan, N.; ben-Avraham, D.; Sokolov, I. Dynamics of molecular diffusion of rhodamine 6G in silica nanochannels. *J. Chem. Phys.* **2008**, *128*, 151102.

17. Barrett, E.P.; Joyner, L.G.; Halenda, P.P. The determination of pore volume and area distributions in porous substances. I. Computations from nitrogen isotherms. *J. Am. Chem. Soc.* **1951**, *73*, 373-380.
18. Ravikovitch, P.I.; Neimark, A.V. Characterization of nanoporous materials from adsorption and desorption isotherms. *Colloids Surf. A: Physicochem. Eng. Aspects* **2001**, *187-188*, 11-21.
19. Ravikovitch, P.I.; Domhnaill, S.C.O.; Neimark, A.V.; Schüth, F.; Unger, K.K. Capillary hysteresis in nanopores: Theoretical and experimental studies of nitrogen adsorption on MCM-41. *Langmuir* **1995**, *11*, 4765-4772.
20. Salmio, H.; Brühwiler, D. Distribution of amino groups on a mesoporous silica surface after submonolayer deposition of aminopropylsilanes from an anhydrous liquid phase. *J. Phys. Chem. C* **2007**, *111*, 923-929.
21. Tripp, C.P.; Hair, M.L. Direct observation of the surface bonds between self-assembled monolayers of octadecyltrichlorosilane and silica surfaces: A low-frequency IR study at the solid/liquid interface. *Langmuir* **1995**, *11*, 1215-1219.
22. Fripiat, J.J.; Jelli, A.; Poncelet, G.; André, J. Thermodynamic properties of adsorbed water molecules and electrical conduction in montmorillonites and silicas. *J. Phys. Chem.* **1965**, *69*, 2185-2197.
23. Bascom, W.D.; Timmons, R.B. Hydrolysis of triethylethoxysilane at the silica-carbon tetrachloride interface. *J. Phys. Chem.* **1972**, *76*, 3192-3200.
24. Ritter, H.; Nieminen, M.; Karppinen, M.; Brühwiler, D. A comparative study of the functionalization of mesoporous silica MCM-41 by deposition of 3-aminopropyltrimethoxysilane from toluene and from the vapor phase. *Microporous Mesoporous Mater.* **2009**, *121*, 79-83.
25. Brunauer, S.; Emmett, P.H.; Teller, E. Adsorption of gases in multimolecular layers. *J. Am. Chem. Soc.* **1938**, *60*, 309-319.

5.5 Synthesis of Subphthalocyanines as Probes for the Accessibility of Silica Nanochannels

Mine Ince,[a] Nando Gartmann,[b] Christian G. Claessens,[a] Tomás Torres*[a,c] and Dominik Brühwiler*[b]

[a] Departamento de Química Orgánica, Universidad Autonoma de Madrid, Cantoblanco, 28049 Madrid, Spain

[b] Institute of Inorganic Chemistry, University of Zurich, Winterthurerstrasse 190, 8057 Zurich, Switzerland

[c] IMDEA-Nanociencia, Facultad de Ciencias, Cantoblanco, 28049 Madrid, Spain

Organic Letters **2011**, 13, 4918-4921

Abstract

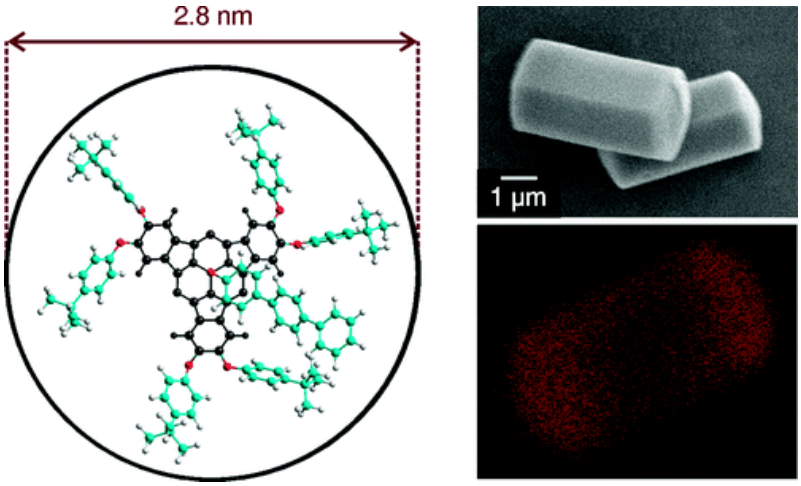

The synthesis of a new subphthalocyanine is reported. Its structural and photophysical properties are ideal for probing the accessibility of arrays of silica nanochannels.

Subphthalocyanines[1] (SubPcs) are lower homologues of phthalocyanines,[2] comprising a 14-π electron non-planar aromatic macrocycle made of three diiminoisoindole units *N*-fused around a central boron atom.[3] Unlike the related planar phthalocyanines, SubPcs possess a peculiar conical structure which provides them with relatively high solubility and low tendency to aggregate. SubPcs exhibit a number of unique properties, which allow a wide range of applications in fields such as nonlinear optics,[4] LEDs,[5] photovoltaics,[6] photodynamic therapy,[7] supramolecular chemistry,[8] as well as in photosynthetic models for studying energy- and electron-transfer processes.[9] SubPcs have also been employed as intermediates in the synthesis of unsymmetrically substituted phthalocyanines through a ring expansion reaction.[10]

Mesoporous silica with ordered pores[11] has become a versatile host material in various fields, including drug delivery[12] and catalysis.[13] These applications typically require functionalization of the mesoporous silica, giving rise to questions concerning the accessibility of the pores and the location of the functional groups.[14] The use of fluorescent probes and confocal laser scanning microscopy (CLSM) offers options for finding answers to these questions.[15] Arrays of silica nanochannels (ASNCs) have proven to be an ideal material for this purpose. ASNCs are hexagonally shaped fibers, each consisting of approximately 200'000 channels that run along the entire length of the particles.[16] Pore sizes of mesoporous materials are traditionally determined from nitrogen sorption data, often by means of the BJH method.[17] However, a pore size distribution does not necessarily provide unambiguous information about the accessibility of the pores.[18] The adsorption of SubPcs in combination with CLSM imaging allows us to draw a correlation between the pore size distribution and the effective accessibility. We show that the frequently used evaulation of pore sizes by the BJH method fails to provide useful data on the pore accessibility.

SubPc **1** (Scheme 1) was prepared in an overall yield of 21% by cyclotrimerization of 4,5-di-(*p-tert*-butylphenoxy)-phthalonitrile[19] **3** in the presence of one equivalent of BCl_3, followed by substitution of the axial chlorine atom by 1,1':4',1"-terphenyl-4-ol **2** in toluene.[20] 1,1':4',1"-terphenyl-4-ol **2** was obtained in 55% yield by Suzuki cross-coupling reaction between 4-bromo-(1,1'-biphenyl)-4'-ol and phenylboronic acid in the presence of tetrakis(triphenylphosphine) palladium(0) as catalyst in DME adapting a previously published procedure.[21] To test the ability of SubPcs to discern pore sizes, we have synthesized ASNCs with different pore size distributions. We found the well-defined morphology of the ASNCs to be extremely sensitive to changes in the synthesis conditions and therefore decided to investigate possibilities for a postsynthetic pore size adjustment. Indeed, physisorption of dodecamethylpentasiloxane and subsequent calcination gave ASNCs with reduced pore sizes (Table 1) but still reasonably narrow pore size distributions (Fig. 1).

Table 1. Structural properties of ASNCs.

	d_{DFT} [a] [nm]	V_{tot} [b] [cm^3/g]	V_P [c] [cm^3/g]	$V_{P(DFT)}$ [d] [cm^3/g]
S-ASNCs	< 2.0	0.24	0.23	0.23
M-ASNCs	2.6	0.57	0.52	0.54
L-ASNCs	3.2	0.75	0.70	0.71

[a] Average pore diameter determined by NLDFT. [b] Total pore volume.
[c] Primary mesopore volume determined by the α_S-plot method. [d] Primary mesopore volume determined by NLDFT.

Physisorption of SubPc **1** on large pore ASNCs (L-ASNCs) gave a uniform distribution throughout the L-ASNCs (Fig. 1). This is in agreement with an assessment of the size of SubPc **1**, resulting in a critical pore diameter of 2.8 nm. The pore size distribution, calculated by a NLDFT (non-local density functional theory) model,[22] of L-ASNCs is positioned almost entirely at values larger than 2.8 nm. The average pore diameter of medium pore ASNCs (M-ASNCs) is 2.6 nm. Intuitively, one would therefore expect that SubPc **1** cannot enter the pores. CLSM images of the SubPc **1** distribution show that this is only partially true. Luminescence can be observed towards the center of the channels. According to the pore size distribution of M-ASNCs, there is a considerable fraction of pores with sizes larger than 2.8 nm, enabling SubPc **1** to access the pore body. Complete exclusion of SubPc **1** is only achieved if the entire pore size distribution is located in a range below the critical diameter of 2.8 nm. This is the case for small pore ASNCs (S-ASNCs). It is interesting to note that there seems to be an accumulation of SubPc **1** at the channel entrances of S-ASNCs as opposed to a uniform coverage of the external particle surface. We have also conducted reference experiments with the smaller SubPc **4** (Fig. 2).[23] In this case, the critical pore diameter for inclusion into the nanochannels is 1.2 nm.

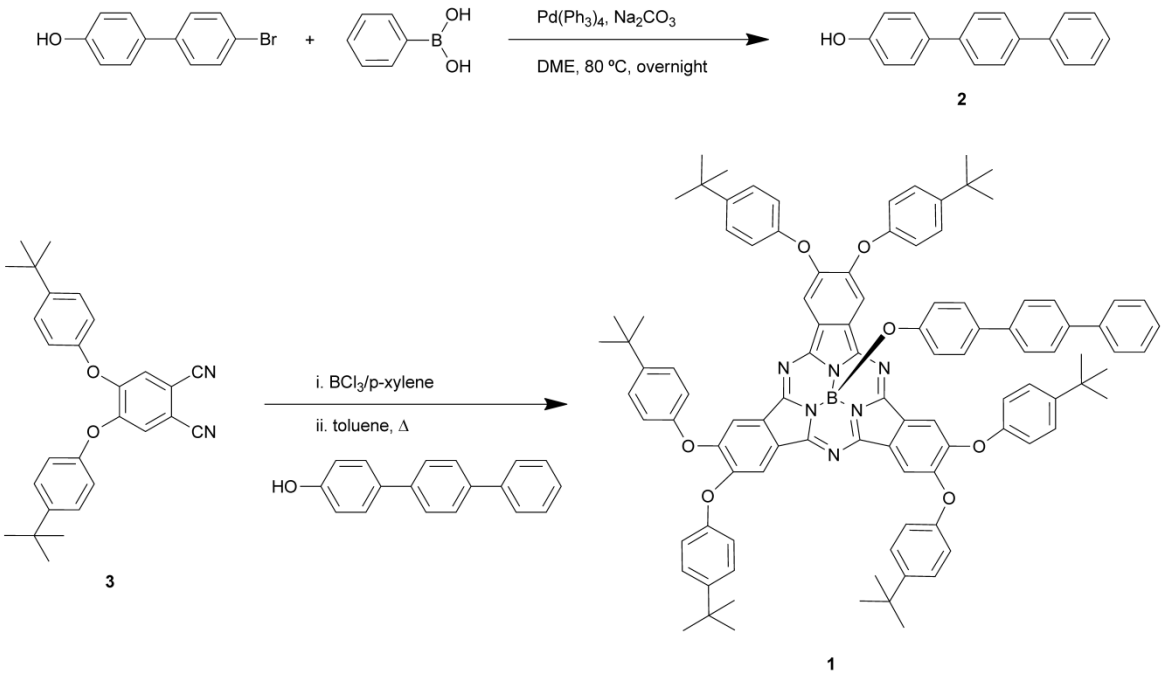

Scheme 1. Synthesis of SubPc **1**.

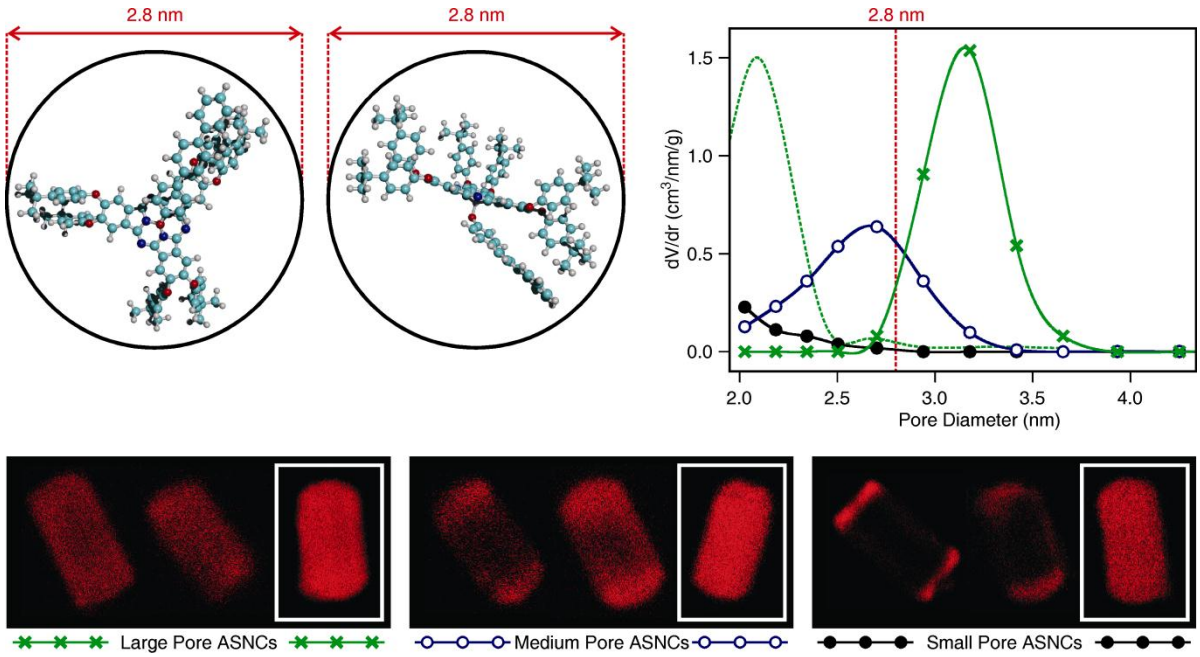

Fig. 1. Top left: Estimation of the critical pore size for the inclusion of SubPc **1** in ASNCs. Top right: Pore size distributions of L-ASNCs (×, green), M-ASNCs (○, blue), and S-ASNCs (●, black) calculated from the nitrogen adsorption isotherms by a NLDFT model. The pore size distribution represented by the dashed green line has been calculated by the classical BJH method using the adsorption isotherm of L-ASNCs. Bottom: CLSM images of ASNCs after deposition of SubPc **1**. The outermost right image of each group (shown in a white frame) was obtained after deposition of SubPc **4**. Optical slices in the center of the particles were selected. The length of the particles is approximately 5 µm.

Contrary to the pore size distribution calculated by NLDFT, the pore size distribution of L-ASNCs determined by the classical BJH method indicates the presence of pores exclusively smaller than 2.8 nm (Fig. 1), which would suggest a complete exclusion of SubPc **1**. This is a clear proof that the BJH method strongly underestimates the pore size of ASNCs. The NLDFT model, on the other hand, adequately describes the accessibility of the pores.

We have functionalized the external surface of L-ASNCs by reaction with 3-aminopropyltris(methoxyethoxyethoxy)-silane (APTMEES) according to the method proposed by Gartmann and Brühwiler.[15] Subsequent labeling with fluorescein isothiocyanate (FITC) and CLSM imaging reveals that the labeled amino groups are indeed accumulated on the external particle surface. Fig. 2A shows that despite the presence of the FITC-labeled amino groups, the pores remain sufficiently accessible to allow the inclusion of SubPc **1**. An external surface area of 53 m^2/g was determined for L-ASNCs. Even in the event of quantitative grafting onto the external surface, the density of amino groups would remain in a reasonable range, i.e., close to one group per nm^2, in the case of 100 µmol of APTMEES per gram of L-ASNCs. Increasing the amount of APTMEES by a factor of 5, on the other hand, would produce a hypothetical density of more than 5 amino groups per nm^2. It can be assumed that in this case, a considerable amount of amino groups is located on the pore surface close to the pore entrances, leading to pore blocking. CLSM images reveal that

the distribution of SubPc **1** on such highly loaded particles indeed tends to be non-uniform (Fig. 2B) with an accumulation of SubPc **1** at the pore entrances. However, the pores are apparently still large enough to enable penetration of SubPc **4** (Fig. 2C).

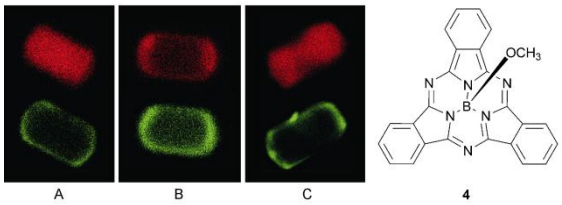

Fig. 2. CLSM images of ASNCs after external surface functionalization with 100 µmol/g (A) or 500 µmol/g (B and C) of APTMEES and labeling with FITC, followed by physisorption of SubPc **1** (A and B) or SubPc **4** (C). The lower (green) images of each panel show the luminescence of the coupled FITC labels, whereas the upper (red) images were obtained upon excitation of the SubPc molecules at 543.5 nm. Optical slices in the center of the particles were selected.

In summary, a new SubPc was synthesized and used in combination with CLSM to probe the accessibility of ASNCs. Comparing the results of these studies to predictions based on pore size distributions calculated from the nitrogen adsorption isotherms revealed that an analysis by a model based on NLDFT adequately describes the accessibility of the pores. The classical BJH treatment was found to draw a misleading picture of the accessibility by considerably underestimating the pore size. The SubPc probe was further employed to investigate the effect of surface-grafted functional groups on the accessibility of the pores. The photophysical properties of the SubPc are compatible with those of the frequently used fluorescein labels, allowing independent imaging of the distribution of fluorescein-labeled functional groups and of the distribution of physisorbed SubPc.

Financial support by the European Commission through the Human Potential Program (Marie-Curie RTN Nanomatch, MRTN-CT-2006-035884), the Swiss National Science Foundation (200020-117591), the MICINN and MEC (Spain) (CTQ2008-00418/BQU, PLE 2009-0070, and Consolider-Ingenio Nanociencia molecular CSD2007-00010), and Comunidad de Madrid (MADRI-SOLAR-2, S2009/PPQ/1533) is gratefully acknowledged. We thank Anais Medina for a sample of compound 4.

References

1 T. Torres, *Angew. Chem. Int. Ed.*, 2006, **45**, 2834; C. G. Claessens, D. González-Rodríguez and T. Torres, *Chem Rev*., 2002, **102**, 835.

2 G. de la Torre, C. G. Claessens and T. Torres, *Chem. Commun.*, 2007, 2000.

3 A. Meller and A. Ossko, *Monatshefte Chem*ie, 1972, **103**, 150.

4 B. del Rey, U. Keller, T. Torres, G. Rojo, F. Agulló-López, S. Nonell, C. Marti, S. Brasselet, I. Ledoux and J. Zyss, *J. Am. Chem. Soc.*, 1998, **120**, 12808.

5 D. D. Díaz, H. J. Bolink, L. Cappelli, C. G. Claessens, E. Coronado and T. Torres, *Tetrahedron Lett.*, 2007, **48**, 4657.

6 H. Gommans, T. Aernouts, B. Verreet, P. Heremans, A. Medina, C. G. Claessens and T. Torres, *Adv. Funct. Mater.*, 2009, **19**, 3435.

7 N. Rubio, A. Jiménez-Banzo, T. Torres and S. Nonell, *J. Photochem. Photobiol. A.*, 2007, **185**, 214.

8 C. G. Claessens, M. J. Vicente-Arana and T. Torres, *Chem Commun.*, 2008, 6378.

9 D. González-Rodríguez, E. Carbonell, G. De Miguel Rojas, C. Atienza Castellanos, D. M. Guldi and T. Torres, *J. Am. Chem. Soc.*, 2010, **132**, 16488.

10 N. Kobayashi, R. Kondo, S. Nakajima and T. Osa, *J. Am. Chem. Soc*., 1990, **112**, 9640; A. Sastre, B. Del Rey and T. Torres, *J. Org. Chem*., 1996, **61**, 8591.
11 T. Yanagisawa, T. Shimizu, K. Kuroda and C. Kato, *Bull. Chem. Soc. Jpn.*, 1990, **63**, 988; C. T. Kresge, M. E. Leonowicz, W. J. Roth, J. C. Vartuli and J. S. Beck, *Nature*, 1992, **359**, 710.
12 M. Vallet-Regí, F. Balas and D. Arcos, *Angew. Chem. Int. Ed.*, 2007, **46**, 7548; I. I. Slowing, J. L. Vivero-Escoto, C.-W. Wu and V. S.-Y. Lin, *Adv. Drug Deliv. Rev.*, 2008, **60**, 1278.
13 A. Taguchi and F. Schüth, *Microporous Mesoporous Mater.*, 2005, **77**, 1; J. H. Clark, D. J. Macquarrie and S. J. Tavener, *Dalton Trans*., 2006, 4297.
14 D. Brühwiler, *Nanoscale*, 2010, **2**, 887; I. I. Slowing, J. L. Vivero-Escoto, B. G. Trewyn and V. S.-Y. Lin, *J. Mater. Chem.*, 2010, **20**, 7924.
15 N. Gartmann and D. Brühwiler, *Angew. Chem. Int. Ed*., 2009, **48**, 6354.
16 Y. Kievsky, B. Carey, S. Naik, N. Mangan, D. ben-Avraham and I. Sokolov, *J. Chem. Phys.*, 2008, **128**, 151102.
17 E. P. Barrett, L. G. Joyner and P. P. Halenda, *J. Am. Chem. Soc.*, 1951, **73**, 373.
18 H. Ritter and D. Brühwiler, *J. Phys. Chem. C*, 2009, **113**, 10667; N. Gartmann, C. Schütze, H. Ritter and D. Brühwiler, *J. Phys. Chem. Lett.*, 2010, **1**, 379; H. Ritter, J. H. Ramm and D. Brühwiler, *Materials*, 2010, **3**, 4500.
19 D. Wöhrle, M. Eskes, K. Shigehara and A. Yamada, *Synthesis*, 1993, 194.
20 C. G. Claessens, D. González-Rodríguez, B. del Rey, T. Torres, G. Mark, H.-P. Schuchmann, C. von Sonntag, J. G. MacDonald and R. S. Nohr, *Eur. J. Org. Chem.*, 2003, **14**, 2547.
21 R. J. Edsall, Jr., H. A. Harris, E. S. Manas and R. E. Mewshaw, *Bioorg. Med. Chem*., 2003, **11**, 3457.
22 P. I. Ravikovitch and A. V. Neimark, *Colloids Surf. A: Physicochem. Eng. Aspect*, 2001, **187-188**, 11; P. I. Ravikovitch, S. C. O. Domhnaill, A. V. Neimark, F. Schüth and K. K. Unger, *Langmuir*, 1995, **11**, 4765.
23 K. Kasuga, T. Idehara, M. Handa, Y. Ueda, T. Fujiwara and K. Isa, *Bull. Chem. Soc. Jpn.*, 1996, **69**, 2559.

Electronic Supplementary Information

1. Synthesis of SubPc 1

General details. All chemicals were purchased from Aldrich and used without further purification. 4,5-*tert*-butylphenoxyphthalonitrile was prepared according to a published procedure.[1] All reactions were followed by TLC employing aluminium sheets coated with silica gel 60 F254 (Merck).

1,1':4',1''-terphenyl-4-ol (2). A suspension of 4-bromo-4'-hydroxybiphenyl (200 mg, 0.8 mmol), phenylboronic acid (133 mg, 1.09 mmol), tetrakis(triphenylphosphine) palladium(0) (50 mg, 0.04 mmol) and Na_2CO_3 (2 ml of a 2 N aqueous solution) in dimethoxyethane (10 ml) was stirred under argon atmosphere overnight at 80 °C. The suspension was then cooled to room temperature and poured onto a 1 N NH_4Cl solution (100 ml). The mixture was extracted with ethyl acetate (2×100 ml) and the combined organic extracts were washed with brine (20 ml), dried over Na_2SO_4 and evaporated *in vacuo*. The crude product was purified by recrystallization from ethanol to yield 108 mg (55%) of a white solid. IR (KBr): ν = 3387, 3033, 2360, 1608, 1509, 1454, 1402, 1373, 1263, 1002, 822 cm^{-1}. ^1H NMR ($CDCl_3$, 300 MHz): 7.69 (d, J = 4 Hz, 6H), 7.53 (d, J = 9 Hz, 2H), 7.45 (t, J = 7 Hz, 2H), 7.22 (t, J = 7 Hz, 1H), 6.93 (d, J = 9 Hz, 2H), 4.75 (s, 1H); MALDI-TOF-MS (ditranol): M/*z*: 246.1 [M^+].

SubPc 1. In a 25 ml two-necked round-bottomed flask, equipped with a condenser, magnetic stirrer and rubber seal, BCl_3 (0.38 ml, 1 M solution in *p*-xylene) was added to 4,5-di-(*p-tert*-butylphenoxy)phthalonitrile (163 mg, 0.38 mmol) under argon atmosphere. The reaction mixture was refluxed at 150 °C for 2 h. After cooling down to room temperature the unreacted BCl_3 and solvent were quickly removed *in vacuo*. 1,1':4',1"-terphenyl-4-ol (475 mg, 1.92 mmol) and dry toluene (5 ml) were added to the crude mixture and stirring was continued at 100 °C for 3 h. The solvent was removed by vacuum distillation and the remaining dark solid was washed with a 4:1 mixture of methanol/water. The crude compound was purified by column chromatography on silica gel using a mixture of hexane/ethyl acetate (9:1) as eluent to give 40 mg (21%) of a reddish solid. IR (KBr): ν = 2922, 1735, 1603, 1508, 1261, 1180, 1107 (B-O), 891 cm^{-1}. ^1H NMR ($CDCI_3$, 300 MHz): 8.28 (s, 6H), 7.59-7.52 (m, 4H), 7.45-7.37 (m, 17H), 7.12-7.05 (m, 12H), 7.0 (d, J = 9 Hz, 2H), 5.38 (d, J = 9 Hz, 2H), 1.41-1.33 (m, 54H). UV/Vis ($CHCI_3$): λ_{max} [log ε ($dm^3mol^{-1}cm^{-1}$)]: 573 (4.9), 518 (4.3), 357 (4.5), 283 (5.0). HR-MALDI-TOF-MS (Matrix: DCTB) calc. for $C_{102}H_{97}BN_6O_7$ [$M]^+$: M/z: 1528.7522, found 1528.7498.

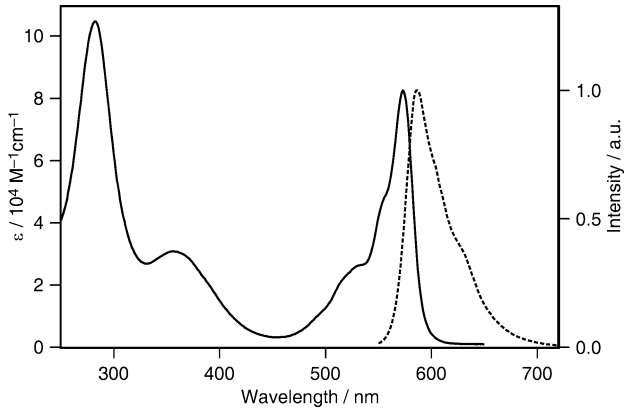

Figure S1. UV/Vis (solid) and photoluminescence spectrum (dashed) of SubPc **1** in $CHCl_3$.

2. Synthesis and Functionalization of Arrays of Silica Nanochannels (ASNCs)

ASNCs were synthesized according to a published procedure.[2] However, as our comparative studies require larger batches of starting material, the procedure was upscaled by a factor of 3. Briefly, an amount of 14.55 g of hexadecyltrimethylammonium chloride (Acros, 99%) was dissolved in 228 ml of double distilled H_2O and 180 ml of 32% aqueous HCl by stirring for 1 min at ca. 1000 rpm in a polypropylene beaker. The solution was cooled to 0 °C for 15 min without stirring, followed by the slow addition of 6 ml of cold tetraethoxysilane (Aldrich, 99.999%) and further stirring for 30 s. The resulting mixture was kept at 0 °C under quiescent conditions for 3 h. The product was collected by filtration and washed with H_2O. The structure-directing agent (SDA) was removed by first heating at 300 °C for 2 h and calcining at 550 °C for 12 h. Heating rates of 2 °C/min were applied.

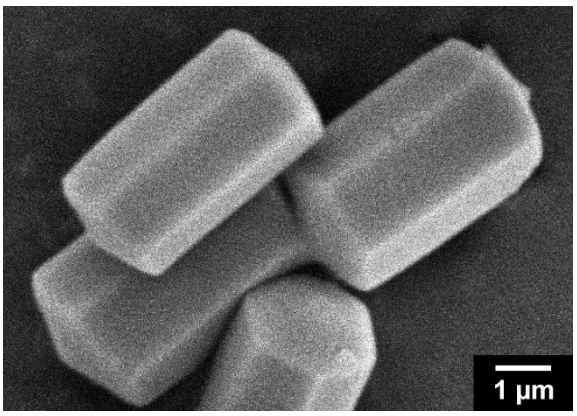

Figure S2. Scanning electron microscopy image of ASNCs.

To reduce the pore size of the ASNCs, an amount of 100 mg of calcined ASNCs was dispersed in 10 ml of hexane. After adding 50 µL of dodecamethylpentasiloxane (Aldrich), the suspension was stirred for 1 h and afterwards left to evaporate. The dry sample was calcined according to the protocol described above for the removal of the SDA. The procedure can be repeated to obtain a stepwise reduction of the pore size. Due to a certain

degree of non-uniformity of the dodecamethylpentasiloxane distribution in the channels, the width of the resulting pore size distribution increases upon pore size reduction. Reducing the pore size by the straight-forward approach of using a SDA with a shorter alkyl chain length was not successful, failing to produce particles with the well-defined morphology of ASNCs. The advantage of the postsynthetic modification with dodecamethylpentasiloxane is the conservation of the particle morphology, allowing comparative studies of the spatial distribution of molecules in the channels by means of CLSM.

Functionalization of the external surface of ASNCs was carried out as follows:[3] An amount of 200 mg of calcined ASNCs was dispersed in dry toluene (10 ml) and 3-aminopropyltris-(methoxyethoxyethoxy)silane (APTMEES, ABCR Karlsruhe) was added (20 µmol or 100 µmol). After the mixture had been stirred for 10 min, the functionalized ASNCs were recovered by filtration and cured in an oven at 80 °C for 16 h. The amount of grafted amino groups was analyzed by the fluorogenic derivatization reaction with fluorescamine.[4] In the investigated range of amino contents, the average relative error of this analysis method is below 10%.[5] For the sample prepared with 20 µmol of APTMEES, the grafting yield was close to quantitative, in agreement with previous results.[3] The sample prepared with 100 µmol of APTMEES had a grafting yield of 42%. The amino-functionalized ASNCs were labeled by stirring in absolute ethanol containing 1.5 equivalents (relative to the amount of APTMEES) of fluorescein 5-isothiocyanate (FITC, Fluka) for 24 h at room temperature. The labeled samples were washed with ethanol until the washing solution became colorless.

Adsorption of SubPc **1** on ASNCs was accomplished as follows: An amount of 0.1 µmol of SubPc **1** was dissolved in 1.3 ml of hexane and added to 15 mg of ASNCs. After shaking the resulting suspension for 1 h, the solvent was left to evaporate under ambient conditions. Adsorption of SubPc **4** was conducted in the same manner, using dichloromethane instead of hexane as a solvent, due to the insolubility of SubPc **4** in hexane.

3. Physical Measurements

^{1}H NMR spectra were obtained using a Bruker Avance 300 spectrometer. UV/Vis spectra were recorded on a Hewlett-Packard 8453 and a Varian Cary 50 instrument. Photoluminescence spectra were measured on a Perkin-Elmer LS50B spectrofluorometer equipped with a red-sensitive photomultiplier (Hamamatsu R928). Infrared spectra were recorded on a Bruker Vector 22 employing solid samples (KBr pressed disks). MALDI-TOF mass spectrum was obtained in a Voyager-DE STR mass spectrometer. Nitrogen sorption isotherms were collected at 77 K using a Quantachrome NOVA 2200. Samples were vacuum-degassed at 80 °C for 3 h. The total pore volume V_{tot} was calculated from the amount of nitrogen adsorbed at a relative pressure of 0.95. The primary mesopore volume V_P and the external surface area were determined from the linear part of the α_S-plot ($\alpha_S > 1$).[6] A NLDFT model developed for silica exhibiting cylindrical pore geometry (NOVAWin2 software, Version 2.2, Quantachrome Instruments) was employed to calculate the pore size distributions.[7] The adsorption isotherms were used for the calculations. Scanning electron microscopy images were acquired on a JEOL JSM-6060. The CLSM setup consisted of an Olympus BX 60 microscope with a FluoView confocal unit and lasers operating at 488 and 543.5 nm.

References

1 D. Wöhrle, M. Eskes, K. Shigehara and A. Yamada, *Synthesis*, 1993, 194.

2 Y. Kievsky and I. Sokolov, *IEEE Trans. Nanotechnol.*, 2005, **4**, 490.

3 N. Gartmann and D. Brühwiler, *Angew. Chem. Int. Ed.*, 2009, **48**, 6354.

4 H. Ritter, M. Nieminen, M. Karppinen and D. Brühwiler, *Microporous Mesoporous Mater.*, 2009, **121**, 79.

5 H. Ritter and D. Brühwiler, *J. Phys. Chem. C*, 2009, **113**, 10667.

6 M. Kruk, M. Jaroniec, R. Ryoo and J. M. Kim, *Microporous Mater.*, 1997, **12**, 93; A. Sayari, P. Liu, M. Kruk and M. Jaroniec, *Chem. Mater.*, 1997, **9**, 2499.

7 P. I. Ravikovitch, S. C. O. Domhnaill, A. V. Neimark, F. Schüth and K. K. Unger, *Langmuir*, 1995, **11**, 4765.

PART II

Patterns of Porous Silicates in Polymer Thin Films

1. Introduction

There is a considerable scientific interest in the inclusion of porous silicates such as zeolites and mesoporous silica or of host-guest systems featuring the latter into polymeric structures. Because of the near matching of the refractive index of silicates and polymers like polymethylmethacrylate (PMMA, Plexiglas®), such structures remain optically transparent upon silicate inclusion. The advantages of host-guest systems featuring organic dyes inserted into porous silicates are; (i) the possibility to achieve high local dye concentrations without aggregation, (ii) protection of the organic dyes from environmental influences, thus enhancing their stability and (iii) the possibility to align the guests in a supramolecular arrangement[1] (Fig. 1). Polymer thin films containing organized host-guest systems of this kind can for example be used in light-management (light-harvesting and concentration), optically anisotropic layers and display technology.

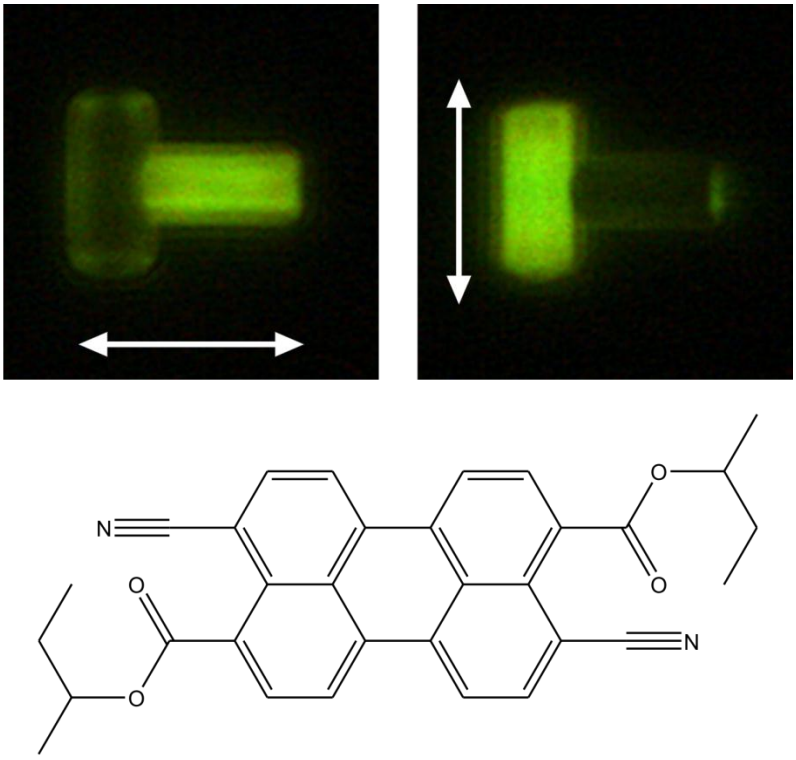

Fig. 1 Fluorescent microscopy image of Lumogen Yellow 083 integrated into zeolite L applying a polarizer in front of the detector (double arrow indicates the orientation of the polarizer). The electronic transition dipole moment of the dye is aligned parallel to the long-axis of the zeolite crystal. The length of the crystals is approximately 5 µm.

An illustrative example for light-management processes featuring silicate-containing polymer thin films is luminescent solar concentrators (LSCs), or color changing media employing ZeoFRET®.[2] Organic fluorescent dyes included in zeolite L allocate themselves in certain orientations, which then can lead to alignment of the electronic transition dipole moments and therefore to efficient Förster resonance energy transfer (FRET). In a system with at least two different luminescent guest molecules, FRET enhances the emission of the dye emitting at longer wavelength.[3]

This concept can be used in both LSCs and color changing media. In LSCs where the concentration of the emitting dye is kept much lower than the concentration of the absorbing dye, the strong red shift of the emitted light leads to avoidance of the self absorption problem.[4] The same energy transfer concept can be applied in color changing media, e.g. in foils for greenhouses, where the conversion of green and yellow light to red light is desirable to enhance photosynthesis.

To apply host-guest systems of porous silicates in display technology, electroluminescent molecules or polymers have to be inserted as guests and the channel openings have to be functionalized with conducting stopcocks.[5] The system can then be used as light emitting diode in a thin film of conducting polymer. If the silicate particles are aligned properly, it would be possible to emit polarized light (Fig. 1) as is applied in 3D displays.

Preliminary work of our group[6] in this field revealed a so far unknown phenomenon. Upon the formation of zeolite containing polymer thin films, a patterned arrangement of the zeolite crystals in the polymer is found. The investigation of the formation mechanism of these patterns is very interesting because of their resemblance to patterns occurring in nature. The investigation of pattern formation of non-living materials is also applied to investigate the organization of cells[7, 8], and to provide insight in the field of developmental biology[9]. Zeolite and mesoporous silica are ideal tools for this investigation, because they can be synthesized in different shapes and sizes[10, 11] and labeled with fluorescent dyes for a facile analysis by fluorescence microscopy[5].

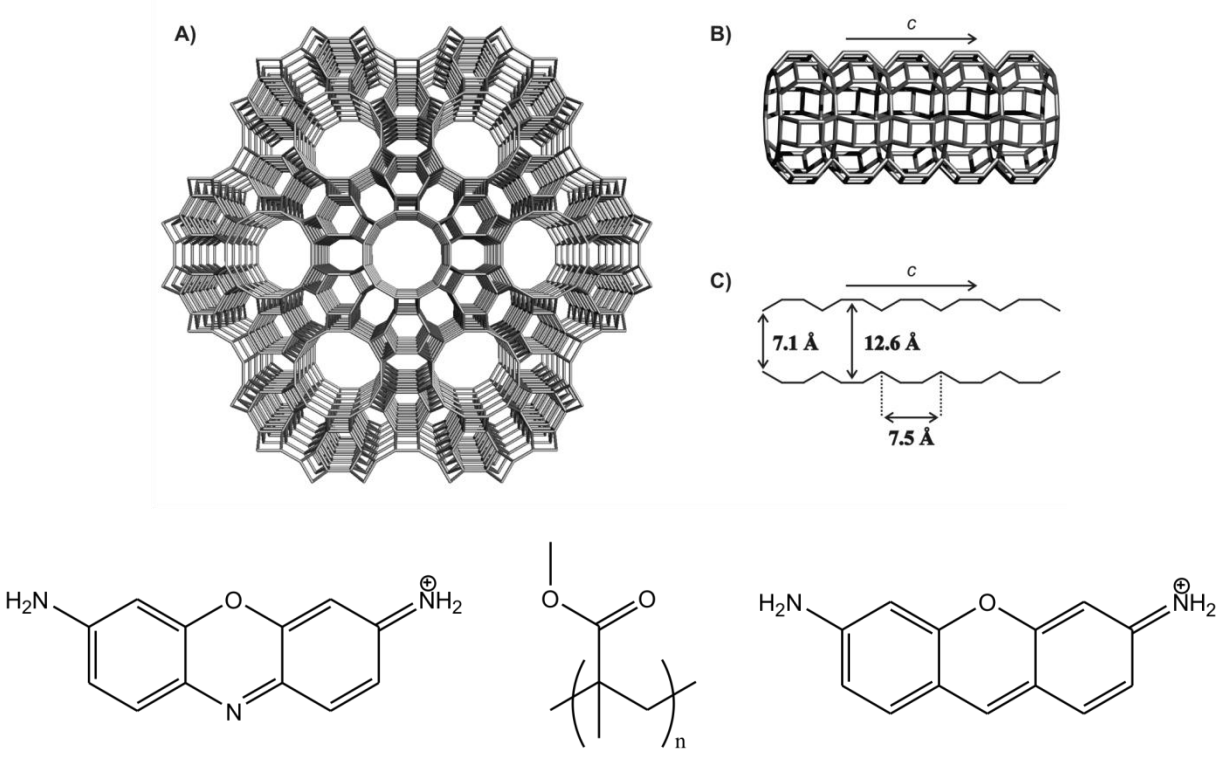

Fig. 2 Top[11]: Structure of zeolite L, view on the channel entrances (A), the structure (B) and dimensions (C) of a single channel. Bottom: Structures of oxonine (left), PMMA (middle) and pyronine (right).

Our work was mainly conducted with luminescent dyes embedded into the channels of zeolite L in a PMMA thin film. Zeolite L is a crystalline aluminosilicate featuring a system of parallel channels (Fig. 2 top). Oxonine and pyronine were used as luminescent guests for fluorescent microscopy imaging. For the experiments featuring mesoporous silica, fluorescein was used as a label.

2. Results and Discussion

2.1 Preliminary Results

Previous work in our group focused on pattern formation as a function of PMMA concentration, and wet film thickness (Fig 3).[6] The preparation of the patterned samples is done as follows: A wet film of PMMA and zeolite L in $CHCl_3$ is applied to a glass surface by doctor blading and the $CHCl_3$ is removed afterwards by evaporation at room temperature without airstream.

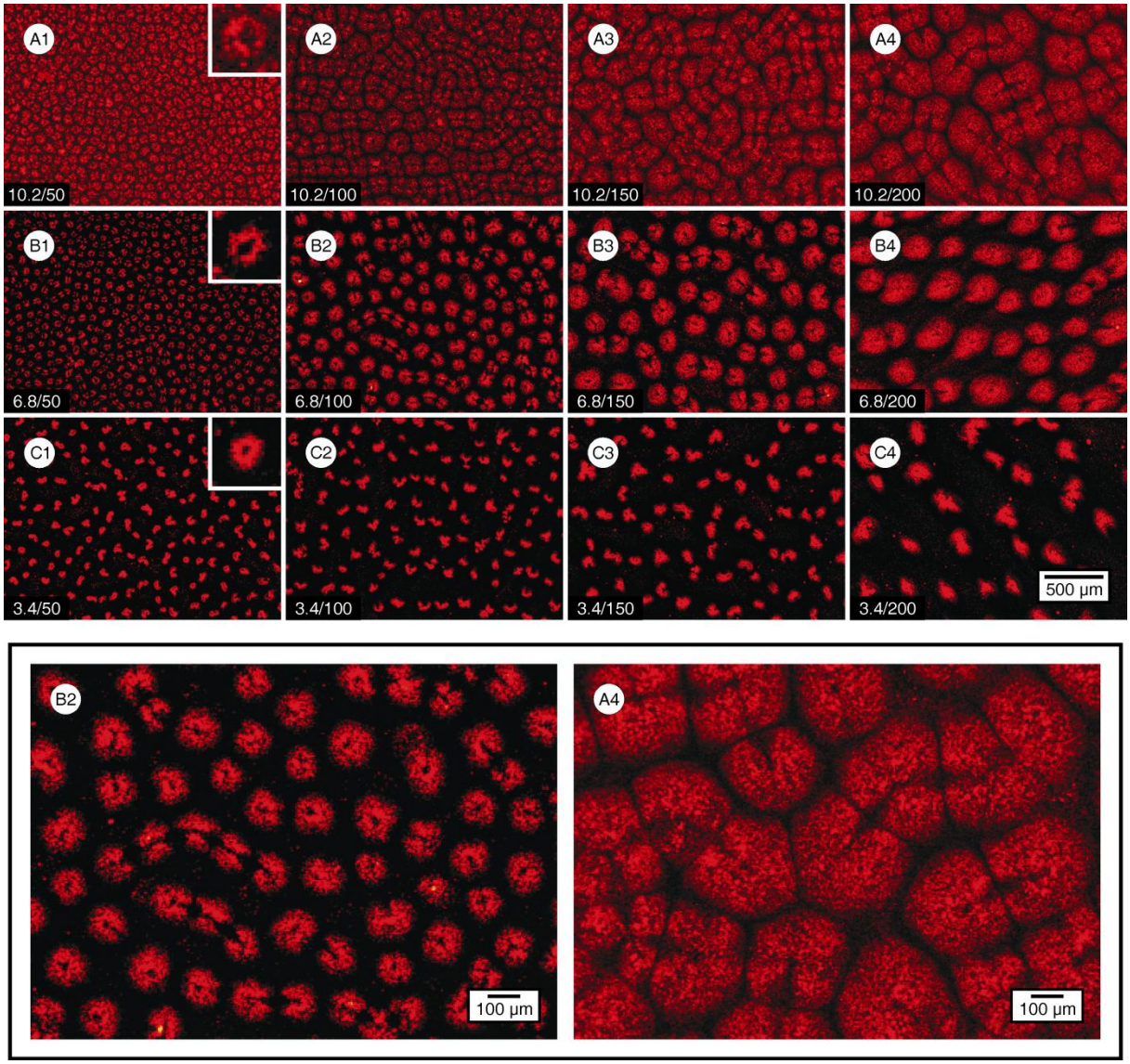

Fig. 3[6] Patterns of oxonine-loaded zeolite L crystals in PMMA thin films imaged by fluorescence microscopy. The number in the lower left corner of each image indicates the PMMA concentration (in [wt%]) and the wet film thickness (in [µm]), respectively.

With an increase of the initial wet film thickness, the size of the zeolite aggregates in the patterns shows a linear increase (Fig. 4 left). At a constant wet film thickness, the size of the aggregates also increases slightly upon the increase of the polymer concentration (Fig. 4 right).

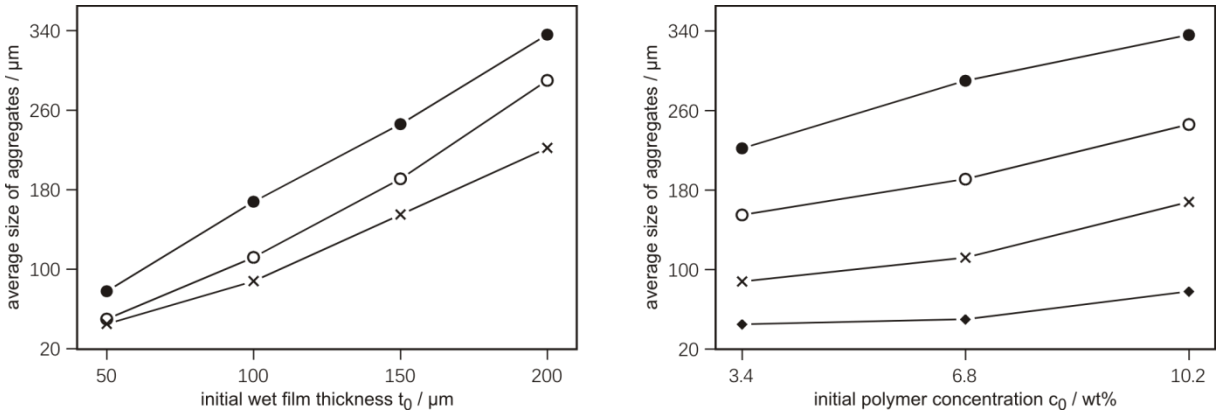

Fig. 4[6] Left: Average size of aggregates of zeolite L crystals as a function of the initial wet film thickness for an initial polymer concentration of 10.2 wt% (●), 6.8 wt% (○), and 3.4 wt% (×). Right: Average size of aggregates of zeolite L crystals as a function of the initial polymer concentration for an initial wet film thickness of 200 µm (●), 150 µm (○), 100 µm (×), and 50 µm (♦). The uncertainty of the average values is typically ± 20 %.

The identification of the mechanism of such a pattern formation is rather complicated, due to the non-equilibrium nature of the system. The formation of the patterns in the zeolite L/$CHCl_3$/PMMA system is assumed to be principally driven by physical processes in an evaporating solution similar to the spatiotemporal dynamics of dewetting[12]. In such systems, the chemical nature of the involved components plays only a minor role in the formation of the patterns, as will be shown later.

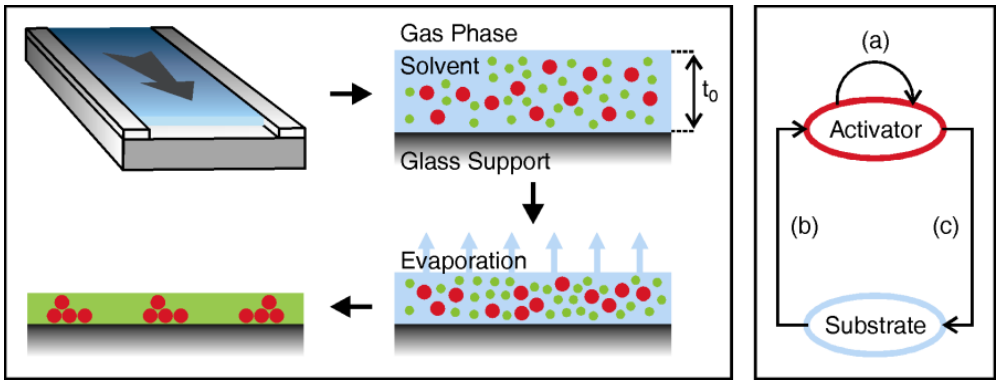

Fig. 5[6] Pattern formation and feedback loops. The left panel illustrates schematically the solvent (blue) evaporation that leads to the formation of patterns of microparticles (red) in a polymer (green). The initial wet film thickness, t_0, is an important parameter controlling the size and shape of the particle aggregates. The right panel shows the feedback loops involved in the pattern formation (activator = microparticles, substrate = solvent). Activating processes (a) and (c) are complemented by an inhibitory process (b).

The pattern formation can be explained with the model of local self-activation and lateral inhibition,[13-15] featuring a short-range positive feedback coupled to a long-range negative feedback.

In the system at hand the positive feedback arises based on the fact that the evaporation of solvent is facilitated in regions with a high local zeolite L concentration (Fig. 5, process (c)). Because of the increasing viscosity in the surrounding medium, the particles in the aggregates are losing mobility, thus leading to a growth of the aggregates and therefore to a further promotion of the local solvent evaporation (Fig. 5, process (a)). The long-range negative feedback in this system (Fig. 5, process (b)) comes from the evaporation of the solvent over the whole surface of the wet film. The less solvent available in the system, the less mobile and penetrable the PMMA phase becomes. With a less penetrable PMMA phase, the further growth of the aggregates is inhibited. The growth of the aggregates is also inhibited by the fact that the larger the aggregates become, the less zeolite L particles are available for further growth.

2.2 Further Investigations

Further experiments were conducted to support the proposed mechanism of pattern formation in the $CHCl_3$/zeolite/PMMA thin film system. On the one hand this was done by showing that the polymer itself does not form any patterns in the absence of zeolite L, on the other hand by

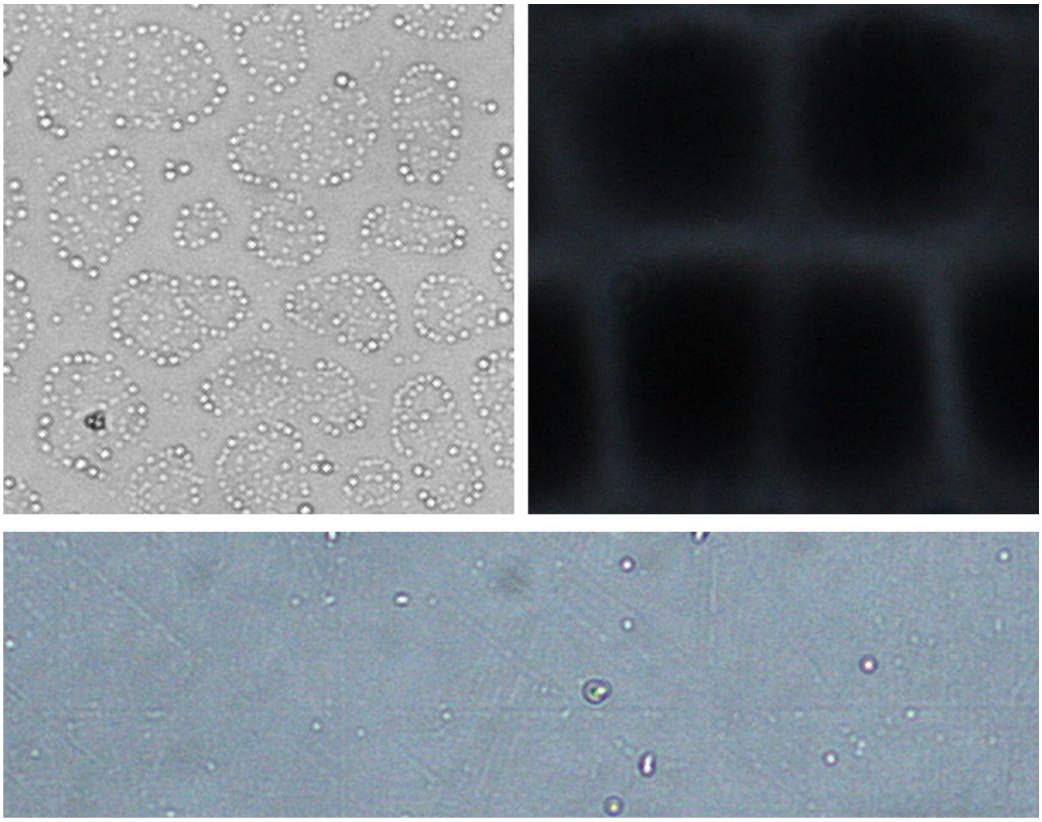

Fig. 6 Top: Thin film of PMMA (left) and polycarbonate (45000 g/mol) (right) cast and evaporated according to the method of Bormashenko et al.[16] Bottom: Thin film of PMMA cast according to our method. The images were taken with a CCD camera at a 100 fold magnification.

proving that the chemical nature of the zeolite itself plays only a minor role, as explained earlier.

Bormashenko et al. found patterns in thin films of different polymers that were created by solvent evaporation in an airstream.[16] They cast the polymer wet films on polypropylene or quartz plates using a brush. Reproduction of these patterns and comparison to our method showed that in the latter the polymer itself does not form any patterns (Fig. 6). This indicates that the patterns indeed arise due to the presence of the zeolites in the wet polymer film, supporting the theory of local activation.

To investigate the influence of the chemical nature of the embedded particles on the pattern formation, we changed the polarity of the external zeolite surface. The external surface of the zeolite was functionalized with octyl moieties applying a well known method of coupling alkyltrialkoxysilanes to the surface silanol groups[17-19]. Fluorescence microscopy of thin films, featuring the octyl-modified zeolites, and mixtures of modified and unmodified zeolites revealed that the patterns are insensitive to the chemical nature of the zeolite surface (Fig. 7). This promotes the fact that the pattern formation is indeed driven by the physical process of the evaporating solvent.

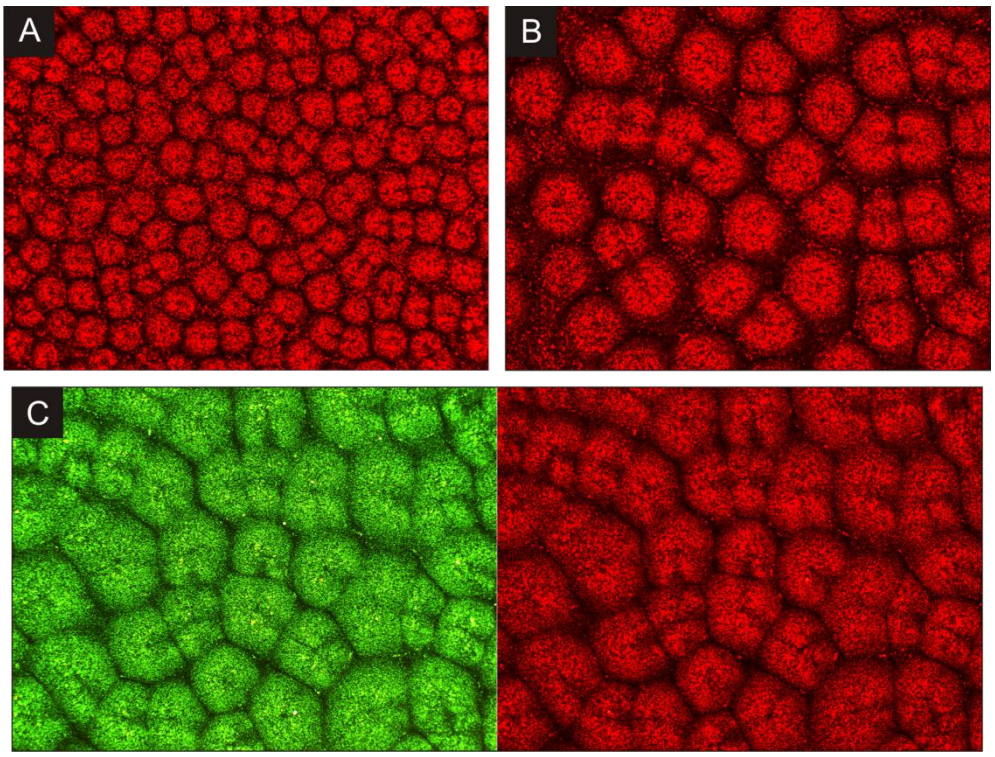

Fig. 7 Top: Fluorescence microscope images of patterns of octyl-modified zeolite L formed with different wet film thicknesses (A = 100 µm, B = 200 µm). Bottom: Pattern of mixed hydrophilic and hydrophobic zeolites in a PMMA thin film. The unmodified hydrophilic zeolites are labeled with pyronine (green), the octyl-modified hydrophobic zeolites are labeled with oxonine (red).

We further investigated the influence of the particle size on the formation of the patterns. In addition to the already applied zeolite L, patterns with nano-sized zeolite L, ASNCs and SBAs were prepared and analyzed.

Silicate	Zeolite L	Zeolite L (nano)	ASNCs	SBAs
Approximate size	1 - 1.5 µm	30 - 60 nm	2 µm × 5 µm	5 - 10 µm
Morphology	hexagonal	hexagonal	hexagonal	spherical

Tab. 1 Approximate particle sizes and morphologies of different silicates used for pattern formation.

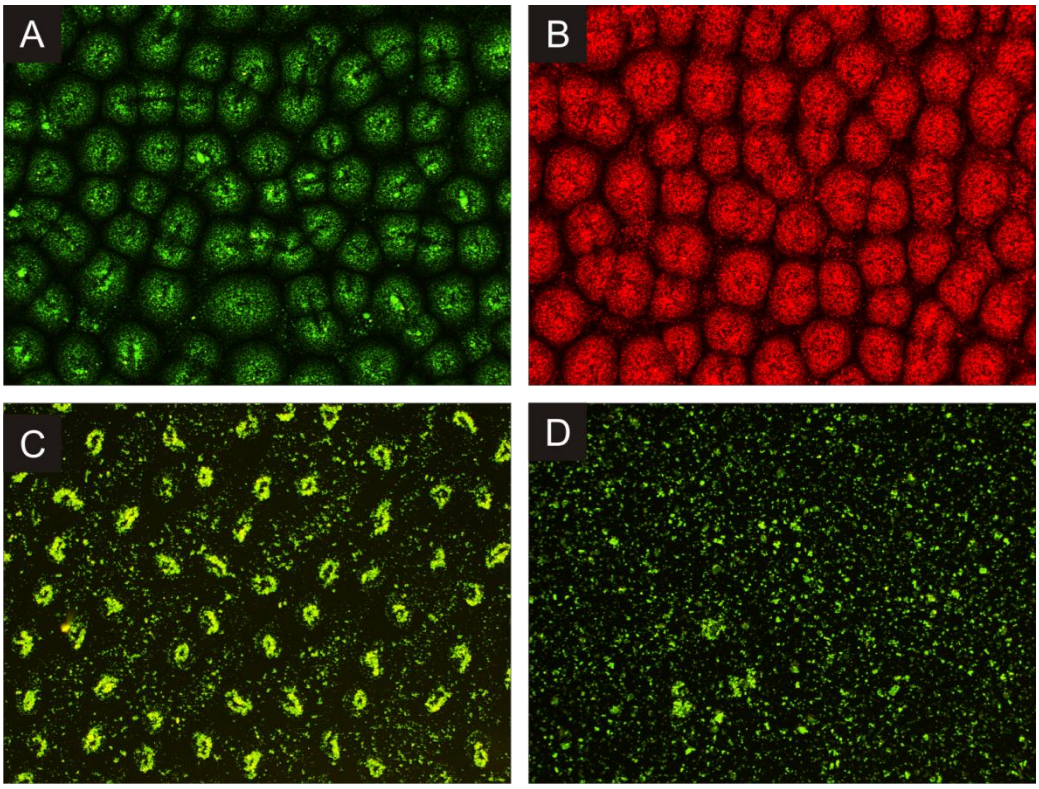

Fig. 8 Fluorescence microscopy images of patterns of different silicate particles formed under the same conditions (wet film thickness of 150 µm and initial PMMA concentration of 6.8 wt%). A: nano-sized zeolite L labeled with pyronine. B: zeolite L labeled with oxonine. C: ASNCs labeled with FITC. D: SBAs labeled with FITC.

Fluorescence microscopy reveals that the size of the particles considerably influences the pattern formation (Fig. 8). The patterns of the regular zeolite and the nano-sized zeolite are quite similar. This is probably due to the formation of micrometer sized aggregates that are known to occur in the applied nano-zeolites. However the pattern changes significantly when going to larger particles. For the large SBAs the pattern formation even ceases to occur. The reason for this is the simple fact that the increase of the particle size decreases the mobility of the particles in the drying wet film.

All results described above support the theory of local self-activation and lateral inhibition.

2.2.1 Experimental

Preparation of the zeolite-free polymer thin films

Method of Bormashenko[16]: Polycarbonate (Acros, 45000 g/mol) or PMMA (Sigma-Aldrich, 120000 g/mol) was dissolved in $CHCl_3$. The concentration of the solution was 6.8 wt%. Clean

glass substrates (cleaned with water and ethanol) were coated with the solutions. The solutions were spread on horizontal glass substrates with a brush and dried in an airstream under ambient conditions.

Our method[6]: PMMA was dissolved in $CHCl_3$. The concentration of the solution was 6.8 wt%. Microscopy glass slides (washed with ethanol and distilled water) were coated with the PMMA solution by doctor blading resulting in a specific initial thickness of the wet PMMA film of 100 µm. Evaporation of the solvent took place in less than 15 s at room temperature. No airstream was applied.

Preparation of dye-loaded zeolite L[20]

70 mg of zeolite L (Lucidot DISC, Clariant) was suspended in an aqueous solution of oxonine chloride or pyronine chloride (4.5 ml, 0.13 mM) and refluxed for 16 h. The crystals were recovered by centrifugation, washed with methanol to remove dye molecules adsorbed on the external zeolite surface, and oven-dried at 60 °C.

Labeling of ASNCs and SBAs

SBAs/ASNCs (100 mg) was suspended in ethanol (15 ml), APTES (2.3 µl, 10 µmol, Acros, 99 %) was added and the suspension was stirred under reflux for 3 h. The resulting modified silica was recovered by filtration and washed thoroughly with ethanol. The modified silica was then labeled with FITC according to the general procedure described in PART I Chapter 3.2.

Preparation of the PMMA/zeolite and PMMA/silica thin films

Dye-loaded zeolite L (5 mg) was dispersed in $CHCl_3$ (0.5 ml) by ultrasonic treatment for 30 min. This suspension was then mixed with a solution of PMMA (M_{av} = 120000 g/mol, Aldrich) in $CHCl_3$ (0.5 ml). The thin films were then prepared the same way as the zeolite-free polymer thin films according to Bauer et al.[6]

3. References

[1] D. Brühwiler, G. Calzaferri, T. Torres, J. H. Ramm, N. Gartmann, L. Q. Dieu, I. Lopez-Duarte, M. V. Martinez-Diaz, *Journal of Materials Chemistry* **2009**, *19*, 8040.

[2] G. Calzaferri, A. Kunzmann, D. Brühwiler, C. Bauer, Patent: CH 698333 and WO 2010/009560.

[3] D. Brühwiler, L. Q. Dieu, G. Calzaferri, *Chimia* **2007**, *61*, 820.

[4] G. Calzaferri, R. Meallet-Renault, D. Brühwiler, R. Pansu, I. Dolamic, T. Dienel, P. Adler, H. Li, A. Kunzmann, *ChemPhysChem* **2011**, *12*, 580.

[5] D. Brühwiler, G. Calzaferri, T. Torres, J. H. Ramm, N. Gartmann, L. Q. Dieu, I. Lopez-Duarte, M. V. Martinez-Diaz, *Journal of Materials Chemistry* **2009**, *19*, 8040.

[6] C. Bauer, N. Gartmann, L. Q. Dieu, N. Zuber, I. Dolamic, J. H. Ramm, D. Brühwiler, *Thin Solid Films* **2011**, *519*, 3674.

[7] E. Karsenti, *Nature Reviews Molecular Cell Biology* **2008**, *9*, 255.

[8] A. S. Mikhailov, G. Ertl, *ChemPhysChem* **2009**, *10*, 86.

[9] J. D. Murray in 'Mathematical Biology', Springer, Berlin, **2008**

[10] L. Sierra, B. Lopez, J. L. Guth, *Microporous and Mesoporous Materials* **2000**, *39*, 519.

[11] A. Zabala Ruiz, D. Brühwiler, T. Ban, G. Calzaferri, *Monatshefte Für Chemie* **2005**, *136*, 77.

[12] O. Karthaus, L. Grasjo, N. Maruyama, M. Shimomura, *Thin Solid Films* **1998**, *327*, 829.

[13] A. Gierer, H. Meinhardt, *Kybernetik* **1972**, *12*, 30.

[14] A. J. Koch, H. Meinhardt, *Reviews of Modern Physics* **1994**, *66*, 1481.

[15] H. Meinhardt, A. Gierer, *Bioessays* **2000**, *22*, 753.

[16] E. Bormashenko, R. Pogreb, A. Musin, O. Stanevsky, Y. Bormashenko, G. Whyman, O. Gendelman, Z. Barkay, *Journal of Colloid and Interface Science* **2006**, *297*, 534.

[17] B. Z. Zhan, M. A. White, M. Lumsden, *Langmuir* **2003**, *19*, 4205.

[18] D. Brühwiler, G. Calzaferri, *Comptes Rendus Chimie* **2005**, *8*, 391.

[19] S. Suárez, A. Devaux, J. Bañuelos, O. Bossart, A. Kunzmann, G. Calzaferri, *Advanced Functional Materials* **2007**, *17*, 2298.

[20] N. Gfeller, S. Megelski, G. Calzaferri, *Journal of Physical Chemistry B* **1998**, *102*, 2433.

APPENDIX

Curiculum Vitae

Personal Data

Name	Nando Gartmann
Personal Address	Loorenstrasse 23, 8305 Dietlikon
	phone: 078 743 5396
Institute Address	Institute of Inorganic Chemistry
	University of Zürich
	Winterthurerstrasse 190, 8057 Zürich
	e-mail: nando.gartmann@aci.uzh.ch
Date & Place of Birth	May 10, 1983, Chur GR
Nationality	Swiss
Marital Status	Married, 1 child

Education

2008-present	PhD in Chemistry
	Thesis Advisor: PD Dr. Dominik Brühwiler
	University of Zürich
2004-2008	BSc and MSc in Chemistry
	University of Zürich

List of Publications and Conference Contributions

Publications

Functionalized Silicate Nanochannels: Towards Application in Drug Delievery an Solar Energy Conversion

D. Brühwiler, H. Ritter, J. H. Ramm, L.-Q. Dieu, C. Bauer, I. Dolamic, N. Gartmann

Chimia (Special Issue on Young Academics in Switzerland) 63 (2009) 8 - 13

Controlling and Imaging the Functional-Group Distribution on Mesoporous Silica

N. Gartmann, D. Brühwiler

Angewandte Chemie 121 (2009) 6472 - 6475 (german version)

Angewandte Chemie International Edition 48 (2009) 6354 - 6356

(Highlighted in ACS Noteworthy Chemistry)

Nanochannels for Supramolecular Organization of Luminescent Guests

D. Brühwiler, G. Calzaferri, T. Torres, J. H. Ramm, N. Gartmann, L.-Q. Dieu, I. Lopez-Duarte, M. V. Martinez-Diaz

Journal of Materials Chemistry 19 (2009) 8040 - 8067

The Effect of Water on the Functionalization of Mesoporous Silica with 3-Aminopropyl-triethoxysilane

N. Gartmann, C. Schütze, H. Ritter, D. Brühwiler

Journal of Physical Chemistry Letters 1 (2010) 379 - 382

Direct Synthesis and Fluorescent Imaging of Bifunctionalized Mesoporous Iodopropyl-triethoxysilane

J. H. Ramm, N. Gartmann, D. Brühwiler

Journal of Colloid and Interface Science 345 (2010) 200 - 205

Microspectroscopic Analysis of Green Fluorescent Proteins Infiltrated into Mesoporous Silica Nanochannels

Y. Ma, P. Rajendran, C. Blum, Y. Cesa, N. Gartmann, D. Brühwiler, V. Subramaniam

Journal of Colloid and Interface Science 356 (2011) 123 - 130

Self-Organized Patterns of Microparticles in Polymer Films

C. Bauer, N. Gartmann, L.-Q. Dieu, N. Zuber, I. Dolamic, J. H. Ramm, D. Brühwiler

Thin Solid Films 519 (2011) 3674 - 3678

Functional Group Distributions on Mesoporous Silica

N. Gartmann, D. Brühwiler

Chimia (Laureates Edition) 65 (2011) 250 - 252

Correlation of Nitrogen Sorption and Confocal Laser Scanning Microscopy for the Analysis of Amino Group Distributions on Mesoporous Silica

N. Gartmann, D. Brühwiler

Materials 4 (2011) 1096 - 1103

Synthesis of Subphthalocyanines as Probes for the Accessibility of Silica Nanochannels

M. Ince, N. Gartmann, C. G. Claessens, T. Torres, D. Brühwiler

Organic Letters 13 (2011) 4918 - 4921

Poster

Functional Group Distributions on Mesoporous Silica

Nando Gartmann, Dominik Brühwiler

Swiss Chemical Society Fall Meeting 2010

(Awarded with the SCS-DSM prize in the section of physical chemisry)